INTEGRATION OF RADAR AND OPTICAL REMOTE SENSING FOR LANDSLIDE INVESTIGATION – CASE STUDY OF KOSLANDA AREA IN SRI LANKA

Ahangama Kankanamge Rasika Nishamanie Ranasinghe

(118027 L)

Degree of Doctor of Philosophy

Department of Civil Engineering

University of Moratuwa

Sri Lanka

January 2018

INTEGRATION OF RADAR AND OPTICAL REMOTE SENSING FOR LANDSLIDE INVESTIGATION – CASE STUDY OF KOSLANDA AREA IN SRI LANKA

Ahangama Kankanamge Rasika Nishamanie Ranasinghe

(118027 L)

Thesis submitted in partial fulfilment of the requirements for the degree of Doctor of Philosophy

Department of Civil Engineering

University of Moratuwa

Sri Lanka

January 2018

Declaration

I declare that this is my own work and this thesis does not incorporate, without acknowledgement, any material previously submitted for a Degree or Diploma in any other University or Institute of higher learning, and to the best of my knowledge and belief, it does not contain any material previously published or written by another person except where the acknowledgement is made in the text.

Also. I hereby grant to University of Moratuwa the non-exclusive right to reproduce and distribute my thesis, in whole or part in print, electronic or other medium. I retain the right to use this content in whole or part in future works (such as articles or books).

Signature: Date:

The above candidate has carried out research for the PhD Thesis under my supervision.

Name of the Supervisor: Prof. U. G. A. Puswewala

Signature of the Supervisor: Date:

Name of the Supervisor: Dr. T. L. Dammalage

Signature of the Supervisor: Date:

Abstract

Koslanda, in Sri Lanka is an area that remains in the memories of people due to frequently occurring landslides as the area is made vulnerable by both climatic and geomorphological settings. Additionally, the aftermath of the landslide, i.e. the debris flow, causes more damages when compared to the landslide itself. As such, this study focuses on the integration of radar and optical remote sensing for landslide investigation with inclusion of debris flow. The significance of the data types derived from radar and optical images are examined in terms of sensor characteristics and spectral information.

Radar and optical images before and after the event, geometrically registered and radiometrically normalized, are used to delineate the landslide area by different change detection techniques. Detected landslide areas are compared with the area determined by GPS field surveying. At the comparison stage, landslide detection capacity of the optical images was 76% while it was 86% with the radar images. This is mainly due to inherent nature of radar being able to collect data under any climatic condition.

The Information Value method uses bivariate analysis without radar induced factors (BiNR), and bivariate analysis with radar induced factors (BiWR), while the Multi Criteria Decision Analysis based on AHP uses multivariate analysis without radar induced factors (MNR), and multivariate analysis with radar induced factors (MWR). When utilizing the multivariate method, an increase in the area showing high and moderate susceptibility to landslides was observed as 5% and 3% from the total area, respectively. With the inclusion of radar induced factors (surface roughness, near surface soil moisture from delta index, and forest biomass), high and very low susceptible regions to landslide increased by 7% and 4% when using the bivariate method, while it was 3% for both cases when using the multivariate method. Landslide prediction analysis is enhanced by incorporating debris flow analysis with DEM derived factors, as appropriate for a country like Sri Lanka, where data scarcity of acceptable accuracy is high for smaller scale studies.

Key Words – Radar, Optical, Landslide, Prediction, Debris

ACKNOWLEDGEMENT

First and foremost, I wish to thank my main supervisor, Prof. UGA Puswewala, for accepting me as a PhD candidate, and for his untiring support throughout the work. I am indebted to him for his encouragement and the understanding, but most of all, for the patience extended to me during the most difficult times of my PhD. I am really thankful to you Sir. Secondly, I wish to extend my sincere gratitude to my second supervisor, Dr. TL Dammalage, for providing me wonderful support, especially proper directions at the perfect time, and for 'pumping' me up with enough confidence during my lowest points. Thank you very much for being a mentor in its complete sense, and for showing me the way to learn from mistakes. My sincere gratitude to Dr. Ranmalee Bandara. Though you are not my supervisor in the conventional sense, thank you for sharing all the experiences, providing expert reviews, and encouraging me to “find the light at the end of the tunnel”. Your guidance during the last stage when I needed it most, especially when I was lost and wandering around (and feeling completely lazy to write my thesis), is truly appreciated.

I also wish to acknowledge the HETC project, Ministry of Higher Education, for providing the financial support for my PhD studies. Special appreciation and gratitude to Prof. Lalith Munasinghe, Project Coordinator, HETC grant, for without his enormous support and understanding in financial matters, I would never have been able to come to this point of completion. Prof. Joachim Ender and Dr. Nies from ZESS, University of Siegen, Germany, are remembered with profound gratitude for giving me the opportunity and space at ZESS for four months, and for providing their fullest support in collecting and initial processing of the TerraSAR-X and TanDEM-X images from DLR, Germany. The DLR, Germany, is remembered with appreciation for providing radar images for free, and the GSMB, Sri Lanka for providing me, freely, the geological data necessary for my PhD research work.

Additionally, I wish to acknowledge the OTS office, and all the academic, academic support, and non-academic staff of Sabaragamuwa University and University of

Moratuwa, for providing me the peaceful environment needed for my research studies. I wish to convey my sincere gratitude to the Dean, all Heads of Departments, and all my colleagues in the academic staff, and all academic support staff of the Faculty of Geomatics, Sabaragamuwa University, for giving me a home away from home, with enough peace and facilities to complete this task successfully.

I also wish to express my deepest appreciation to a number of very special individuals who stood by me during this crucial period of my life. Among them, Darshana, Jayan, Tharaka, Chandima, Pussella, Mahesh, Charith, Amali, Samanthi, Dr. DR Welikanna, Prof. PI Yapa, and Dr. Jayathissa (from NBRO) are remembered dearly.

When I sat down to write my acknowledgement, many people and memories swamped my mind. It would not be possible for me mention all of them by name, as the list would be endless. But each of you is dear to me, and I am blessed to have had you all coming into my life at one time or other, helping me overcome troubles, and supporting me through hard and harsh times, and making my life easier and more meaningful. Thank you!

I wish to extend my gratitude and love to my family. My mother Babyhami Ekanayake, and my late father Cyril Ranasinghe, who sacrificed their whole life for the betterment of our future. My father would be the happiest about my achievement if he was with us today. He always believed in me, and had unshakable faith in my capacity. That faith and trust gave me strength to crawl over the worst points and periods in my life. Thank you! You are the best Father a daughter could ever have. My sincere gratitude to my sisters, Niranjala, Thushari, Inoka and Manori, and brothers Nadeera and Pradeep, and their families, for making my life easier during the most difficult time in the past years. I am indebted to my father-in-law Gunapala, mother-in-law Premawathi and sister-in-law Niluka and her family, for their kindness and love towards my family when I was away from home.

My deepest appreciation, gratitude, and love to my loving husband Lakmal, the pillar of strength and backbone of my life, and my lovely kids Geeth, Hasi and Thinu. Thank you for being patient with me when I had to work, for being understanding when I had to miss important activities in your life, and for coping by yourselves when I was away from home. Thank you for all the sacrifices you made to support my studies, especially by accepting my long absence from home graciously.

Ahangama Kankanamge Rasika Nishamanie Ranasinghe

30 January 2018

TABLE OF CONTENTS

LIST OF FIGURES

LIST OF TABLES

LIST OF ABBREVIATIONS

AHP – Analytic Hierarchy Process

ALOS - Advanced Land Observation Satellite

ASTER - Advanced Spaceborne Thermal Emission and Reflection Radiometer

AUC - Area Under Curve

AVNIR-2 - Advanced Visible and Near Infrared Radiometer type 2

CI – Consistency Index

CR - Consistency Ratio

CVA - Change Vector Analysis

DEM - Digital Elevation Model

DFR - Debris Flow Regions

DGPS - Differential Global Positioning System

DI – Delta Index

DInSAR – Differential Interferometric SAR

DLR - German Aerospace Center

DMC – Disaster Management Center

DN - Digital Numbers

DT - Decision Tree

EEC - Enhanced Ellipsoid Corrected

EM-DAT - Emergency events data base

ENVISAT – Environmental Satellite

EO - Earth Observation

ERDAS - Earth Resource Data Analysis System

ERTS - Earth Resources Technology Satellite

ERS - European Remote Sensing

ESA - European Space Agency

EW - Extra Wide swath

FR - Frequency Ratio

GCP - Ground Control Points

GEC - Geocoded Ellipsoid Corrected

GIS – Geographical Information System

GPS – Global Positioning Systems

GRD - Ground Range Detected

GSMB - Geological Survey Mines Bureau

IDW - Inverse Distance Weighting

InfoVal - Information value

InSAR - Interferometric SAR

IRS – Indian Remote Sensing

IW - Interferometric Wide swath

JICA - Japan International Co-operation Agency

LST – Land Surface Temperature

MCDA – Multi Criteria Decision Analysis

MGD - Multi look Ground range Detected

MSL – Mean Sea Level

NBRO - National Building Research Organization

NDVI - Normalized Difference Vegetation Index

NIR - Near Infrared

OCN – Ocean

OLI - Operational Land Imager

PALSAR - Phased Array type L-band Synthetic Aperture Radar

PCA – Principle Component Analysis

PRISM - Panchromatic Remote-sensing Instrument for Stereo Mapping

RDFD - Relative Debris Flow Density

RFD - Relative Failure Density

ROC - Receiver Operating Characteristics

SAFE - Standard Archive Format for Europe

SAR - Synthetic Aperture Radar

SI - Statistical Index

SM - Strip Map

SMI – Soil Moisture Index

SPI - Stream Power Index

SRTM - Shuttle Radar Topographic Mission

SSC - Single look Slant range Complex

SVM - Support Vector Machine

T - Temperature

TauDEM - Terrain analysis using DEM

TFSI - Terrain Failure Susceptibility Index

TIRS - Thermal Infrared Sensor

TM - Thematic Mapper

TOA - Top-Of-Atmosphere

TWI - Topographical Wetness Index

UDA – Urban Development Authority

WOE - Weight of Evidence

CHAPTER 1 : INTRODUCTION

This research focuses on developing a versatile approach for predicting and detecting landslides through the integration of radar and optical satellite data. It should be pointed out that both optical and radar data have their own advantages and disadvantages, and integrating the two would complement each other, especially within the context of landslide studies. The current research first generates the prediction model for landslide using landslide failure map from the study area, then moves onto a detailed study of the recent Meeriyabedda landslide (in Sri Lanka), and concludes with analysing the debris flow path of the landslide in order to define the consequential damages.

"One generation *goeth* (disappears/goes), and another generation *cometh* (comes); and the earth *abideth* (waits/stays) forever. The sun also *ariseth* (rises), and the sun *goeth* (sets/goes) down, and *hasteth* (hastens) to his place where he *ariseth* (arose). The wind *goeth* (goes/blows) towards the south, and *turneth* (turns) about unto (towards) the north. It *turneth* (turns) about continually in its course, and the wind *returneth* (returns) again *unto* (into) its circuits. All the rivers run in to the sea, yet the sea is not full; *unto* (towards) the place *whither* (where) the rivers go, *thither* (there) they go again..... That which *hath* (has) been is that which shall be..... Is there a thing whereof men say, see this is new? it *hath* (has) been already, in the ages which were before us" (Ecclesiastes). Although this had been written several thousand years ago, it confirms current geologic thinking that "the Past and Present are the keys to the Future" (James Hutton Circa, 1800 A.C.).

“Nature has its ways in the mountains, building them up and planning (bringing) them down, but rejuvenating them again in geologic time. Landslide forms as part of this process. The hills and valleys are sculptured by exposure to weathering, erosion, gully formation, instability, rock falls, creep and landslide etc. leading to peneplanation,

sedimentation and maturity before mountain building gets repeated again, with igneous activity and metamorphism occurring at different times in between. Landslides have therefore gone on for millions of years, but naturally there have been no readily available records for our use" (Sithamparapillai, 1994).

1.1 Problem Statement

Landslides are unexpected momentary geographical events that consists of the rapid downward motion of soil and rock materials on sloping terrains. The triggering system may include extreme precipitation or rain, deforestation or earthquakes which affect the natural stability of the slope. The result would be falling, sliding or flowing of soil and rock materials under gravity, destroying human lives and property (Singhroy and Mattar, 2000). The immediate priority after a landslide disaster is to carryout relief and rescue operations, which are often disturbed by lack of timely information on the location, number and size of landslides, particularly in inaccessible mountainous areas. Even afterwards, for monitoring and mapping of the landslide, the role of a remote tool would be of utmost importance. Every level of disaster management process requires specific landslide maps that must match their objectives since larger scales require quantitative maps, whereas at smaller scales, qualitative maps are more suitable. With the absence of historical records and a complete landslide inventory system, predicting and studying landslide hazards is a challenging task (Abella *et al.*, 2008). Though field surveys can provide accurate and reliable data, it is not capable of satisfying all of the requirements of landslide studies at a smaller scale, and for active sliding.

Presently, remote sensing technology has been used extensively to provide landslide-specific information for emergency managers and policy makers in terms of disaster management activities in the world (Martha *et al.*, 2011). In recent years, there is an increasing demand for high resolution satellite data to be used for extracting geometric object information and mapping. The spatial resolution of space-borne optical data is now less than 1m in panchromatic images, and at the same time, the interest in

Synthetic Aperture Radar (SAR) sensors and related processing techniques has also increased. Radar is considered to be unique among the remote sensing systems, as it is all-weather, independent of the time of day, and is able to penetrate into the objects through the atmosphere.

Additionally, radar images have been shown to depend on several natural surface parameters such as the dielectric constant and surface roughness. The dielectric constant is highly dependent on soil moisture due to the large difference in dielectric constant between dry soil (having typical dielectric constants in the range of 2-3) and water (dielectric constant in the range of 80) (Kseneman *et al.*, 2012). Estimating soil moisture from radar has received much attention in the scientific community and it has proven that quantitative analysis of soil moisture estimation of radar is possible (Dubois *et al.*, 1995).

Since this research is based on the steep slope terrain areas in Koslanda, Sri Lanka, in order to reduce geometrical disturbances in radar and optical images, terrain correction has to be performed. In addition, since data is coming from different data sources as radar, optical and other available data in raster and vector formats, accurate geometric co-registration for pixel-based analysis is most important. Hence, there is a necessity of producing high resolution DEM (Digital Elevation Model) for optical image ortho-rectification and terrain correction of radar images with the available data and required accuracy concerns.

Radar and optical data present many differences and similarities at the same time. Although in the past, one side-lined the other, nowadays the usefulness and the effectiveness of both of them are fully appreciated. Today, the idea of complementary use of radar and optical data for mapping and monitoring applications has emerged (Ioannidis and Vassilaki, 2008; Stramondo *et al.*, 2006). Hence, the main focus of this research is to examine the real contribution of the integration of radar and optical remote sensing techniques in landslide prediction and detailed landslide studies. The

purpose is to present improved landslide prediction and detection procedures using different native characteristics of radar and optical satellite images before and after the landslide event.

1.2 Koslanda

Koslanda is one of the most beautiful valleys in Sri Lanka, being the home for the breath-taking waterfall of Diyaluma at 210 m being the sixth highest waterfall in the world. Koslanda is situated in the Haldummulla DS Division, Uva Province, in Sri Lanka, and geographically located at 06° 44' 00" North and 81° 01' 00" East coordinates. Koslanda is a remote, hilly area, with geographically difficult access, facing many hard weather conditions. Badulla, which is the capital of the Uva province, is located about 28 km away from Koslanda. The air displacement from Koslanda to Colombo, the capital of Sri Lanka, is approximately 131 km and the route distance is 195 km.

During the period of colonial rule, British planters found that the climate of the hill country to be too cold and the low country to be too hot most of the time. Yet, between the high hill country of Bandarawela and the low country of Wellawaya and Hambantota, they found that Koslanda at 700 m elevation has a climate that is most suitable for plantations. As a result, during British times, tea and rubber estates came up in the Koslanda region, along with good roads and other government facilities.

1.3 Research Objectives

The main objective of this research is to examine the integration of radar and optical remote sensing for landslide prediction through a detailed study of landslides.

The sub-objectives are:

- Conducting a detailed study of the recent Meeriyabedda landslide using different change detection techniques inherent to radar and optical data sources.
- Identifying the most prominent landslide pre-disposing factors from remotely sensed sources, i.e. DEM, Optical and Radar.
- Building landslide prediction models from bivariate and multivariate statistical methods.
- Investigating the performance of the landslide prediction model, with the integration of landslide causal factors derived from radar remote sensing.
- Comparing the performance of the differently built landslide prediction models.
- Investigating the post disaster effects from debris flow due to landslide failures.

1.4 Outline of Approach

This study focuses on the integration of radar and optical remote sensing approaches for landslide studies and to investigate the radar performances for landslide prediction and detections. Hence, it involves the landslide predictions with and without radar induced factors (12 factors derived from optical images, DEM and other auxiliary data with 3 radar induced factors as soil moisture index, surface roughness and forest biomass) using (i) bivariate, information value method, and (ii) multivariate, MCDA (Multi Criteria Decision Analysis) based on the AHP (Analytic Hierarchy Process) technique. The landslide inventory map was then separated into two parts as (i) 'training sample' for prediction analysis, and (ii) 'validating sample' for the validation of results. Fifteen spatial factors (elevation, slope, aspect, planar, curvature, profile curvature, surface roughness, distance to hydrology, TWI (Topographical Wetness Index), rainfall, surface soil moisture, soil moisture index, land use, forest biomass, geology and lineament) for prediction analysis are generated with radar, optical, DEM, field data and other available data sources.

All spatial factors are then converted to the thematic maps and the landslide susceptibility weights assigned using the training samples from the landslide inventory map. Prediction analysis is then performed in bivariate and multivariate environments. Prediction models are evaluated with the separate validation sample from the landslide inventory map, and prediction performances are investigated through success rate and prediction rate curves of the landslide susceptibility analysis. Though landslide studies are wider in the discipline of geology at a larger scale, this research attempts to point out the possibilities of working at a smaller scale with different accuracy levels.

This study investigated, in detail, the Meeriyabedda landslide in the study area. The landslide area is detected by using change detection analysis inherent to radar and optical data sources. In order to incorporate debris flow analysis for landslide predictions, as well as to introduce a low cost and rapid method for landslide prediction better suited for a country like Sri Lanka, terrain failures and debris flow susceptibility analysis are performed using DEM in a GIS (Geographic Information System) environment. Four main terrain factors, which contribute to the terrain instability, are extracted from DEM as slope, aspect, planar curvature and profile curvature. Debris flow analysis is performed using the TauDEM (Terrain analysis using DEM) open source software as an external tool in the ArcGIS environment.

This work consisted of three main tasks; (i) generating the prediction model for landslide using landslide failure map from the study area, (ii) performing a detailed study of the Meeriyabedda landslide with area delineation using change detection techniques, and (iii) analysing the debris flow path in order to define the damaged regions from the land failures using all the susceptible areas extracted from DEM derived parameters as slope, aspect, planar curvature and profile curvature [Figure 1-1].

Land use, slope, elevation, aspect, planar curvature, profile curvature, distance to hydrology, geology, rainfall, soil moisture, soil roughness and forest biomass were

selected as major causal factors of the land failures, and were extracted from DEM, radar, optical images and available data. Ultimately, this approach aims to introduce a methodological enhancement to the landslide susceptibility analysis through the integration of radar remote sensing and debris flow analysis. Hence, in developing an enhanced technique by means of remote sensing as a tool for predicting and detecting areas subjected for sliding, its possible causes will assist the current national landslide inventory and hazard mapping in mountainous areas in a small-scale domain. The radar and optical images before and after the event had been pre-processed so as to minimize the radiometric and geometric errors. Since this study focuses on a mountainous area, working with temporal data in different data formats presented a challenge due to the complexity of the co-registration procedures.

Once data processing is completed for analysis, the selected major causal factors are generated as thematic maps from the DEM, radar and optical images. The presented method combines the landslide inventory map with each thematic map to determine the weight of influence on terrain instability for each parameter class, and the Log function is used to control the large variation of weights in calculations. The weights are then added to bivariate and multivariate environments to obtain the terrain failure susceptibility index for each pixel. Based on these values, landslide susceptibility regions are delineated into four classes as very low, low, moderate and high. All the analyses are performed with and without radar induced factors in order to examine the performance of predictions with radar image sources. Prediction performances are investigated using success rate curves and prediction rate curves.

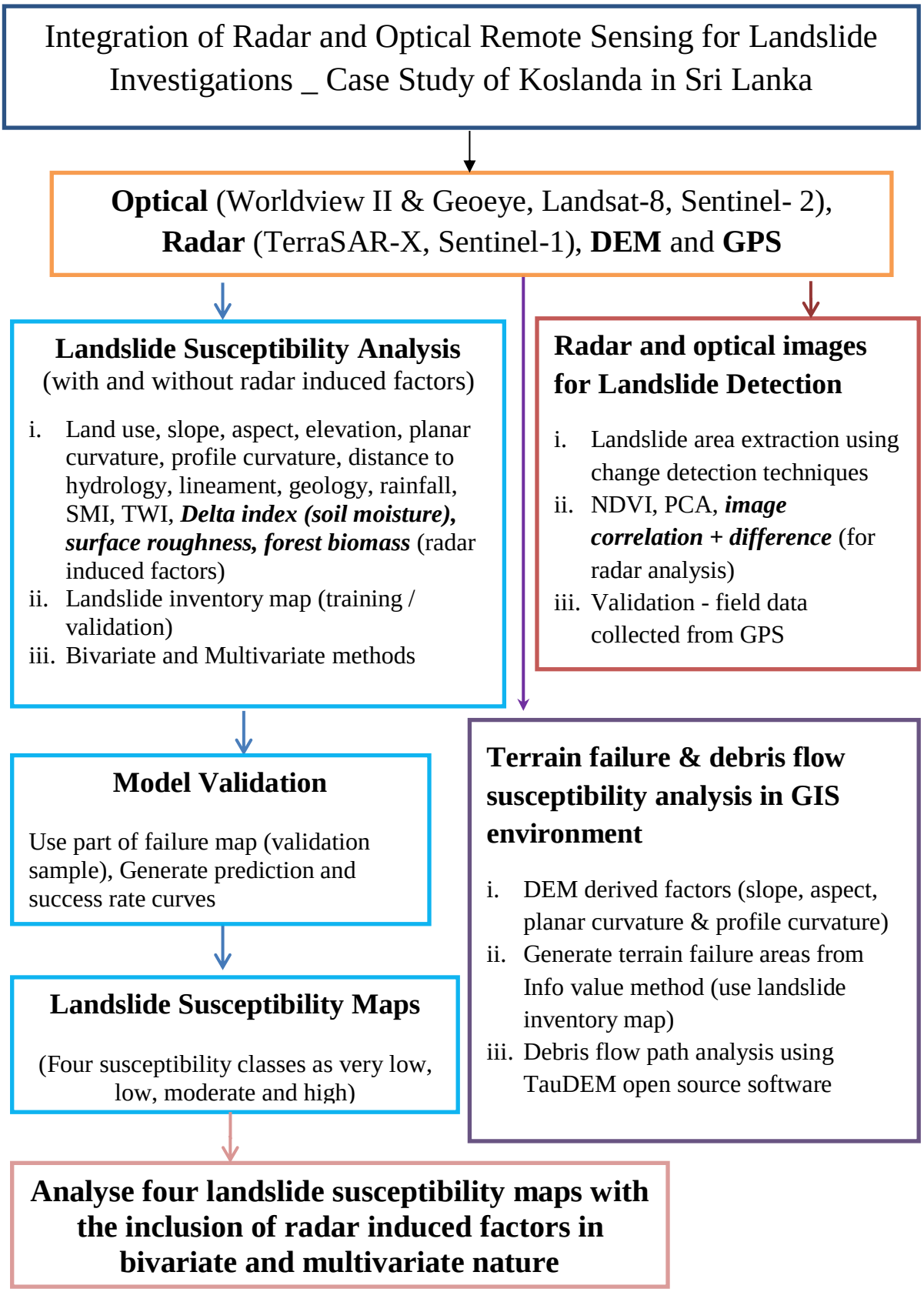

Figure 1-1 : Conceptual methodology for radar and optical remote sensing for landslide investigations

Finally, four landslide susceptibility maps obtained with and without radar induced factors in bivariate and multivariate statistical nature are compared in order to analyse the performance of radar induced factors in landslide susceptibility analysis.

1.5 Thesis Organisation

This thesis consists of seven chapters, with **Chapter2** describes the study area, Koslanda in Badulla District, the probability of landslide occurrence due to its geomorphological, geological and climatic nature and the types of radar, optical and other auxiliary data used. **Chapter 3** describes the related work and scientific literature including an introduction to landslides and landslides in global and regional context, modes of landslide investigations, landslide prediction models, statistical analysis in landslide susceptibility analysis and their validations, change detection techniques for landslide extraction, and finally, debris flow analysis for landslide prediction modelling. **Chapter 4** develops an empirical model using data pre-processing, selecting, generating and weighting spatial factors, to predict the landslide and ultimately validating the model with the recent landslide that occurred in Meeriyabedda area. **Chapter 5** analyses the detection of Meeriyabedda landslide from change detection techniques with the combination of radar and optical images. **Chapter 6** investigates the terrain failure regions derived from the four main terrain factors identified as slope, aspect, planar and profile curvature, and the analysis of the debris flow susceptibility regions in Koslanda area. The final chapter of the thesis, **Chapter 7** provides conclusions of the research and recommendations for future work.

CHAPTER 2 : STUDY AREA AND DATA USED

This chapter describes the basis for selecting Koslanda (in Sri Lanka) as the study area for landslide prediction, and detailed landslide studies. The natural formation of the area itself, based on topographical and geological context, makes it most vulnerable for landslide disasters. Previous landslides experienced in this area are described including damages to both human life and property. Many primary data types derived from radar and optical images, DEM generated from aerial photogrammetric techniques, and other auxiliary data used in this analysis are described. GPS (Global Positioning System) surveying is carried in order to obtain GCPs (Ground Control Points) for image pre-processing as the method is better suited for pixel-based analysis, and to demarcate the margin of the damaged area due to landslide for validation of the results from change detection analysis. This chapter ends with a detailed discussion on the selection of radar images, optical images and other auxiliary data.

2.1 Introduction

Sri Lanka is the pearl of the Indian Ocean and is known for her beauty, as well as being gifted with some of world's most beautiful gems and quality teas fulfilling about a quarter of the tea requirement of the world. It is located between northern latitudes of 05°55' and 09°51' and eastern longitudes of 79°42' and 81°52', approximately 24 km to the southeast of India. The country occupies an area of nearly 65,000 km^2, stretching to 435 km from north to south and 224 km from east to west. The country, as a whole, has experienced extensive land degradation primarily due to soil erosion, existing geology, unsafe land use practices and denudation processes. These factors, together with the common triggering factor, intensive and prolonged rainfall due to the south west and north east monsoonal and inter monsoonal rains, increases the incidence of landslides in the central hilly region and abutting sloping terrain of the country. From the land extent of Sri Lanka, an area of nearly 20,000 km^2 encompassing 10 districts is prone to landslides. These districts are Badulla, Nuwara Eliya, Kegalle, Ratnapura,

Kandy, Matale, Kaluthara, Matara, Galle and Hambantota. NBRO (National Building Research Organization), is the organization responsible for landslide studies in Sri Lanka. Their studies indicates that haphazard and unplanned land use, inappropriate construction methods, and wanton human intervention have led to an increase in landslide susceptibility.

According to the statistics from NBRO, it has been revealed that the landslide frequency has been increased in the Badulla district with the increases of human activities, forest degradation and unplanned developments in hilly areas. Parallel to this, unplanned land clearing for tea and other plantations, changing the existing natural drainage patterns and dramatically reduced vegetation covers, make for far larger areas to be more vulnerable to landslides (Bandara, 2005; DMC, 2010).

2.1.1 Climate in Koslanda

The climate is tropical in Koslanda, with a significant rainfall during most months of the year, with a short dry season. The annual rainfall in Koslanda is 1,500 mm, with an annual average temperature of 20°C. April and May are the warmest months of the year with an average temperature of 21.5°C while January is the coldest month, with the temperatures averaging at 19°C (CLIMATE_DATA_ORG 2016). The average minimum and maximum monthly temperatures from year 2000 to 2012 in Koslanda area are described in Figure 2-1.

The highest temperature is observed during the months of February, March, April and May, with April being the warmest month and October and November being the coolest months with high precipitation. The data presented in Figure 2-1 has been obtained from the weather station covering Nuwara Eliya (Sri Lanka), which is the nearest to Koslanda, at a distance of 54.6 km.

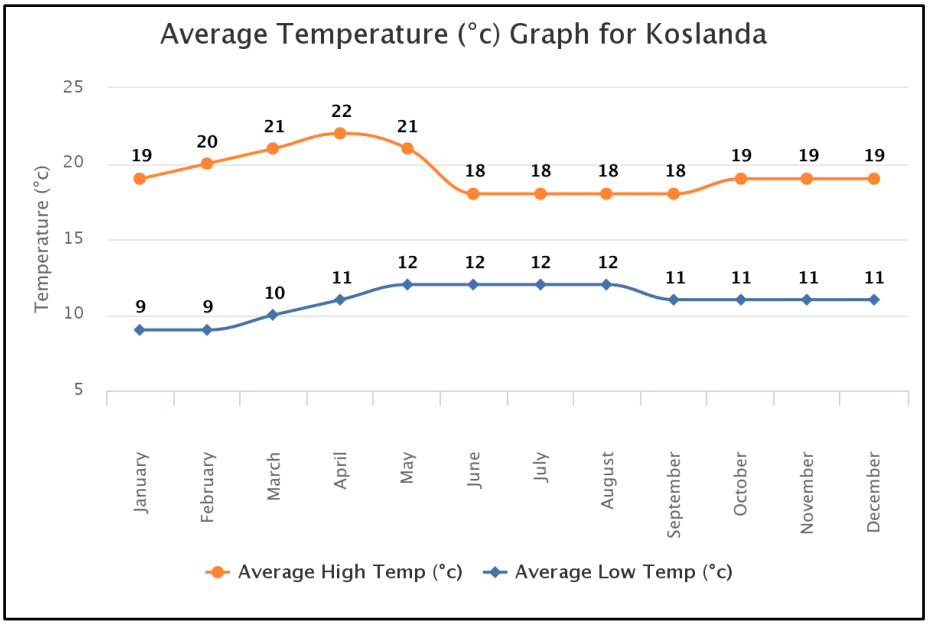

Figure 2-1 : Average minimum and maximum monthly temperature from year 2000 to 2012 in Koslanda
Source:http://www.worldweatheronline.com/koslanda-weather-averages/uva/lk.aspx, accessed on 06th February 2016.

The precipitation (in mm) and average rainfall (30 days) from year 2000-2012 are shown in Figure 2-2, for the weather station at Nuwara Eliya. It is observed that the driest month is February with the lowest precipitation. Most of the precipitation falls during October and November, averaging to 200 mm.

2.1.2 Geomorphology of Koslanda

The geomorphology of Koslanda area has been described as “the area is a gently inclined talus slope, where a thick, loosely compacted colluvium deposit is observed at the foot of the near vertical rocky scarp and is situated at the middle part of the slope. The lower area shows a fairly steep surface as well. The composition of the colluvium deposit includes a randomly arranged mixture of weathered clayey and sandy products and organic material that can act as a sponge with high water content. The area was an abandoned tea cultivated land in which the properly maintained surface drainage

system has been neglected. This colluvium deposit is underlain by garnet biotite gneiss bedrock, which is highly foliated and jointed" (Somaratne, 2016). Such geological formation, together with improper land use management practices, has made the Koslanda area extremely vulnerable to landslide events.

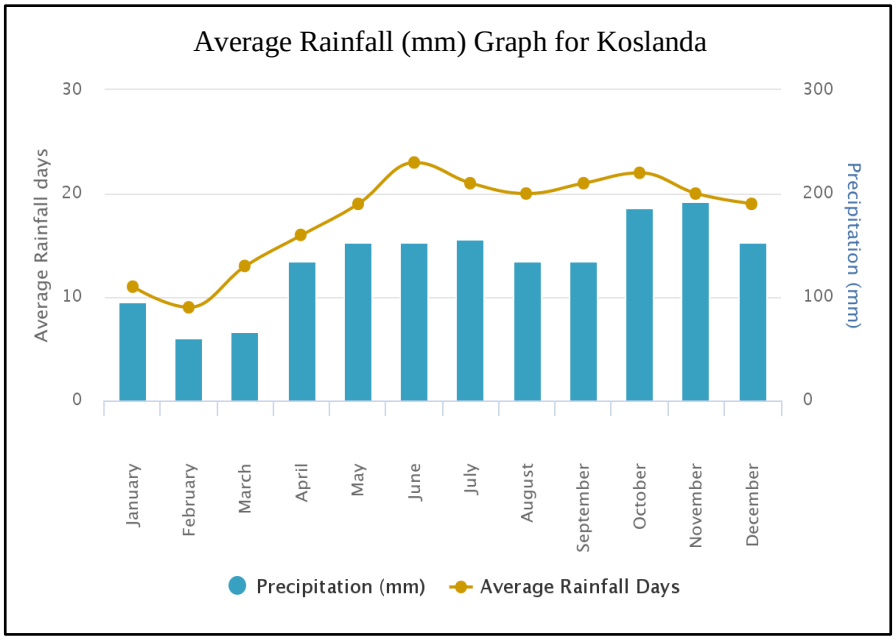

Figure 2-2 : Precipitation and average monthly rain fall from year 2000-2012 in Koslanda
Source:http://www.worldweatheronline.com/koslanda-weather-averages/uva/lk.aspx, accessed on 06th February 2016.

2.1.3 Landslides in Koslanda

Generally, landslides occur in slopes with gradients over 30^0 in lands that had been made unstable by clearing for various cultivations such as tea and homestead gardens with improper land use practices, including soil management. Especially in tea estates, due to non-maintenance of contour drains and blockage of natural water courses in steep areas, the area is highly vulnerable for terrain failures. With prolonged heavy rain, the soil covers get saturated, ultimately resulting in a mass movement comprising of mud and debris (Somaratne, 2016).

Koslanda has been the site for of several massive landslides over the years, and both the Naketiya landslide in the year 1997, and Meeriyabedda landslide in the year 2014, are very distinct [Figure 2-3]. As the name suggests, “Naketiya” is landslide-prone, and within two years, major landslides have occurred three times at the same location, destroying the road from Beragala to Wellawaya. NBRO has recognized this area as highly vulnerable to landslides, with many studies being carried out for identifying potential mitigatory measures.

Figure 2-3 : Locational map for Koslanda, Sri Lanka with historical landslide experiences from Google earth.

2.1.4 Meeriyabedda Landslide

On 29th October 2014, at around 7.30 am, a severe landslide occurred in Meeriyabedda area [Figure 2-4] in Kotabathma Grama Niladhari division within the Haldummulla Divisional Secretariat Division in Badulla District. Rainfall data from the Poonagala gauging station, which is closer to the area revealed that the amount of precipitation that poured into the area for three consecutive days from 26th to 29th October, 2014, has exceeded 500 mm.

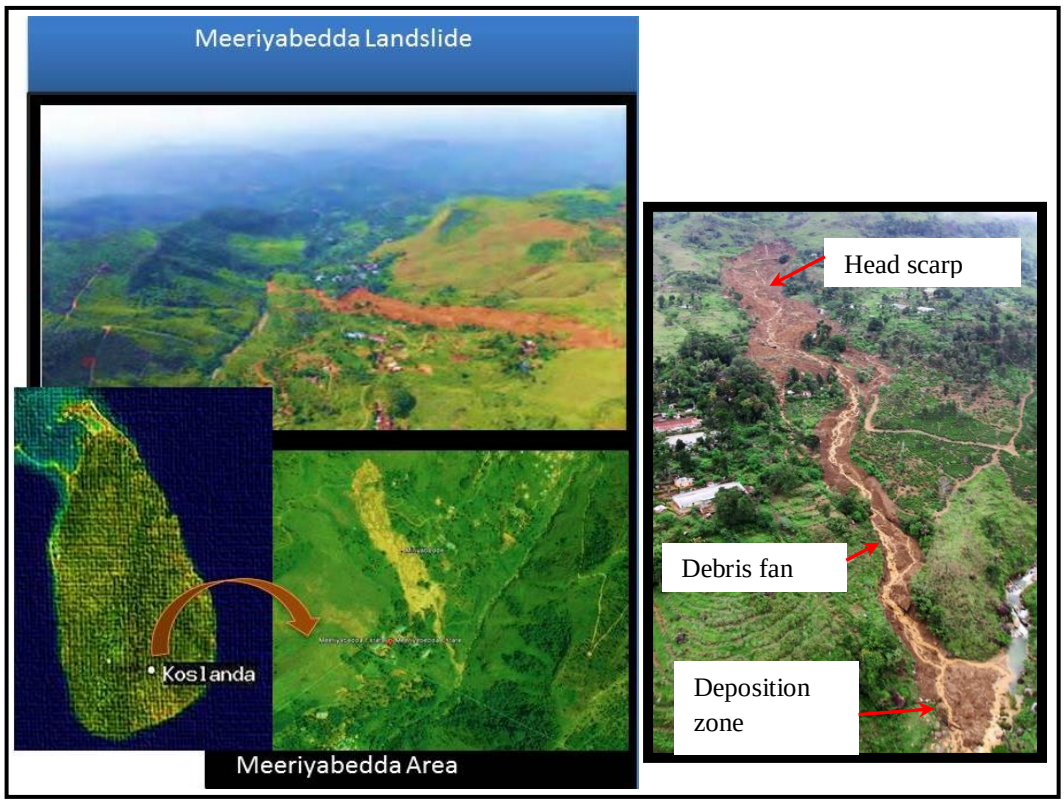

Figure 2-4 : Nature of Meeriyabedda Landslide in 29th October, 2014

The impact of the landslide affected around 330 people of 57 families in Ampitikanda tea estate. 16 deaths were confirmed, and 192 persons went missing. The total number of buildings destroyed were 63, including houses, Kovil, community center, dairy collection centers, boutiques, telecommunication center, and 3 estate bungalows. [Figure 2-5]. Out of the total number of children who attended the school, 75 children were orphaned.

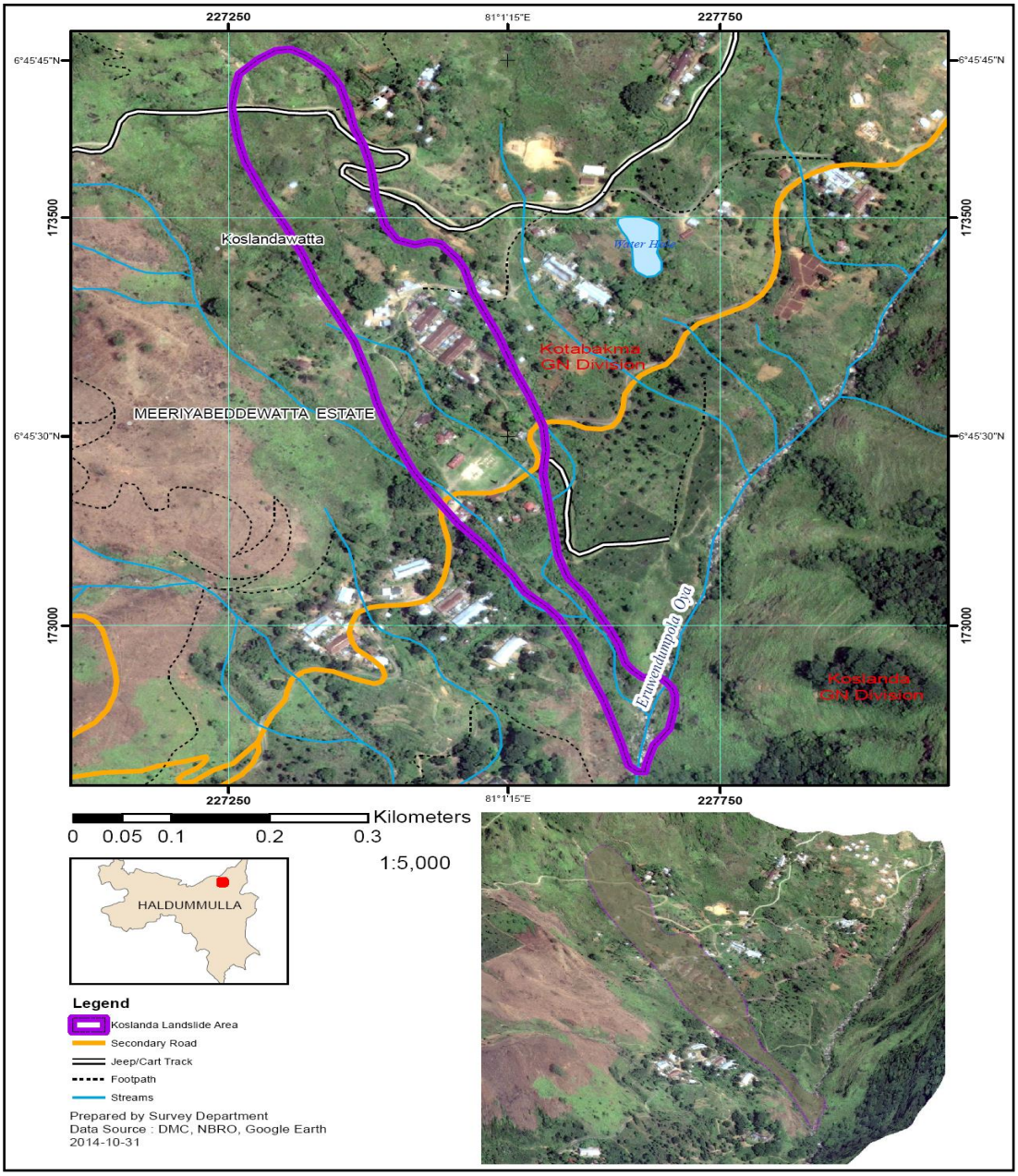

Figure 2-5 : Meeriyabedda landslide disaster and its damages
Source: Prepared by Survey Department of Sri Lanka, Data Source: DMC, NBRO, Google Earth, 31-10-2014

Usually, almost all landslides indicate advanced warning signals via the appearance and expansion of tension cracks on the ground, floors and walls of buildings located in upper slope areas, disappearance of springs and drying up of wells on the upper slopes, appearance of springs and increase of water levels of wells located at lower

slope areas, muddy water out-pouring from springs at lower slope areas, ground subsidence of the upper slopes, tilting of poles and trees, and so on, prior to the main movement (Bandara, 2005). In the case of Meeriyabedda landslide, some of these warning signals like appearance and widening of tension cracks on the upper estate road, floor and ground cracks of line houses, and small local ground subsidence, happened at times in the middle part of the damaged area. Moreover, water seepage out of the ground surface at elevated locations on the slope have been observed prior to the incident.

As short-term mitigation measures, surface drainage control, application of erosion control measures can be applied. Simultaneously, if the risk is high, the vulnerable community must be evacuated and proper temporary shelters must be provided immediately. When providing permanent resettlement, new places should comprise more facilities than the original place. If such a system is available, any community will not resist resettling in a more comfortable location (Bandara, 2005).

2.1.5 Debris Flow

Most of the destructions from landslides occurred due to the combined effect of terrain failures and debris flow. According to the definition of Iverson and Denlinger (2001), debris flows consist of a mixture of fine material (sand, silt and clay), coarse material (gravel and boulders), with a variable quantity of water, which flow rapidly down a slope under the influence of gravity. Three distinctive elements are distinguishable in a debris flow: the source area, the main track (transportation area) and the depositional fan. Debris flows are of primary concern due to their long run-out and the resulting destructive impacts.

Meeriyabedda landslide was the worst natural disaster after the tsunami in 2004 that killed over 38,000 people along the coastal belt of Sri Lanka. A thirty-foot mudslide

buried approximately 200 human lives and their properties, with the area becoming a pool of mud that was unapproachable. About 500 military personnel were involved in the rescue operation, and heavy machinery had been deployed to speed up the rescue efforts.

2.2 Satellite Images and Auxiliary Data

As this research focuses on the integration of radar and optical remote sensing for landslide prediction and detailed landslide studies, the types of radar, optical and other auxiliary data used in the research are explained. Since the study area is undulated, all the satellite images had to be corrected for the terrain before doing any analysis. Thus, DEM plays a significant role in both image pre-processing and final data analysis.

2.2.1 DEM from Aerial Photogrammetry

Topography influences both initiation of sliding and movement of mass due to landslides. DEM data can be used to derive most prominent causative factors for landslide as elevation, slope, aspects, hill shading, slope curvature and qualitative classifications of landform, including hydrological parameters as flow direction, flow path, basin and river network and so on (Bonachea *et al.*, 2009; Yawen, 2011).

The DEM for this study is generated using aerial photogrammetry. Automatic procedures for DEM extraction using photogrammetric techniques produce high precision terrain models within a short time, thereby reducing manual editing. The accuracy of the DEM is strictly related to the image quality and terrain features. A DEM of 7 m resolution is derived from aerial triangulation, using stereo aerial photographs from year 1993. The Imagine photogrammetry tool in ERDAS Imagine 2014 (Earth Resource Data Analysis System) software is used to generate the DEM from aerial photographs [Figure 2-6]. Camera calibration, interior orientation, and

exterior orientation are performed in order to generate the DEM from aerial triangulation, by using 25 GCPs obtained from a GPS survey of the study area.

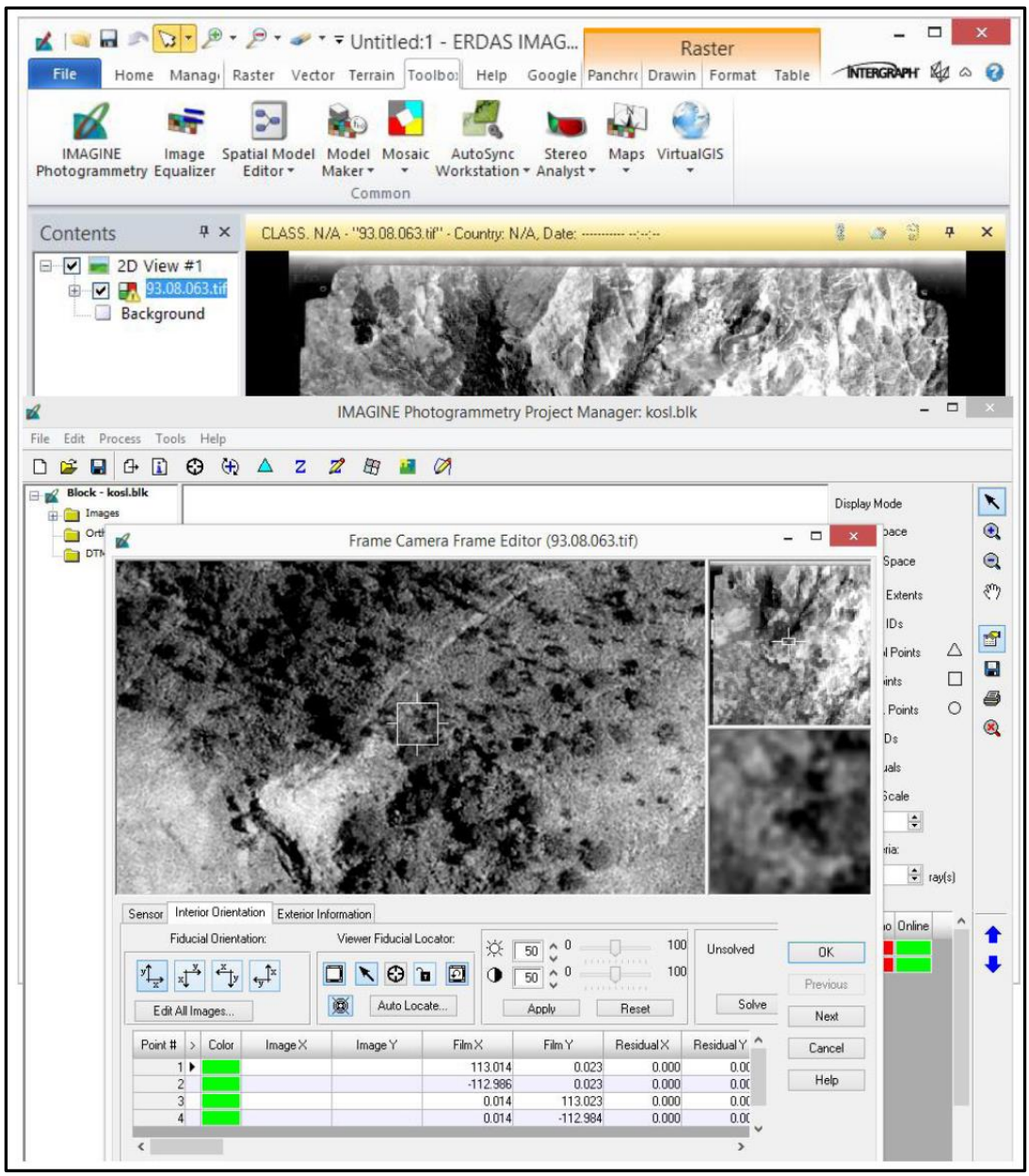

Figure 2-6 : DEM Generation from Imagine photogrammetry tool from ERDAS Imagine 2014

2.2.2 Radar Images

Due to their inherent characteristics, the significance of radar images for disaster studies have been proven by the scientific community. The capabilities of day and night observation, under all weather conditions, offer quick responses in all phases of disaster management studies.

Sentinel-1

This study uses a series of Sentinel-1 images in landslide detection, with soil moisture and surface roughness parameters used in the landslide prediction analysis. All images are level-1 GRD (Ground Range Detected) products consisting of focused SAR data, multi-looked and projected to ground range using an earth ellipsoid model. The resolution is dependent upon the amount of multi-looking performed. Hence, the study uses a 10 m resolution, multi-looked, square pixel images calibrated for radar backscatter in decibels, filtered for speckle using the enhanced Lee filter, and corrected for terrain using the SRTM (Shuttle Radar Topographic Mission) 30 m DEM data.

Sentinel-1 is a space mission funded by the European Union, and carried out by the ESA (European Space Agency) within the Copernicus Programme, consisting of a constellation of two satellites. The Sentinel-1 is a Synthetic Aperture Radar in C band that provides continuous imagery in day, night, and all weather conditions. Sentinel-1A was launched on 03rd April 2014, and Sentinel-1B was launched on 25th April 2016 with an operational lifespan of 7 years (Sentinel_1, 2016).

Sentinel data products are made available systematically and free of charge to all data users including the general public, scientific and commercial users. Radar data are delivered within an hour of reception for emergency response, within three hours for priority areas and within 24 hours for systematically archived data. All data products are distributed in the SAFE (Standard Archive Format for Europe) format. Sentinel-1

productions are at SAR Level-0, Level-1 SLC, Level-1 GRD, and Level-2 OCN (Ocean). Data products are available in single polarisation (VV or HH) for Wave mode and dual polarisation (VV+VH or HH+HV) and single polarisation (HH or VV) for SM (Strip Map), IW (Interferometric Wide swath) and EW (Extra Wide swath) modes. The Sentinel-1 mission is sun-synchronous, near-polar, and circular, with an orbit height of 693 km at an inclination of 98.18°, with a repeat cycle of 175 orbits in 12 days (Sentinel_1, 2016).

TerraSAR-X

TerraSAR-X, a radar earth observation satellite, is a joint project between the German Aerospace Center (DLR), and EADS Astrium. TerraSAR-X was launched on 15th June 2007 and has been in operational service since January 2008. TanDEM-X was launched on 21st June 2010 as its twin satellite, and together acquire the data for generating the World DEM, which is available from 2014. TerraSAR-X contains a phased array Synthetic Aperture Radar antenna with X-band (wavelength 31 mm, frequency 9.6 GHz), circles the earth in a sun-synchronous polar orbit with a temporal resolution of 11 days, at an altitude of 514 km (TerraSAR_X, 2016).

Spot Light mode (up to 1 m resolution) has a 10 × 5 km^2 scene size, while Strip Map mode (up to 3 m resolution) contains a 30 × 50 km^2 scene size. Scan SAR (up to 16 m resolution) covers an area of 100 × 150 km^2 for one scene of the earth. Depending on the desired application, TerraSAR-X provides data products at different processing levels as SSC (Single look Slant range Complex), MGD (Multi look Ground range Detected), GEC (Geocoded Ellipsoid Corrected), and EEC (Enhanced Ellipsoid Corrected). The TerraSAR-X spotlight image, GEC product, with 2 m resolution taken on 02nd November 2016, just after the Meeriyabedda landslide, is used for forest biomass estimation, by taking forest biomass as radar induced causative factor for landslide prediction modelling (TerraSAR_X, 2016).

2.2.3 Optical Images

High resolution and free medium resolution optical satellite images are used in various parts of the analysis. Several causative factors for landslide prediction analysis are derived from the free Landsat -8 and Worldview -2 images. Detailed landslide detection using different change detection techniques are done using WorldView -2 and GeoEye -1 satellite images.

WorldView II

WorldView-2 is a commercial earth observation satellite possessed by Digital Globe. WorldView-2 provides panchromatic imagery of 0.46 m resolution, and eight-band multispectral imagery with 1.84 m resolution. It was launched on 08th October 2009 and takes images of any place on Earth every 1.1 days. WorldView -2 comprises of 8 Multispectral bands with four standard colors (Red, Blue, Green, Near-IR) and four new colors (Red edge, Coastal, Yellow, Near-IR2) (WorldView_2, 2016).

Red edge band aids in the analysis of vegetative conditions and is directly related to plant health revealed through chlorophyll production. The coastal band supports vegetation identification and analysis, and supports bathymetric studies based on its chlorophyll and water penetration characteristics. Further, this band is subjected to atmospheric scattering and can be used to investigate atmospheric correction techniques. Yellow band is used to identify "yellow-ness" characteristics of targets, important for vegetation applications. Also, this band will assist in the development of "true-color" hue correction for human vision representation. NIR 2 band overlaps the NIR 1 band but is less affected by atmospheric influence and supports vegetation analysis (WorldView-2 2016). This research uses the WorldView –2 image with four standard colors from 16th May 2013 as the pre-image for the landslide prediction and detailed landslide detection analysis.

GeoEye-1

GeoEye-1 is very high-resolution satellite that was successfully launched on September 6, 2008 with a 0.46 m resolution. The GeoEye -1 satellite sensor features the most sophisticated technology ever used in a commercial remote sensing system and is owned and operated by Digital Globe. This sensor is optimized for large projects, as it can produce over 350,000 $km^2$of pan-sharpened multispectral satellite imagery every day (GeoEye-1 2016). The GeoEye -1 satellite image with four standard colors taken on 06th November 2014, covering the Koslanda area, was used as the post landslide image in the landslide detection analysis.

Landsat-8

On 23rd July 1972, the first Earth Resources Technology Satellite (ERTS) was launched from Vandenberg Air Force Base in California. In 1975, it was renamed as Landsat 1 and since then, six more Landsat satellites have followed, collectively capturing millions of images of Earth, and creating an impressive archive that has been available at no charge since 2008. Over the past five decades, the Landsat program and other international Earth-observation programs have matured. Landsat satellites monitor forest health, mobilize food resources to drought-stricken areas, observe climate change impact on polar ice caps, monitor crop health and stress, measure the impacts of carbon escaping into the atmosphere, and map rates, causes, and consequences of land cover changes and so on (Landsat– 8, 2016). Table 2-1 describes the sensor characteristics and band information of WorldView -2, GeoEye-1 and Landsat -8. The research uses the Landsat – 8 images taken on 03rd July 2015 for analysing the soil moisture index by using Red, NIR and Thermal bands.

Landsat -8 OLI (Operational Land Imager) and TIRS (Thermal Infrared Sensor) were launched on 11th February 2013, and consists of nine spectral bands with a spatial resolution of 30 m for Bands 1 to 7 and 9. The new band 9, ultra-blue, is useful for coastal and aerosol studies, and cloud detection. The resolution for Band 8 (panchromatic) is 15 m. Thermal bands 10 and 11 are useful in providing more

accurate surface temperatures and are collected at 100 m resolution. Approximate scene size is 170 km north-south by 183 km east-west (Landsat–8, 2016).

Table 2-1 : Sensor characteristics and spectral information for WorldView -2, GeoEye-1 and Landsat -8 Satellite images

	WorldView -2	**GeoEye -1**	**Landsat -8**
Resolution	0.46 m PAN +1.85 m MS	0.41 m PAN + 1.65 m MS	15 m PAN + 30 m and 100 m MS
Swath width	16.4 km	15.2 km	190 km
Average Revisit	1.1 Days	2.1 Days	16 Days
Orbit Type	Sun-synchronous	Sun-synchronous	Sun-synchronous
Orbit Altitude	770 km	681 km	705 km
Orbit Period	100 minutes	98 minutes	98.9 minutes
Spectral Bands	PAN + 8 MS Bands	PAN + 4 MS Bands	PAN + 10 MS Bands
Spectral Range	Red(630-690 nm), Green(510-580nm),Blue(450-510 nm), Near Infar Red 1(770-985 nm), Near Infrared 2 (860-040 nm), Coastal Band (400- 450 nm), Yellow Band (585-625 nm), Red Edge Band (705-745 nm)	Panchromatic (450-800nm), Blue (450 – 510nm), Green (510-580nm), Red (655-690nm), Near Infrared (780-920nm)	Coastal aerosol (430–450nm),Blue (450-510 nm), Green (530–590 nm), Red (640– 670 nm), NIR (850– 880 nm), SWIR 1 (1570–1650nm), SWIR 2 (2110– 2290 nm), PAN (500–680nm),Cirrus (1360–1380nm),TIRS1(10600–11190 nm), TIRS 2 (11500– 12510 nm).

Sentinel-2

Sentinel-2 is an Earth observation satellite developed by ESA which consists of 13 multispectral bands in visible, near infrared, and short-wave infrared regions of the spectrum. Four bands at 10 m resolution (490 nm (nano meter) (B2)), 560 nm (B3), 665 nm (B4), 842 nm (B8)), six bands at 20 m resolution (705 nm (B5), 740 nm (B6),

783 nm (B7), 865 nm (B8a), 1610 nm (B11), 2190 nm (B12)) and three bands at 60 m resolution (443 nm (B1), 945 nm (B9) and 1375 nm (B10)) (Sentinel_2, 2016).

In order to achieve recurrent revisits and data availability, two identical Sentinel-2 satellites (Sentinel-2A and Sentinel-2B) are planned to operate simultaneously. The first satellite, Sentinel-2A was launched on 23rd June 2015 and Sentinel-2B was scheduled to be launched in March 2017. The most important aspect is the free and open data policy for data dissemination (Sentinel_2, 2016). Free Sentinel-2A image dated 10th October 2016 is utilized for the production of the land cover map, and the lineament density map of the study area for landslide prediction modelling.

2.2.4 Auxiliary Data

Many data types produced from radar and optical remote sensing techniques are used in all analysis within this research work. However, there are some data types that are really important for landslide prediction analysis that are obtained from available data sources as (a) landslide failure map, (b) geological map, (c) soil map, (d) monthly average rainfall data, and (e) GCPs coordinate and Meeriyabedda landslide boundary from GPS survey.

The Geological map of Sri Lanka at 1:100 000 scale from GSMB (Geological Survey Mines Bureau)), Sri Lanka, Soil map of Sri Lanka for the intermediate zone (Mapa *et al.*, 2005) and average rainfall data interpolated for the study area are used for preparing causative factors for landslide prediction analysis. Since the study area is highly undulated, all the satellite images were corrected for the terrain for better registration of the images. Hence, a GPS survey was carried out for obtaining the GCPs covering the particular area, and for the accurate boundary demarcation of the landslide damaged regions, especially for the Meeriyabedda landslide. All prediction analysis and validation are based on past landslide experiences in the chosen area,

thereby minimizing bias and errors from human intervention. Hence, producing the landslide failure map using the landslide data-base for the study area is of utmost importance.

(a) Landslide Failure Map

The landslide failure map shows the landslide locations, dimensions and geographical extent of each landslide. One of the main clues to the location of future landsliding is the distribution of past movement. Hence, the maps that show the location and size of landslides are helpful in predicting the landslide hazard for the entire area [Figure 2-7].

Figure 2-7 : Landslide failure map of the Koslanda area with two different training and validating samples with Google image as background

A landslide inventory is a data set that may represent a single event, a regional event, or multiple events. Small-scale maps may show only landslide locations, whereas large-scale maps may distinguish landslide sources from deposits and classify different kinds of landslides and show other pertinent data. Hence, this work generates the landslide failure map by considering the past movements from the landslide database from the NBRO, Sri Lanka. Mapping was depended on the aerial photographs obtained in 1993 and 1997, WorldView -2 and GeoEye – 1 image, and a series of temporal google earth images. Basically, the landslide failure map was separated in to two samples as training and validating for the landslide susceptibility analysis through the entire research [Figure 2-7].

(b) Geological Map

A geological map is a special purpose map made to show the geological features of the Earth. Rock or geologic strata are shown by colour or symbols to indicate where they are exposed at the surface. Bedding planes and structural features such as faults, folds, foliations, and lineation are shown with symbols describing the three-dimensional orientations of the features. Contour lines may be used to illustrate the surface of a selected stratum that describing the subsurface topographic trends of the strata. It is not always possible to properly show this when the strata are extremely fractured, mixed, in some discontinuities, or where they are otherwise disturbed. A geological map with 1:100,000 scale (Sheet No 17) from GSMB, Sri Lanka is used. There are 21 geological maps of 1:100,000 scale covering the entire land mass of the country. Required geological boundaries of the study area were extracted and made use of as a causative factor for the landslide prediction analysis.

(c) Soil Map

Soil map is a geographical representation which shows the diversity of soil types and soil properties (soil pH, textures, organic matter, depths of horizons and so on) in the area of interest. It is typically the end result of a soil survey inventory. Sri Lanka is basically divided in to three climatic zones as Wet, Dry and Intermediate zones. The

soil maps at smaller scale (1:400,000) for these three climatic zones are accomplished by monitoring the long-term changes of the morphological, physical, chemical and other important properties of the soil. Basically Koslanda is in the high-land intermediate zone comprising soil type as Badulla-Mahawalathenna complex (Mapa *et al.,* 2005). When considering the extent, and the location of study area, the soil type could not be considered as a causative factor for this landslide prediction analysis because the study area consists with one soil type. However, it should be noted that the soil type is one of the most prominent factor in landslide susceptibility analysis.

(d) Monthly Average Rainfall Data

Rainfall is the most common causal factor for the landslide occurrence and the majority of landslides are triggered by heavy and prolonged rainfall. Especially in Sri Lanka, the atmosphere is extremely dynamic due its location closer to the equator. The basic wind system over Sri Lanka is mostly the monsoons which seasonally alternate between northeast (December–March) and southwest (May – September). The inter-monsoonal periods are also there from March to April and October to November. The Koslanda area is located in the intermediate zone and receives rainfall from southwest monsoon and inter-monsoonal period from October to November. According to the historical landslide record in Koslanda area, most of the rainfall induced devastating landslides and mass movements occurred during October to November.

The study uses monthly average rainfall data in year 2014 from 10 nearby stations to Koslanda as Buttala, Konketiya, Diyatalawa, Badulla, Gangeyaya, Gleanore, Haputale factory, Poonagala, Suriyawewa, Thenamalwila and Wellawaya. All the monthly rainfall data from the 10 rain gauge stations are averaged, and the average rainfall map for the study area is generated using the IDW (Inverse Distance Weighting) interpolation method from ArcGIS environment.

(e) GPS Survey

A GPS survey was carried out for obtaining 40 GCPs covering the whole study area, and the accurate boundary for landslide damaged regions in Meeriyabedda. GCPs and the boundary points extracted from the GPS Survey were most important for image pre-processing and validation of the final results. The GPS survey was carried out for three days starting from 17th October 2015. Leica Handheld GPS and RTK GPS (Real Time Kinematic GPS) units had been used with a reference station in order to achieve more accuracy with DGPS (Differential GPS) techniques. During the first two days, three survey groups collected all the GCPs with 30 minutes of observation, and on the third day, all groups collected location data on the boundary of the landslide damaged area from Meeriyabedda landslide.

2.3 Chapter Summary

This research study is based on the integration of radar and optical remote sensing for landslide prediction and detailed landslide detection. This chapter discussed the justifications of selecting Koslanda as the study area for the research. The climatic and geomorphological settings of the area that are most vulnerable to landslides were discussed, using the recent devastating landslide that occurred in Meeriyabedda area. Significance of each data type derived from radar and optical remote sensing for the analysis were investigated in terms of sensor characteristics and spectral information. Other auxiliary data available, along with their processing stages in order to apply them for enhancing the ultimate results for these analyses, were described. A GPS survey was carried out in order to obtain the GCPs for satellite image pre-processing and to extract the landslide damaged boundary from Meeriyabedda landslide for validating the results from change detection analysis.

CHAPTER 3 : RELATED WORK - SCIENTIFIC LITERATURE

This chapter focuses on viewing landslides as a disaster, and discussing the importance and contribution of previous scientific work that motivated the successful accomplishment of the work discussed in this thesis. The chapter starts with the importance of remote sensing for landslide investigations, which comprises mainly of landslide susceptibility analysis and post landslide detections. It is followed by a discussion on the integration of radar, with its inherent characteristics, in natural disaster studies for landslide susceptibility analysis and landslide detections. The different landslide prediction models with different causative factors, and statistical analysing techniques for modelling and model validation that are currently available are investigated next. Then the various change detection techniques that are presently available to detect the geographical and geomorphological changes due to landslides are presented. Finally, the inclusion of the concept of debris flow path for reliable landslide susceptibility zonation is investigated. This chapter also discusses gaps in the theoretical capabilities between radar and optical remote sensing for landslide prediction and detection with diverse causative factors of different nature.

"Destructive outcomes of landslides in relation to human life and the overall economic system of many nations around the globe are very severe. Accurate susceptibility mapping can be key information for a large variety of users from both private and public sectors, from governmental departments and the scientific community on both local and international levels. Recently, landslide susceptibility mapping has been made possible due to the accessibility and variety of remote sensing data and thematic layers as causative factors data using GIS. Most of these landslides are referred to as significant geomorphic processes which usually form an important landscaping aspect in humid tropical mountain surroundings. Records have shown that in Asia, steep hill slopes, seasonally dry periods, excessive rainfall intensities, and unstable soils are the main causes of frequent landslides. Landslide

investigation is difficult since the landslides are generally covered by dense vegetation and the cloudy and rainy weather conditions are often undesirable for optical remote sensing. Consequently, it is necessary that new techniques and accurate data are used in landslide susceptibility mapping in the tropical environment. In recent years, radar which has the capability of data collection day and night under all weather conditions has added a new dimension to disaster management research by providing real-time and precise information. "

-Extracted from – Himan Shahabi and Mazlan Hashim, Scientific Report, 22nd April 2015-

3.1 Landslides

A frequently used definition for a landslide is "a movement of mass of rock, earth or debris down a slope" (Cruden, 1991). They may occur in many types of terrain with the right conditions of soil, rock, land use/ cover, moisture conditions and slope. Soil material can experience a reduction in shear strength due to ingress of water causing increase of pore water pressure and subsequently a mass of soil can slide down due to shear failure along a surface inside the soil mass. This movement can occur as a fall, topple, slide, spread or flow. The speed of the movement may range from the very slow to rapid, and the mass of moving material can destroy property along its path of movement and cause death to people and livestock (Kumar and Tapas, 2007).

A landslide classification had been proposed by (Varnes, 1984b), based on the types of movements and materials. The landslide classification was described by two nouns; the first describes the material and the second describes the movement. The materials can be rock, debris, earth or a mix of them. The movements can be a fall, topple, subsidence, lateral displacement or flow. Thus, a landslide can be named as a rock fall, or debris flow. Falling occurs as the soil or rock materials on a higher elevation falls down freely as fragments or splinters. Toppling occurs when the rock boulders separated from the bedrock along joint lines are subjected to toppling. They may drop

directly on to the ground, or may roll over along slopes. Subsidence is the process where a portion of the terrain subsides, or dips, from its natural topographic relief level with reference to its surrounding. Lateral displacement is a slow, gentle, circular movement of a soil mass laterally or downwards along the slip surface. The flow is the downward motion of muddy water and soil of different particle sizes and stone, which occurs mostly on escarpments with a rapid speed causing much destruction (Bandara, 2005).

Figure 3-1 is a graphical illustration of a landslide with the commonly accepted terminology describing its features and geometry. Although landslides occur mostly in mountainous regions, they can also be seen in areas of generally lower reliefs. Landslides happen as cut and fill failures in road and building excavations, river bluff failures, collapses of mine-waste piles, and a wide variety of slope failures (e.g. slides, falls, topples, and flows) in low relief terrain (USGS, 2004).

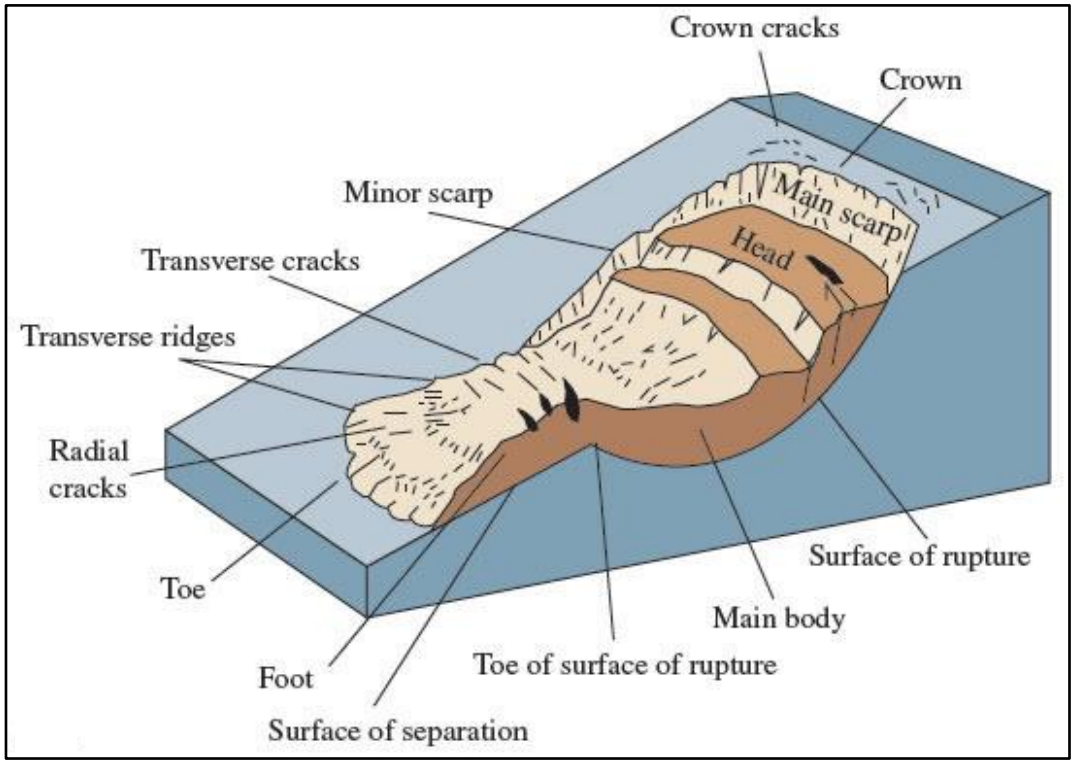

Figure 3-1 :Block Diagram of a Landslide showing commonly used nomenclature, Source : (USGS, 2004)

The upper most part of the sliding terrain, or where the landslide originated, is known as the crown, and this region is usually subjected to subsidence and cracking. The body of the landslide is the middle part of the sliding mass below the crown. This area is usually wide, and contains most of the sliding materials (USGS, 2004).

Areas vulnerable to landslides can be identified with some general indications given by nature itself. If any area is vulnerable to landslides, subsidence of the ground and tension cracks could be seen towards the upper region of the slope, while tall trees may slant towards the hill. Additionally, if cracks are observed on the wall and floors of houses located in down slopes, and if these cracks enlarge progressively, it is an indication that a landslide is active in the area. Furthermore, water springs may appear suddenly, while at the same time, the water in the wells become muddy. Small streams or water courses may also disappear suddenly before the occurrence of landslide in the area (Bandara, 2005; Weerasinghe *et al.*, 2008).

3.1.1 Landslides in the World

Landslides are significant geological hazards that can destroy human life and property, and are recognized as the third worst type of natural disasters. Mostly, people living in mountainous areas, and their properties, face critical danger from landslide disasters. Landslides are triggered due to unsustainable anthropogenic activities such as mining, road cutting, urbanization, as well as natural causes like earthquakes and rainfall (Cruden and Varnes, 1996; Klose *et al.*, 2014; Singhroy and Mattar, 2000). The recent statistics of landslide disasters per continent, from year 2000 to 2016 are summarized in Table 3-1. During this period, landslides caused around 14,000 deaths while 4 million people were affected worldwide.

Table 3-1: World Statistics for Landslides. Source: EM-DAT Database for the period 2000-2016 (OFDA/CRED, 2016)

Continent	Disaster type	Disaster sub type	No of Events	Total deaths	Total affected
Africa	Landslide	Landslide	24	738	43091
Americas	Landslide	--	2	43	379
Americas	Landslide	Landslide	56	2387	256705
Americas	Landslide	Rock fall	1	33	0
Asia	Landslide	--	2	48	330
Asia	Landslide	Avalanche	29	1305	46244
Asia	Landslide	Landslide	168	9310	3739969
Asia	Landslide	Rock fall	1	12	55
Asia	Landslide	Subsidence	1	287	2838
Europe	Landslide	Avalanche	4	164	0
Europe	Landslide	Landslide	7	40	2852
Oceania	Landslide	Landslide	7	143	11095

Abella *et al.*, (2008) are of the opinion that most of the damages to human life, as well as manmade and natural features associated with earthquakes and meteorological events, are caused by landslides. Such damages are attributed to major events, leading to considerable underestimation of the available statistical data on the landslide impact. Figure 3-2 illustrates the chain of natural events causing landslides, and their reporting.

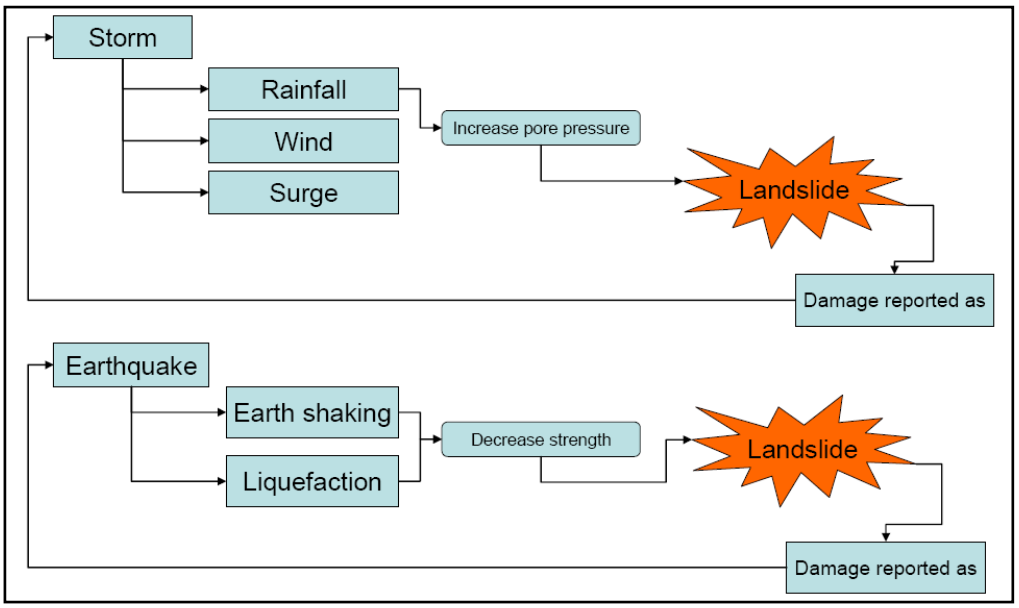

Figure 3-2: Chain of natural events causing Landslides and their reporting
Source: (Abella *et al.*, 2008)

Many recent detailed studies illustrate that the catastrophic nature of landslides in the world has mismatches with the official Emergency events data base (EM-DAT). This is due to the manner in which events were recorded, and the adopted minimum threshold for deaths and economic impacts. Consequently, statistical data about landslide impacts vary considerably among the records of different organizations. Thus, there is a basis to assume higher losses for both humans and economy by landslides than reported, due to the following reasons (Abella *et al.*, 2008):

- Most landslides are secondary phenomena, and their statistics appear under the principle disaster, as Earthquakes or Hurricanes.
- Landslides occur recurrently, and they do not cause significant level of damage per event as compared with the minimum threshold of disaster impact. Hence, most landslides are not recorded in the EM-DAT database.
- Even under similar natural conditions, landslide records from different countries have large variations.

- Landslides in mountainous areas with low risk, but high hazard vulnerability, may not be recorded.

3.1.2 Landslides in Sri Lanka

Sir Lanka is a tropical island with a mountainous central region. The combination of geology, unsafe land use practices, and heavy rainfall due to two monsoons have caused irregular landslides throughout the hill country. Landslide causal factors can be identified as preparatory and triggering. A particular factor may perform either or both functions, depending on its amount of action. However, globally rainfall and earthquakes have been identified as the two main causes.

Many studies have been more concerned about the statistical relationship for creating correlation models and producing forecasting models based on the rainfall threshold values for landslides (Jakob *et al.*, 2006; Lee *et al.*, 2017; Yilmaz, 2009; Zezere *et al.*, 2005). In Sri Lanka, almost all reported landslides are associated with the intense or prolonged rainfall. According to the statistics of NBRO, the nodal governmental agency engaged in landslide studies in Sri Lanka, the annual average number of landslide records did not exceed 50 until 2002. However, there was a sudden increase in the occurrence of landslides from 2003 to 2010 as shown in Figure 3-3.

The most recent devastating incident was recorded from Meeriyabedda area in Badulla District on 29th October 2014. Meeriyabedda Landslide in section 2.1.4 describes, in detail, the impact of the landslide with damages for human life and property (Landslide, 2014).

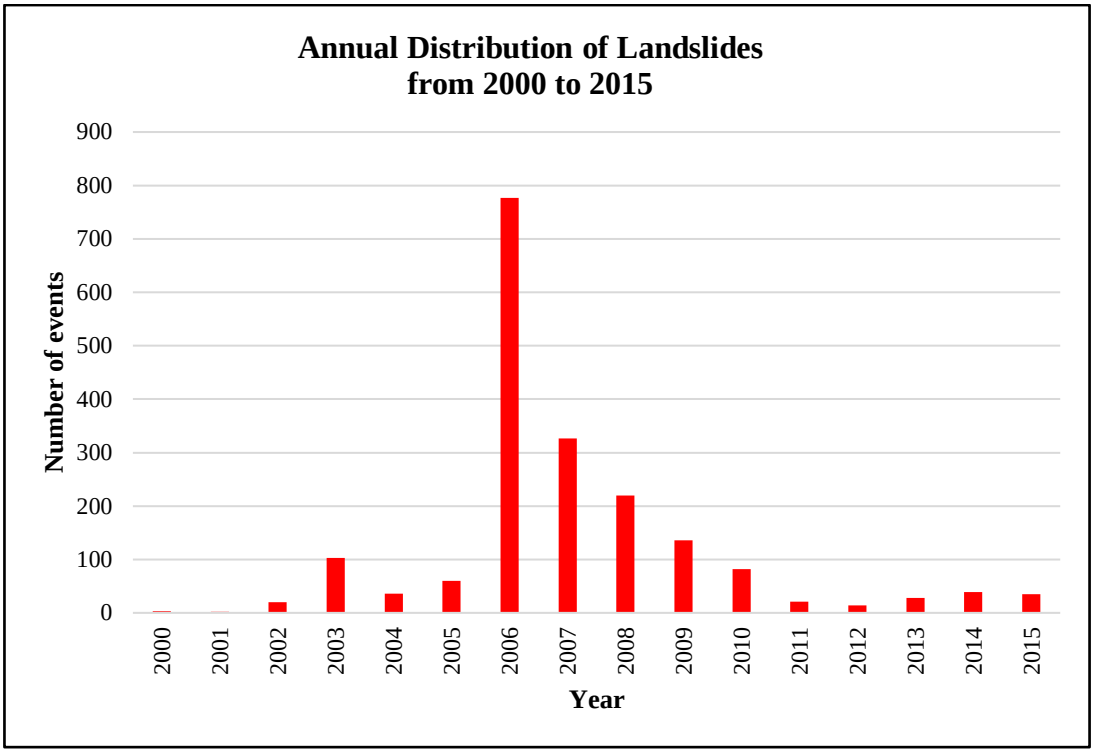

Figure 3-3 : Annual distribution of Landslides in Sri Lanka from year 2000 to 2015. (Source: www.desinventar.lk, accessed on 10th January 2016)

Sri Lanka gets a significant amount of precipitation during the months from October to march due to the northeast monsoon. The climate is tropical in Koslanda, and the rainfall is significant throughout the year, where the short dry season has little effect. Especially from October to December, due to a long spell of rains, the number of landside occurrences increases as shown in Figure 3-4.

NBRO has revealed that the landslide frequency has increased in the Badulla District with the increase of human activities, deforestation and unplanned developments in hilly areas. Hence, a detailed study about the landslide as a disaster, and its causes for disaster mitigation with improved zonation mapping could be more beneficial for fast and reliable landslide management activities in Sri Lanka.

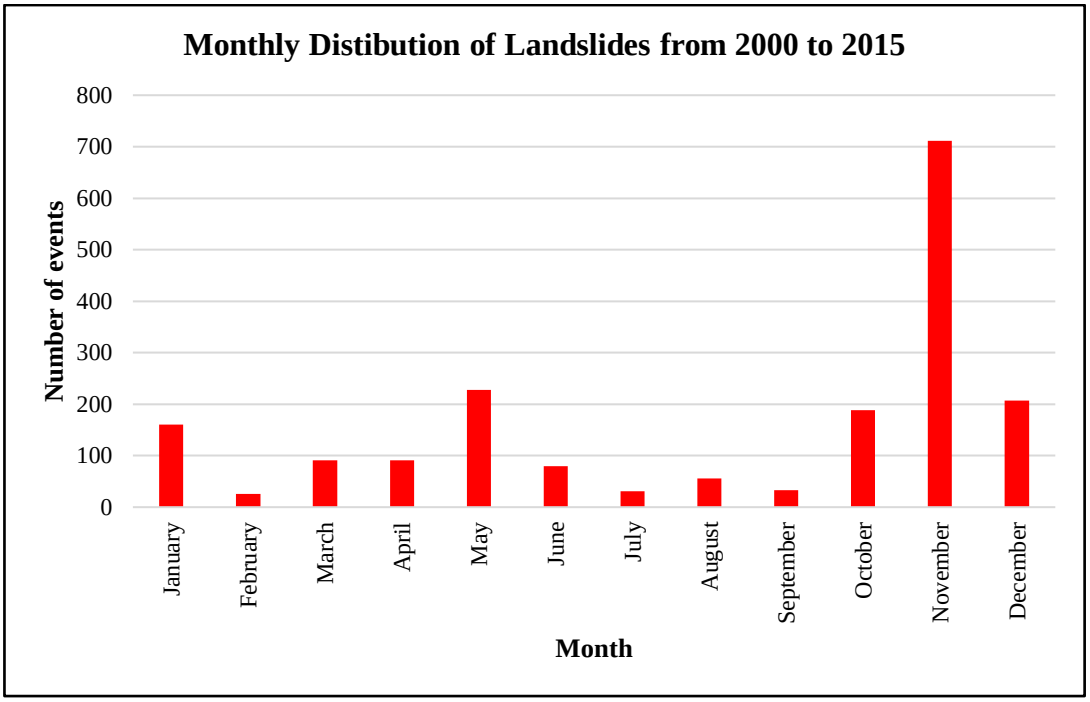

Figure 3-4 : Monthly distribution of Landslides (Source :www.desinventar.lk, accessed on 10th January 2016)

3.1.3 Present Landslide Studies in Sri Lanka

NBRO is a premier research and development institution in Sri Lanka that was established in 1984. The aim of this institution is to create a disaster-free built environment for the nation by providing better technical services, research, and development. NBRO focuses mainly on landslide disaster management, and is continuously engaged in landslide hazard identification, risk evaluation, appropriate construction and land use practices, cost effective mitigation measures, and real time landslide early warning and forecasting.

Landslide Research and Risk Management Division of NBRO has implemented a landslide hazard zonation mapping programme within the 10 landslide prone districts of Kalutara, Galle, Hambantota, Nuwara Eliya, Matale, Kandy, Kegalle, Ratnapura, Matara and Badulla. Mapping is carried out at 1:50,000 scale and at 1:10,000 scale, but 1:10,000 maps are still in progress. 1:50,000 scale maps covering the entire

districts of Kalutara, Galle, Hambantota, Nuwara Eliya, Matale, Kandy, Kegalle, Ratnapura, Matara, Badulla, Moneragala and Kurunegala are available for the use of planners, developers, decision makers, and general public. Available geographical and geomorphological data from mapping organizations are used in this programme. However, the necessity of the most recent data at a smaller scale, with sufficient accuracy, has arisen through the current technological developments. Moreover, there is a need for landslide inventories to be detailed and to be up-to-date than the present situation. Hence, there is a necessity for NBRO to refresh the routine work with the current technological enhancement in order to reach its objectives (NBRO, 2011).

3.2 Integration of Radar and Optical Remote Sensing for Landslide Studies

The use of radar and optical satellite images for remote sensing applications has a history longer than three decades. At the very beginning, the low resolution of images, and the limited processing capabilities had restricted the use of such data for a wider range of applications. However, with the recent developments of satellite images with high spatial and temporal resolutions, the situation has changed, increasing the variety of applications using remote sensing as a tool (Ioannidis and Vassilaki, 2008). In the event of natural disasters, remote sensing is a valuable source of spatial information whose utility has been proven on many occasions around the world (Joyce *et al.*, 2009).

The significant differences between the characteristics of the radar and optical data structures have not encouraged their combined use. In most cases, optical remote sensing technology has been used in obtaining landslide specific information for disaster management activities, while radar sensors have been used in detecting soil moisture and surface roughness. Yet, their combined use could provide complementary information and better results in remote sensing applications (Ioannidis and Vassilaki, 2008). In this work, the combined use of radar and optical images assumes special interest. (Singhroy *et al.*, 1998) integrated the RADARSAT (RADAR Satellite) and TM (Thematic Mapper) images with InSAR (Interferometric

SAR) techniques to characterize landslides in both high and low relief areas. Martha *et al*., (2011) recommended the use of radar data for landslide studies, as landslide studies are greatly benefitted from radar remote sensing with its rapid response system providing landslide specific information. However, the removal of geometric distortions in this instance is quite challenging.

Advantages of the combined use of radar and optical satellite data for other applications have been highlighted. For example, Bignami *et al.*, (2004) studied the combined use of ERS1 (European Remote Sensing 1), ERS2, ENVISAT-ASAR and IRS (Indian Remote Sensing)) satellite images for extracting the earthquake damages from the earthquake in Izmit in (Turkey) 1999 and the earthquake in 2003 in Bam (Iran). A similar study was conducted by Stramondo *et al.*, (2006), with the combination of ERS1, ERS2, IRS, TERRA-ASTER and ENVISAT-ASAR for earthquake damage detection. Multi-temporal ENVISAT-ASAR and Quick Bird images were integrated by Orsomando *et al.*, (2007) to extract the urban changes. In addition, instances are available in the literature of feature extraction from high-resolution InSAR data and optical images (Soergel *et al.*, 2007; Sportouche *et al.*, 2009; Stilla *et al.*, 2005; Tupin and Roux, 2003), ortho image production (Cheng, 2007), and coastal zone management (Raouf and Lichtenegger, 1997).

3.3 Landslide Investigations

Landslide studies are widely documented in literature and comprehensive reviews, and in these, landslide investigations are classified into three main groups as; (i) landslide recognition, classification, and post landslide analysis, (ii) landslide monitoring (i.e., monitoring the activity of existing landslides), and (ii) landslide susceptibility and hazard assessment, even though these classes have some fuzziness at their borders (Mantovani *et al.*, 1996; Metternicht *et al.*, 2005; Scaioni, 2013; Scaioni *et al.*, 2014).

Landslide recognition includes all the activities aimed at recognizing past or active landslide events in a specific region. All the techniques available for landslide recognition can be used for building and updating the landslide databases or inventories. The landslide inventory map is a spatial distribution of landslides represented at a predefined cartographic scale in a given area. Landslide maps prepared by collecting historical information on landslide events are called 'Geomorphical Inventory Maps' (Malamud *et al.*, 2004; Mantovani *et al.*, 1996). Landslide monitoring engages in both ground deformation measurement, and the analysis of any other changes in land use and vegetation cover with the time. Monitoring is necessary in predicting the behavior of physical processes of landslides and their movements. In addition, multi-temporal landslide inventories can be used for landslide monitoring, as they show the evolution of landslides over time.

The capabilities of remote sensing techniques with their data sources, spatial, spectral and temporal resolutions, and availabilities for landslide investigations are being studied for more than two decades Landslide susceptibility analysis investigates the probability of a potentially damaging phenomenon or areas in a given region, with the use of predisposing or causal factors related to landslide occurrences. Most landslide hazard maps are of qualitative nature, providing relative indicators for spatial probability of landslide occurrences. Remote sensing techniques represent a powerful tool for all the phases in landslide investigations. (Mantovani *et al.*, 1996; Metternicht *et al.*, 2005).

3.4 Remote Sensing for Landslide Investigations

Remote sensing techniques have greatly aided in the investigation of landslides, at both local and regional scales. Remote sensing techniques for landslide studies in terms of landslide detection, monitoring, and susceptibility analysis are exploited in several research studies. The advantages and limitations of conventional methods for landslide

investigations, and the capability of different remote sensing techniques within the context of disaster analysis, are discussed here.

3.4.1 Remote Sensing for Landslide Detection

In order to study landslides and their behaviour for the detection and classification, it is important to examine the size and contrast of landslide features and the morphological arrangements of the topography within and around the landslide. Some of the pertinent parameters might be the type of movement that has occurred, the degree of present activity of the landslide, and the depth to which movement has occurred.

Most popular conventional methods for landslide detections are geomorphological field surveys and aerial photo interpretation. Advantages and limitations of these two methods were comprehensively discussed by Guzzetti *et al.*, (2012) and Malamud *et al.*, (2004). The difficulty of using field survey arises due to multiple causes as; (i) the size of the landslide, often too large to be seen completely in the field, (ii) the viewpoint of the landslide investigator, frequently insufficient to see all parts of a landslide (e.g., the scarp, lateral edges, deposit, toe), (iii) landslide boundary is often indistinct or fuzzy and the old landslides are partially or totally covered by forest, and so on (Cardinali *et al.*, 2006; Santangelo *et al.*, 2010).

Landslide detection through the visual analysis of aerial photography is a pragmatic and uncertain technique that requires experience, training, a systematic methodology, and well-defined interpretation criteria (Antonini *et al.*, 2002; Speight, 1977). The methodologies do not contain any standards. The interpreter detects and classifies the morphological formation of the landslide based on his experience, and set of characteristics or signatures of land failures that can be identified on the aerial photographs. These include shape, size, photographic colour, tone, texture, pattern of

objects, site topography, and morphological setting. Yet, due to the large inconsistency of landslide occurrences, landslides will not be clearly and easily recognizable in the field, from the aerial photographs or the satellite images. Individual landslides, immediately after an event, are fresh and usually can be clearly identified. The boundaries between the failure areas and the unaffected terrain are usually distinct, making it relatively simple for the landslide investigators to detect the landslide areas (Fiorucci *et al.*, 2011; Santurri *et al.*, 2010).

Now a days, landslide investigations are mainly carried out by using the integration of remote sensing techniques. There are four main remote sensing data sources that are commonly used in landslide recognition as; (i) optical, (ii) thermal, (iii) microwave radar images, and (iv) laser scanning data. Optical and thermal remote sensing techniques are usually based on airborne and spaceborne platforms and rarely from ground-based platforms. Microwave sensors are mounted on airborne, spaceborne and ground-based platforms. Laser scanning is basically employed on airborne and ground-based platforms (Baroň *et al.*, 2014; Pesci *et al.*, 2011; Vohora and Donoghue, 2004). Hence, remote sensing techniques are more advantageous than field-based techniques especially in landslide investigations in smaller scale domain.

3.4.2 Remote Sensing for Landslide Monitoring

Landslide monitoring is typically conducted via the comparison of landslide conditions over time, including the extent of the landslide, speed of movement, and the change in the surface topography. On the other hand, remote sensing techniques measure quantitative changes on the surface of the slopes. This is because the slope change is one of the primary indicators that is available to understand the progress of a landslide (Farina *et al.*, 2006).

There are several remote sensing techniques that are generally used for landslide monitoring as; (i) optical images from any available platform, (ii) spaceborne and ground-based microwave data, and (iii) airborne laser scanning and terrain laser scanning data (Delacourt *et al.*, 2007). In optical remote sensing, measurement of deformation requires a series of temporal optical images, which are geometrically co-registered for accurate change detection. If 3D deformation monitoring is required, at least one pair of stereo images for one temporal observation of a particular scene is needed. In the case of a large landslide, monitoring has to be done through computation of the earth volume (Baker *et al.*, 2011; van Westen and Lulie, 2003). Microwave remote sensing, coupled with the Differential Interferometric SAR (DInSAR) technique, has been widely used for monitoring slow moving landslides in millimetre scale (Colesanti and Wasowski, 2006; Wasowski and Bovenga, 2014). Monitoring landslides through laser scanning is beneficial, given that it contains data on the complete displacement of the landslide body. However, laser scanning is limited for measuring the velocity of the landslide (Akbarimehr *et al.*, 2013).

3.4.3 Remote Sensing for Landslide Susceptibility Analysis

Landslide susceptibility is the probability of a landslide occurrence, in a given area within a specific period of time. Landslide susceptibility mapping performs the division of a particular area into homogeneous regions by using ranks or weights of influences of landslide occurrences (Varnes, 1984a). These homogeneous regions represent the different hazard zonation or classes, and for the derivation of these zones, analysis of causative and triggering factors is required. Most landslide susceptibility maps are of qualitative nature with a relative indicator of the spatial probability of landslide occurrence (van Westen *et al.*, 2008).

Many research studies investigated the role of remote sensing and GIS for landslide susceptibility analysis. It is accepted in the scientific community that remote sensing techniques do offer an additional tool for extracting the information on the causes of

landslides and their occurrences. Especially for deriving various parameters related to the landslide predisposing and triggering factors in global and regional scales, remote sensing plays a vital role (Corominas *et al.*, 2014; Muthu *et al.*, 2008). Most importantly, landslide susceptibility analysis has greatly aided the prediction of future landslide occurrences and it is important for humans who reside in areas surrounded by unstable slopes. Hence, remote sensing techniques are more valued in order to extract the landslide susceptibility regions by providing most suitable landslide predisposing factors in smaller scale.

3.5 Integration of Radar and Optical Remote Sensing for Landslide Investigations

Remote sensing data sources play a vital role in all phases of disaster management studies by providing remotely sensed data on space, where physical measurements are restricted. Especially in disaster situation, rapid investigations on very large area with prevailing bad weather conditions are complicated. Promising alternatives are the use of optical and radar images acquired from the space. Applicability of optical sensors with high resolution data sources is still limited because their acquisition depends on solar radiation. High resolution SAR are active sensors that produce their own incident radiation and thus are able to acquire images regardless of the weather and illumination conditions. The wavelength they use is also longer than the one of the optical sensors, allowing measurement of different characteristics of the imaged area. Thus, the integration of optical and radar remote sensing provide different but complementary capabilities for disaster management studies (Scaioni *et al.*, 2014).

This concept is proven with the incorporation of optical and radar satellites, or through a simultaneous existence of optical and radar sensors in the same satellite. For example, the ALOS (Advanced Land Observation Satellite) satellite consists of three remote sensing instruments as; (i) PRISM (Panchromatic Remote-sensing Instrument for Stereo Mapping) for digital elevation models, (ii) AVNIR-2 (Advanced Visible

and Near Infrared Radiometer type 2) for precise land coverage observation, and (iii) PALSAR (Phased Array type L-band Synthetic Aperture Radar) for day-and-night and all-weather land observation and enabled precise land coverage observation. The most famous example of cooperation of satellites is the joint CNES/ASI Orfeo program, where the optical component of this programme is developed by France and consists of two optical satellites with sub-meter accuracy; the radar component is developed by Italy and consists of four SAR satellites with meter accuracy. The Brazilian SAOCOM constellation, which consists of four satellites, is also planned to be synchronized with the Cosmo-Skymed constellation (Ioannidis and Vassilaki, 2008).

The way for this recently announced cooperation at sensor level has been opened with scientific studies about the integrated use of optical and SAR data. It has been shown that not only is it possible to combine optical and radar products, but it is also efficient. Nowadays, it is being examined what specific needs can be covered with a combined use of SAR and optical data (Ioannidis and Vassilaki, 2008). Hence, the present research explores the integrated use of radar and optical data sources for landslide investigations. This work is mainly focused on the landslide detections and susceptibility analysis in a smaller scale domain.

3.6 Landslide Susceptibility Analysis

Landslide susceptibility analysis is a valuable information source for disaster mitigation activities and creating awareness among the local authorities on potential unstable and hazard prone areas. Additionally, such information can be better utilized in decision making for helping the general public, planners, and engineers to reduce losses to lives and property in particular areas. The results of the landslide susceptibility assessment can help to identify the degree of susceptibility for potential landslide risk zones. Production of accurate, up-to-date and reliable landslide susceptibility maps is very important for landslide-related studies. In recent years, many qualitative and quantitative methods have been applied and evaluated in the

literature for producing landslide susceptibility maps (Bui *et al.*, 2011; Kouli *et al.*, 2010).

Landslide susceptibility analysis depends on a rather complex knowledge of slope movements, and other causal factors like land use, geology, soil moisture, etc. The reliability of landslide susceptibility analysis relies mostly on the amount and quality of available data, the working scale, and the selection of the appropriate methodology of analysis and modelling. The process of creating these landslide susceptibility maps involves several qualitative (e.g. geomorphic and map combination) or quantitative (e.g. bivariate and multivariate) approaches (Aleotti and Chowdhury, 1999; Guzzetti *et al.*, 1999; Soeters and van Westen, 1996).

3.7 Landslide Prediction Models

There are inherent limitations and uncertainties in landslide susceptibility analysis. Several methods for landslide prediction modelling have been utilized and successfully applied in the past. Such methods implemented have been of qualitative and quantitative nature. Generally, qualitative methods are based on expert opinions while the quantitative approaches, such as statistical and probabilistic approaches, depend on the past landslide experiences (Kanungo *et al.*, 2009).

3.7.1 Qualitative Methods

Qualitative methods simply make use of landslide inventories to identify areas with similar geological and geomorphologic properties that are susceptible for land failures. These methods can be divided into two groups as geomorphologic analysis, and map combination. In geomorphologic analysis, the landslide susceptibility is determined directly either in the field or by the interpretation of images trough geomorphologic analysis (Bui *et al.*, 2011; Kouli *et al.*, 2010; Rupke *et al.*, 1988). Map combination is

based on combining a number of predisposing factor maps for landslide susceptibility analysis. However, map combination analysis comprises of a semi-quantitative nature by integrating the ranking and weighting of landslide susceptibility (Ayalew *et al.*, 2004; Barredol *et al.*, 2000; Kavzoglu *et al.*, 2014; Onagh *et al.*, 2012; Saaty, 1980; Soeters and van Westen, 1996).

3.7.2 Quantitative Methods

The analyses based on the quantitative approaches depends on numerical data and statistics, expressing the relationship between instability or predisposing factors with landslides (Bui *et al.*, 2011). These methods are categorized into two groups as bivariate and multivariate statistical analysis. Within the context of this work, popular bivariate and multivariate methods are compared with respect to their performances in landslide susceptibility modelling.

(a) Bivariate Method

In bivariate analysis, each predisposing factor, obtained as a thematic map, is combined with the landslide inventory map, and weights for each factor are calculated based on landslide densities. There are several methods in using bivariate statistics for the landslide susceptibility assessment as; (i) FR (Frequency Ratio), (ii) InfoVal (Information Value method) or SI (Statistical Index), and (iii) WOE (Weight of Evidence) based on the Bayesian probability model.

(i) FR Method

Frequency Ratio calculates the probabilistic relationship between dependent (landslides) and independent variables (e.g. slope, aspect, land use, geology.). FR analysis estimates the densities of landslide occurrences within each predisposing factor, and generates the weight of index based on the landslide density in class

distributions (Akgun *et al.*, 2008; Demir *et al.*, 2013; Sarkar *et al.*, 1995; Yilmaz, 2009). Greater the weight index, higher the landslide susceptibility, and vice versa. After calculating the weight of indices for each predisposing factor, they are aggregated for generating the LSI (Landslide Susceptibility Index).

$$LSI = \sum (FR)_i (i = 1, 2, \ldots . n) \quad (1)$$

Where FR is the Frequency Ratio of each factor and n is the number of predisposing factors.

(ii) InfoVal or SI Method

Information Value Method (InfoVal or SI) is another bivariate statistical algorithm that has been employed to determine landslide susceptibility (Bui *et al.*, 2011; Cevik and Topal, 2003; Saha *et al.*, 2005; van Westen, 1993, 1997; Yalcin, 2008; Yilmaz *et al.*, 2012; Yin and Yan, 1988). This method overlay all individual predisposing factors as thematic maps with the landslide inventory map to calculate the density of the landslide detachment zones for each class of the selected factors. The density of landslide pixels represents the weight of influence of each predisposing factor.

$$W_i = Log\left(\frac{Densclass}{Densmap}\right) = Log\left(\frac{N_{pix}(S_i)/N_{pix}(N_i)}{\sum_{i=1}^{n} N_{pix}(S_i)/\sum_{i=1}^{n} N_{pix}(N_i)}\right) \quad (2)$$

Where, W_i is the weight given to the parameter class, $Densclass$ is the landslide density within the parameter class and $Densmap$ is the landslide density within the entire map. $Npix(Si)$ is the number of landslide pixels within parameter class i, and $Npix(Ni)$ is the total number of pixels in the same parameter class. It means that, if the parameter class contains no landslide occurrence, it will have no correlation with the landslide inventory map (Bui *et al.*, 2011; Conforti *et al.*, 2011; Kavzoglu *et al.*, 2015).

(iii) WOE Method

Bayesian probability model, using the WOE approach, has been applied for many studies in landslide susceptibility assessment (Armas, 2012; Nandi and Shakoor, 2009; Regmi *et al.*, 2010; Schicker and Moon, 2012; van Westen *et al.*, 2003). This method is applied when ample data are available to estimate the relative importance by statistical means. The basic theory behind the WOE method is the concept of prior and posterior probability. The research studies mentioned before have described the applicability of this method for landslide prediction modelling. A pair of weights, W^+(positive weights) and W^-(negative weights), is calculated for the predisposing factors using the following equations;

$$W^+ = \ln\left[\frac{\frac{Landslide\ area\ in\ the\ perticular\ class}{Total\ Landslide\ area}}{\frac{Stable\ area\ in\ the\ sameclass}{Total\ stable\ area}}\right] = \ln\left[\frac{\frac{w_1}{w_1+w_2}}{\frac{w_3}{w_3+w_4}}\right] \quad (3)$$

$$W^- = \ln\left[\frac{\frac{w_2}{w_1+w_2}}{\frac{w_4}{w_3+w_4}}\right] \quad (4)$$

Where, $w_1$is the number of landslide pixels present in the selected factor class, w_2 is the number of landslide pixels not present in the same factor class, w_3 is the number of stable pixels within the same factor class and w_4 is the number of stable pixels not present in the same factor class. The positive weights (W^+) represent the positive correlation between the presence of the landslide in each predisposing factor, while the negative weights (W^-) indicate the absence of the landslide probability in same predisposing factor class (Dahal *et al.*, 2008; Kavzoglu *et al.*, 2015).

(b) Multivariate Method

Multivariate models integrate all the independent predisposing factors and historical landslides occurred in a particular area for landslide susceptibility analysis. However, the multivariate model, unlike the bivariate model, evaluates the relative contribution of each factor by assigning more emphasis on the variables known to contribute to landslide occurrence (Kavzoglu *et al.*, 2015; Nandi and Shakoor, 2009). Several methods based on multivariate theory are suggested and applied by the scientific community for landslide susceptibility assessment. Here, the most popular multivariate methods, namely (i) AHP (Analytical Hierarchy Process), (ii) SVM (Support Vector Machine), and (iii) DT (Decision Tree) analysis are discussed with their robustness for the multivariate analysis.

(i) AHP

AHP (Analytic Hierarchy Process) is a semi quantitative method, and a flexible tool for analysing complicated problems on site selection, suitability analysis, urban and regional planning, and landslide susceptibility analysis. AHP is a multi-criteria decision making and multi-objective approach, allowing expert opinions to derive the scale of preferences of each predisposing factor. All the factors are arranged in a hierarchical order, and numerical values are assigned based on the relative importance of each factor. Each factor is then synthesized based on the assigned proprieties, and the reciprocal pair-wise comparison matrix is generated for utilization in AHP (Park *et al.*, 2013; Sar *et al.*, 2016; Shahabi *et al.*, 2013; Shahabi and Hashim, 2015). In the preparation of pair-wise comparison matrix, each factor is rated against all other factors by assigning relative dominant values between 1 and 9 [Table 3-2].

Table 3-2 : Fundamental scale of absolute number between two parameters in AHP (Saaty, 2000)

Intensity of Importance	Degree of preference	Explanation
1	Equally	Contribution to objective is equal
3	Moderately	Attribute is slightly favoured over another
5	Strongly	Attribute is strongly favoured over another
7	Very Strongly	Attribute is very strongly favoured over another
9	Extremely	Favouring one attribute is the highest degree possible for an affirmation
2,4,6,8	Intermediate values	When compromise is needed
Reciprocals	Opposites	Used for inverse comparison

In pair-wise comparison matrix, when the factor on vertical axis is more important than the factors in the horizontal axis, relative values vary between 3 and 9 and conversely, the values vary between the reciprocals as 1/3 and 1/9. Finally, all the values in pair-wise comparison matrix are normalized, in order to obtain the relative weights for each predisposing factor. Weights calculated for each factor from AHP technique are incorporated for performing the weighted overlay for generating the final landslide susceptibility analysis. For the AHP model, final results include the weights of the derived factors and a calculated CR (Consistency Ratio). The CR can be described as an index of inconsistency, and is generally used to indicate that the matrix judgments were randomly generated (Saaty, 1980).

$$CR = \left(\frac{CI}{RI}\right) \quad (5)$$

where, RI is the average of the resulting consistency index depending on the order of the matrix given by Saaty, (1980) and CI is the Consistency Index that can be expressed as;

$$CI = \left(\frac{Y_{max} - n}{n-1}\right) \quad (6)$$

where, Y_{max} is the largest or principle eigen value of the matrix, and can be easily calculated from the matrix of order n. Since the CR is a ratio between the matrix's inconsistency index and random index, it ranges 0 to 1. A CR of 0.1 and less is a reasonable level of consistency, and above 0.1 requires revision of the pair-wise comparison matrix due to an inconsistent rating of some factors.

(ii) SVM

SVM (Support Vector Machine) is a kernel based, advanced learning algorithm that can be used for complex classification and regression analysis. The basic idea behind the SVM for binary classification is to find an optimal separation by considering the nearest training data. SVM plots the original input space into a higher dimensional feature space and consequently, in the feature space, the optimal hyper plane is determined by maximising the margins of class boundaries. The training data that are closest to the optimal hyper plane are support vectors. Once the decision space is confirmed, it can be used for new data for the same classification (Kavzoglu *et al.*, 2014; Peng *et al.*, 2014; Pourghasemi *et al.*, 2013).

There are two main concepts inspiring the SVM classification. One is establishing an optimum linear separating hyper plane that separates data patterns, while the second is the use of kernel functions for converting the original non-linear data patterns into a linearly separable higher dimensional feature space [Figure 3-5] (Ballabio and Sterlacchini, 2012; Kavzoglu *et al.*, 2015; Lee *et al.*, 2017; Pradhan, 2013).

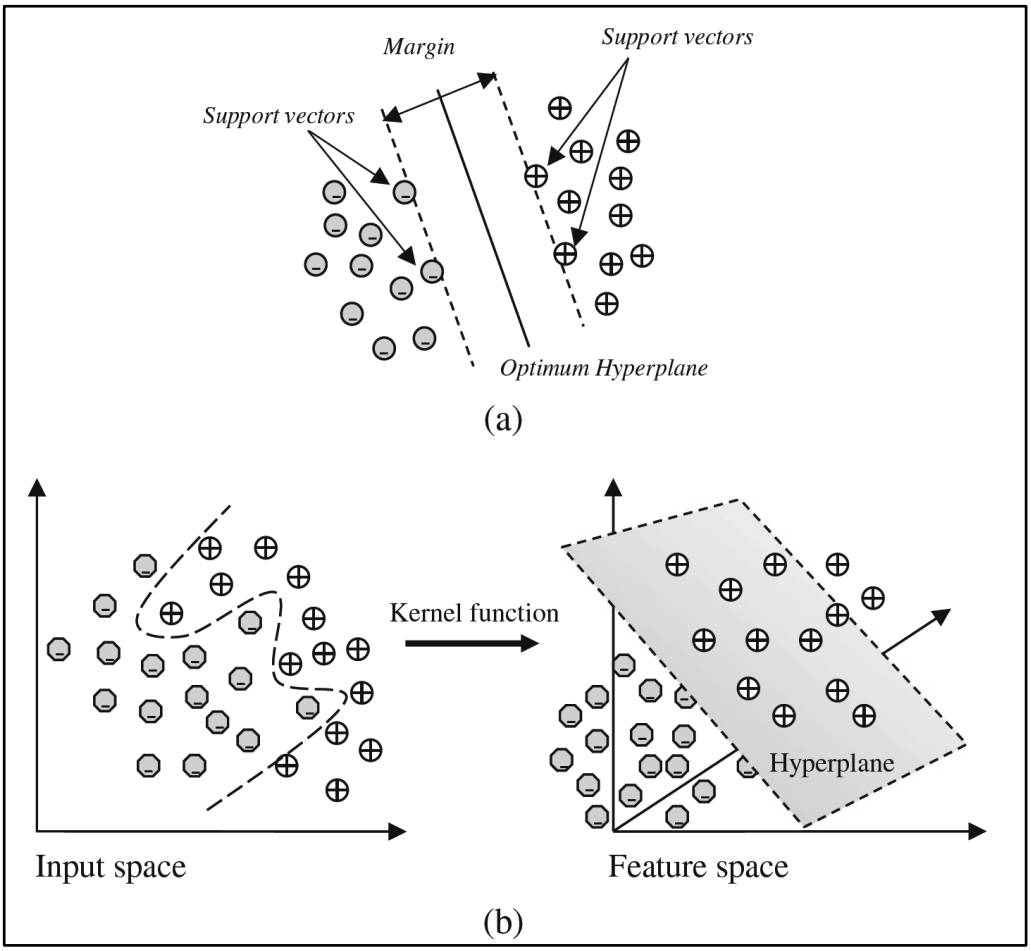

Figure 3-5 : Hyper-planes for (a) linearly separable data and (b) non-linear separable data (Kavzoglu *et al.*, 2014).

(iii) Decision Tree

A DT (Decision Tree) is a supervised learning method composed of decision rules that performs the recurrent splits of independent variables into homogeneous zones (Breiman *et al.*, 1984; Bui *et al.*, 2012; Niuniu and Yuxun, 2010). The structure of DT is similar to a flow chart tree structure, comprising of root nodes containing all the data, and a set of internal nodes with terminal nodes. Each node of the tree structure generates binary decisions based on the training data for either one class or for some other class [Figure 3-6]. DT is involved in the binary repetitive partitioning of whole data into a set of homogeneous subsets on the basis of test data (Cho and Kurup, 2011; Kavzoglu *et al.*, 2015; Myles *et al.*, 2004; Pradhan, 2013).

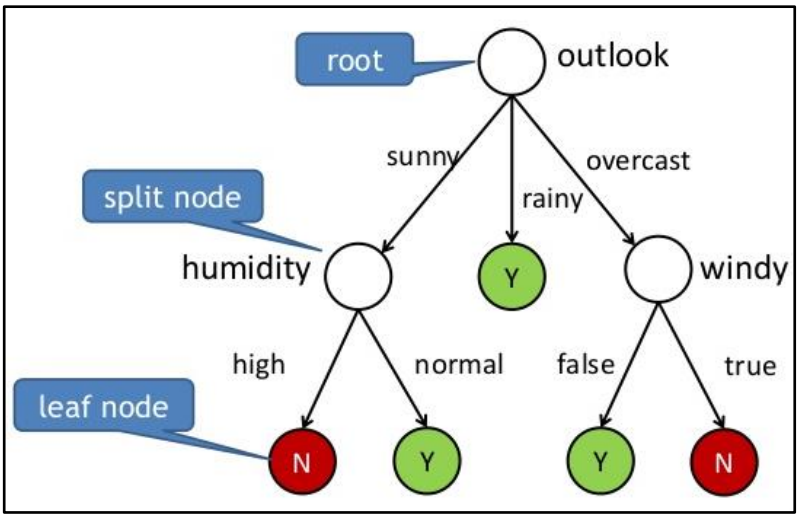

Figure 3-6 : Distributed decision tree learning for mining big data streams, (Murdopo, 2013)

Many research studies examined the performance of bivariate and multivariate techniques for landslide prediction analysis (Bui *et al.*, 2011; Kavzoglu *et al.*, 2015; Park *et al.*, 2013; Pradhan, 2013; Saha *et al.*, 2005; Sar *et al.*, 2016; Shahabi *et al.*, 2013; Yalcin, 2008; Yilmaz *et al.*, 2012). When considering the results from the above studies, it was observed that the accuracy level reached from multivariate methods, when compared with the bivariate methods, was statistically significant. However, the accuracy level is dependant not only on the technique applied, but also with some other factors such as the quality of data, and distribution of training and validation samples.

The main drawback of the statistical methods is their dependence on the data structure. Statistical methods require assumptions that the statistical properties of samples are in a normal distribution. In addition, the size of the training data set is also very important if statistical estimates are to be reasonable. In the case of a limited training set size, it is difficult to define decision boundaries in the feature space. Therefore, the effectiveness of statistical methods depends on the size of the dataset, and its distribution.

3.8 Predisposal Factors for Landslide Susceptibility Analysis

It is generally believed that landslides may occur as consequences of complex predisposing and triggering factors. Topographical and geological factors, together with local climatic conditions, lead to landslide occurrences. The selection of these factors, and preparation of corresponding thematic data layers, are vital for models used in landslide susceptibility analysis (Lee *et al.*, 2017; Sarkar and Kanungo, 2004). There are no universal guidelines regarding the selection of predisposing factors in landslide susceptibility analysis. Some parameters may be important factors for landslide occurrences in a certain area but not for another one. van Westen *et al.*, (2003) stated that every study area has its own particular set of predisposal factors, which condition landslides.

Determining of appropriate causal factors is a difficult task, and no specific rule exists to define how many factors are sufficient for a specific landslide susceptibility analysis. Hence, the selections of predisposing factors are dependent on the nature of the study area, opinions of the experts, and the availability of data for generating the appropriate spatial and thematic information (Kavzoglu *et al.*, 2015; Shahabi and Hashim, 2015). The instability factors responsible for landslide occurrences include; lithology, geological structure, slope steepness, seismicity, morphology, climate, land use, stream evolution, ground water conditions, vegetation cover, and human activities. Among these basic factors, the predisposing factors that have been selected in most popular research studies are tabulated in Table 3-3.

The effect of landslide predisposing factors for the accuracy of landslide susceptibility analysis has been investigated by several researches. (Costanzo *et al.*, 2012) analysed the relationship between prior ranking of predisposing factors, and their predictive performances. Results indicate that the slope angle, surface roughness, land use, and TWI are the major causative factors for that landslide prediction analysis.

Table 3-3 : Number of causative factors used for Landslide susceptibility analysis in recent literature

Study and Year	No. of Predisposal Factors	Predisposal Factors
(Conforti *et al.*, 2011)	7	Lithology, Land use, Slope, Aspect, Planar curvature, Distance to fault, Distance to stream
(Pradhan, 2013)	8	Altitude, Slope, Soil type, Planar curvature, Distance from drainage, Distance from road, TWI, NDVI
(Pradhan *et al.*, 2013)	14	Slope, Aspect, Altitude, Planar curvature, Profile curvature, Tangential curvature, Surface area ratio (SAR), Lithology, Land use, Distance from faults, Distance from rivers, Distance from roads, Topographic wetness index (TWI) and Stream power index (SPI)
(Chalkias *et al.*, 2014)	7	Elevation, Slope, Aspect, Lithology, Land cover, Mean Annual Precipitation and Peak Ground Acceleration
(Shahabi and Hashim, 2015)	10	Slope, Aspect, Soil, Lithology, NDVI, Land cover, Distance to road, Distance to drainage, Precipitation, Distance to fault
(Kavzoglu *et al.*, 2015)	16	Slope, Lithology, Land cover/use, Aspect, Soil depth, NDVI, Elevation, TWI, Distance to lineaments, Slope length, Distance to road, Distance to drainage, Planar curvature, Profile curvature, Topographic Position Index, Relative relief
(Lee *et al.*, 2017)	17	Slope, Aspect, Planar curvature, SPI, TWI, Geology, Distance from fault, Soil depth, Soil drainage, Soil material, Soil texture, Soil topography, Timber type, Timber diameter, Timber age, Timber density, Land use.

Hasekiogullari and Ercanoglu, (2012), examined the effect of causative factors for landslide susceptibility analysis using AHP techniques. For the modelling process, 7 combinations of 9 parameters were tested, starting from 3 factors and by adding each new factor till all the factors were included. The best performance was obtained when all the factors were considered. In the study of (Suzen and Kaya, 2012), they found that 10 causative factors out of 20 of all contributing parameters provided the best performance for landslide susceptibility analysis. (Pradhan, 2013) explored 5 combinations of 8 causative factors (commencing with 4 factors while adding a new factor till all factors were included) by using decision tree and support vector machine for landslide susceptibility analysis, and determined the most suitable factors as elevation, slope, planar curvature, distance from drainage, distance from road, soil type and NDVI (Normalized Difference Vegetation Index).

3.9 Evaluation of Landslide Prediction Models

The validation is of utmost importance in any prediction analysis. Once the landslide prediction analyses are performed, the overall performance of the prediction model can be investigated by using the ROC (Receiver Operating Characteristics) curve. In statistics, ROC is a graphical plot that illustrates the performance of classification, and this analysis is considered as a powerful method for the validation of landslide susceptibility analysis.

There are two types of plots in ROC curve, the success rate and prediction rate curves, and these have frequently been used in landslide susceptibility analysis (Chung and Fabbri, 2003). The success rate assesses how many landslides are successfully captured by the susceptibility map, and the prediction rate calculates the percentage of the independent landslides captured with the susceptibility map of the validation dataset (Neuhäuser *et al.*, 2012). Hence, the prediction performances and validation performances can be calculated with the use of training and validation samples separately [Figure 3-7].

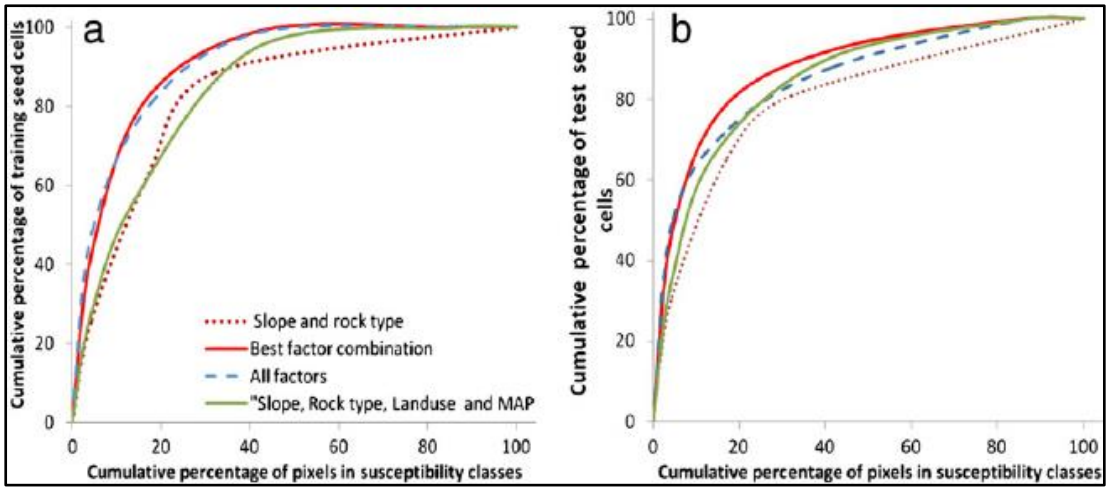

Figure 3-7: Prediction performance of multiple factor combinations. (a). success rate curve from the training data set; (b). prediction rate curve from the validation data set (Che *et al.*, 2012).

In practice, the AUC (Area Under Curve) is a good indicator and performs very well for measuring the prediction performance analysis [Figure 3-8]. The AUC of the success rate and prediction rate curves measure the prediction performances and validation performances respectively (Chalkias *et al.*, 2014; Fawcett, 2006; Frattini *et al.*, 2010; Jaafari *et al.*, 2014; Kavzoglu *et al.*, 2014; Naghibi *et al.*, 2015; Nandi and Shakoor, 2006; Pourghasemi *et al.*, 2012; Youssef *et al.*, 2015).

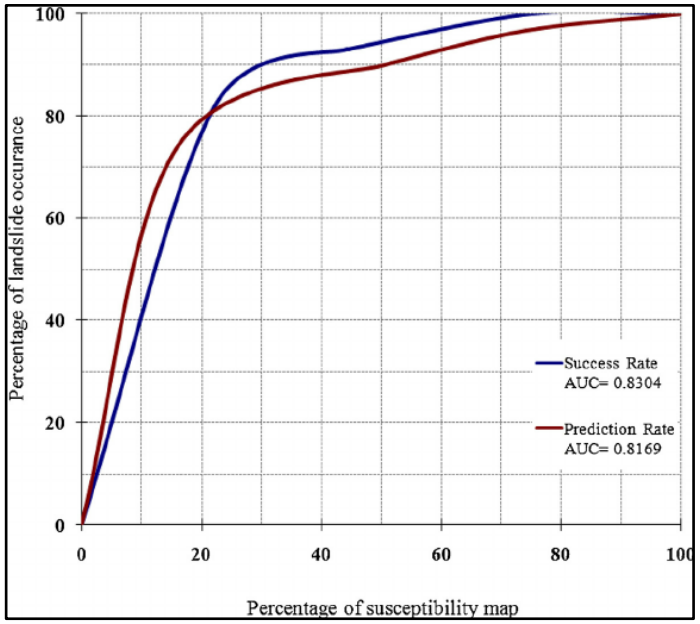

Figure 3-8 : Success rate and prediction rate curves for the landslide susceptibility map (Jaafari *et al.*, 2015)

The AUC value ranges from 0.5 to 1.0 and values closer to 1.0 are considered as a perfect fit, whereas a value closer to 0.5 indicates a random fit. The higher the AUC, i.e. the steeper the curve's slope, the better is the prediction (Kamp *et al.*, 2008). Here, the AUC of the success rate and prediction rate is 0.8304 and 0.8169 respectively. Hence, it can be concluded that the predicted susceptibility levels are in good agreement with past landslide occurrences, and therefore that the map is trustworthy for susceptibility analysis.

3.10 Landslide Detections

Landslide detection is an important prerequisite in pre and post disaster analysis. In the past, landslide detection was done through time consuming, cost-intensive, field surveys and visual orthophoto interpretation. Recently, with the advancement of satellite remote sensing technology in spatial, spectral and temporal domain, they offer new opportunities for fast, reliable, and accurate landslide identification at smaller scales. Especially SAR data proves to be useful in the aftermath of an event, as radar sensors are mostly independent of illumination and weather conditions, and therefore the data is more likely to be available. However, more research is needed to make the best integration of optical and radar data for landslide detection in different environments.

With the increase of earth observation satellites in the constellation, revisit time has been reduced significantly for detecting landslides by visual interpretation. However, the accuracy of landslide detection from visual interpretation using remote sensing images depend on the contrast of images, size of landslide, interpretation method, and professional experience of the interpreter (van Westen *et al.*, 2003). Thus, many researchers investigated the automated processes using spectral information for extracting the spectral signature of the landslide. Change detection is the most commonly used automated process for the detection of landslides.

3.11 Change Detection Techniques for Landslide Detection

Change detection is defined as the process of identifying differences in the state or nature of an object or phenomenon by observing it at different times. The main objective of change detection in remote sensing is in identifying the geographical location, and recognizing and quantifying the type of changes due to some reasons (Devi and Jiji, 2015). Change detection techniques are mainly interrelated with remote sensing data as any change to a geographical phenomenon modifies the spectral behaviour. The factors that are considered in change detection analysis using remote sensing data includes spatial, spectral, thematic and temporal constraints, atmospheric conditions, radiometric resolution and soil moisture conditions (Im and Jensen, 2005).

There are some steps to be followed before using remote sensing data for change detection analysis;

(i) Use of data from the same sensor, radiometric and spatial resolutions, and frequent acquisitions to remove the effects of seasons and sun angle difference (Song and Woodcock, 2003).

(ii) Precise geometric registration between multi-temporal images to avoid false changes being detected due to image displacement (Devi and Jiji, 2015).

(iii) Performance of radiometric corrections to rectify errors caused by the variation in sensor characteristics, atmospheric condition, solar angle, and sensor view angle (Chen *et al.*, 2005).

(iv) Data collection for suitable time period as the data collected ahead of time fail to cover slower change process, whereas data collected in a delayed manner leads to excessive omission errors, which significantly impact the completeness of change detection (Lunetta *et al.*, 2004).

(v) Selection of proper change detection techniques in order to extract the required change (Devi and Jiji, 2015).

Change detection techniques can be categorized as pixel based and object based, grounded on the unit of image analysis. A brief summary of some selected change detection techniques related to the pixels-based analyses are as follows.

(a) Image Differencing

In this technique, two images from the same area from two different times have to be used. Image differencing is performed by subtracting the DN (Digital Number) value of one band from the DN value of the same pixel for the same band of another image. The difference image represents the intensity difference of two images. Mathematically, image differencing is given by;

$$IMG_d = IMG_{t_1} - IMG_{t_2} \quad (7)$$

where, IMG_{t_1} is the image at time t_1 and IMG_{t_2} is the image at time, t_2. IMG_d is the difference image that extracts the changes of the images from time t_1 to time t_2. As changes seem to occur in both directions, the analyst has to decide the order of the image to be subtracted (Singh, 1989).

(b) Image Rationing

Image rationing is similar to the image differencing as images are compared pixel wise. Change results are expressed as a ratio between two co-registered images and unchanged areas would theoretically have 1 as its value.

$$IMG_r = \frac{IMG_{t_1}}{IMG_{t_2}} \quad (8)$$

where, IMG_{t_1} is the image at time t_1 and IMG_{t_2} is the image at time t_2. IMG_r is the ratio image that extracts the changes of the images from time t_1 to time t_2 (Rignot and van Zyl, 1993).

(c) Normalized Difference Vegetation Index (NDVI)

NDVI investigates the data that is related to the green biomass of vegetation. NDVI is calculated by using spectral response from near-infrared and red bands. The main reason for selecting these bands is the high reflectivity of near-infrared band, and the low reflectivity of red band from green vegetation. Two types of pixel-based approaches are integrated in NDVI calculation as image differencing and image rationing.

$$NDVI = \frac{NIR - R}{NIR + R} \tag{9}$$

Where, NIR is the near-infrared band and R is the Red band of the image (Lu *et al.*, 2004).

(d) Principle Component Analysis (PCA)

PCA performs the data redundancy by transforming multivariate data in to a new set of components by assuming that components are not highly correlated. Covariance or correlation matrix is used to arrange the data to uncorrelated components. The first principle component consists of the highest variation of data. The next largest amount of variation consists of the succeeding principal component. Once the appropriate components are selected, change detection techniques, such as image rationing or image differencing, can be applied in order to extract the change (Lillesand *et al.*, 2008).

(e) Change Vector Analysis (CVA)

CVA is a technique that considers multiple image bands simultaneously to detect the change. CVA is not only a change detection method, but also performs the classification of changes. Each pixel value is considered as a vector, and change vectors are computed by subtracting the vectors for all pixels of different images on different dates. The type of change can be investigated from the direction of the change

vector, and the length corresponds to the magnitude of the change. This method is most suitable when the change of interest, and their spectral appearance, is not well recognised. The main limitation of using this method is that it requires the acquisition of remotely sensed data from perfect image registration and radiometric normalization (Ilsever and Unsalan, 2012). Change vector analysis is similar to a multi band version of the image differencing. The direction of the change gives additional information about the type of the change. This information is more valuable than the amount of change as most applications expect some specific type of the change (Chen *et al.*, 2003).

(f) Post Classification

In the post-classification of change-detection technique, each image is pre-processed and classified separately using supervised or unsupervised classification techniques. Then each classification is compared to generate the change matrix that can be used to measure the changes. In order to compare similar classes, the classifications of all images have to be identical. This method provides a complete matrix of change by reducing the impact of atmospheric, sensor and environmental effects. The main limitation of this technique is that the accuracy of the final image is entirely dependent on the classification accuracy of individual image. Thus, accurate, complete, and high-quality training datasets are inevitable to produce an accurate classification. However, acquiring such training datasets, especially for historical image classification, is both a time-consuming and difficult task (Lu *et al.*, 2004).

Developing change detection techniques and tools in remote sensing is an ever-growing research schema. When considering the vast range of applications in change detection analysis, it is a complicated process with no single optimal approach applicable for all the cases. Moreover, with the technological advancements over the last few decades, most applications are allowed to exceed the traditional limits, and attempt new ventures for more robust change detection techniques (Vieira *et al.*, 2012).

3.12 Post Disaster effect from Debris Flow

In the field of natural disasters, landslides receive little attention as they often seem so unexpected. A landslide is simply the sudden movement of terrestrial material with any combination of soil, rocks, mud and water. These materials move slowly and cause damage over a period of time, or move rapidly, destroying property and taking lives suddenly (Canuti *et al.*, 2004; Guinau *et al.*, 2007; Rosso *et al.*, 2006; Schuster, 1996). The danger from debris flow has been recognized by Japanese residents in the mountainous regions, and have used evocative names to debris flows to warn future generations of their danger as "Ja-nuke" (the runoff of the king snake), "yama-tsunami" (mountain tsunami), "yama-shio" (mountain tide) and "phantasmal disaster" (characteristics and mechanisms of debris flows remained poorly understood) (Takahashi, 2007, 2009).

The term 'susceptibility' detects the location of potential landslide failures in a given region based on a set of predisposing factors. Susceptibility analysis investigates the potential of landslides occurring under the same conditioning factors as landslides in the past. Even though these analyses provide information on potentially unstable slopes, they do not offer the information about the debris flow path of the landslide from the failed locations. With the past experiences of damages from landslides, it is obvious that most damages occurred due the debris flow than within the mass failure region. Hence, integration of debris flow path for landslide susceptibility analysis are of utmost importance.

Debris flow investigations within the scientific community started from 1950s with qualitative analysis of debris flows. According to the literature in Japan from (Takahashi, 2009), the debris flow was defined as the gravitational motion of a mixture of sediment and water as a porridge where the volume is much larger than the volume of water. The debris flow behaviour is controlled by several parameters as topography, soil type, land use, debris volume, and so on. With the difficulty of characterising these

parameters for future landslide debris flow analysis, it is hard to determine the runout and the distance reached. However, this situation can be simplified by synthesising that under intense rainfall, debris flow tend to follow the steepest path and merge with drainage network (Parise, 2002).

The open source TauDEM software developed by (Tarboton, 1997), which can be executed as an ArcGIS extension, is used to determine the area prone for landslide debris flows. TauDEM consists of a set of tools to investigate hydrologic processes by using topographical information derived from DEM. Three simple tools can be employed as Pit remove, D-∞flow direction and D-∞ avalanche runout, in order to extract the debris flow path from DEM.

3.13 Chapter Summary

The exploration of previous landslide studies was performed through three basic categories as landslide recognition/classification, landslide monitoring and landslide susceptibility analysis. Landslide recognition identifies the damaged areas from past or active landslides that occurred in a particular area. Landslide monitoring includes the measurements of earth deformation and land use or cover changes along the time. The probability or the potential of land mass failures are determined through the analysis of landslide predisposal factors in landslide susceptibility analysis. Especially in a disaster situation with prevailing bad weather conditions, rapid investigations are really complicated at smaller scale. The promising alternative is the integrated use of radar and optical satellite images for landslide investigations as the radar has the capability of all-weather day and night observation providing complementary information with optical images for the smaller scale landslide investigations. Hence, this research is based on the integration of radar and optical remote sensing for landslide prediction and detection analysis.

Landslide susceptibility analysis involves several qualitative and quantitative methods. Qualitative methods are based on the expert opinions while quantitative methods are dependent on the past landslide experiences. Quantitative methods are bivariate and multivariate and this chapter discussed some popular bivariate and multivariate approaches with their theoretical formations. As the validation is most valuable part in any prediction analysis, this chapter described the use of AUC of ROC curves using separate training and validation samples.

Earlier, landslide detection was based on time consuming, cost-intensive field surveys and visual interpretation of orthophoto generated from aerial photographs. Recently, with the advancement of satellite remote sensing technology in spatial, spectral and temporal domain, new opportunities are emerging for fast, reliable and accurate landslide identification at smaller scales. This chapter focused on several change detection techniques that are most suitable for extracting the landslide signature from satellite imageries.

Landslide susceptibility analysis detects the locations of potential landslide failures in a given area based on a set of conditioning factors. However, these analyses do not provide the information about debris flow path of the landslide from the failed locations. According to the past understandings of damages from landslides, it is noticeable that most damages occurred due the debris flow than the mass failure region. Hence, this chapter finally describes the importance of applying the debris flow path for landslide susceptibility analysis.

CHAPTER 4 : PERFORMANCE ASSESSMENT OF RADAR AND OPTICAL REMOTE SENSING FOR LANDSLIDE SUSCEPTIBILITY ANALYSIS

Through the most recent technological developments of satellite remote sensing in the areas of temporal, spectral, spatial, and global coverage, the availability of such images either at a low cost or free of charge, and the advancement of tools developed in image analysis techniques and GIS for spatial data analysis, a large variety of applications using remote sensing and GIS as tools are promising (Reis *et al.*, 2012). Hence, the goal of this chapter is to generate landslide prediction models using bivariate and multivariate statistical analysis on the causative factors as thematic maps that are produced in GIS and remote sensing environment, with and without radar induced factors. Fifteen topographical, hydrological, geological, land cover, and soil factors are considered in order to determine the landslide susceptibility regions, including three radar induced factors. The prediction levels of susceptibility regions are distinguished and categorized in to four susceptibility classes as very low, low, moderate and high. Currently, the statistical methods are more applicable for landslide prediction analysis than the qualitative approaches. Hence, the Information Value method as a bivariate statistical analysis and MCDA based on the AHP as a multivariate statistical analysis, are performed.

4.1 Study Area

Koslanda is a remote, hilly, area with geographically difficult access, facing various harsh weather conditions. Badulla is the capital of Uva province and is approximately 28 km away from Koslanda. The population is around 5,000 peoples and most of them are working in tea estates. The selected study area has an extent of 19 km^2 within the Koslanda area [Figure 4-1].

A most devastating landslide occurred in Sri Lanka in year 2014 in Koslanda. Earlier in 1997, there was a landslide in Naketiya. As a consequence, many studies on landslide research have focused on Koslanda area as the study area. Even though the study area is most significant in tourism with natural beauty, and rich cultural heritage, due to its topographical and geomorphological formation, Koslanda is better known for its vulnerability to natural disasters such as landslides, rock falls, rock slides, and cutting failures, particularly during the heavy rains (SAARC, 2010).

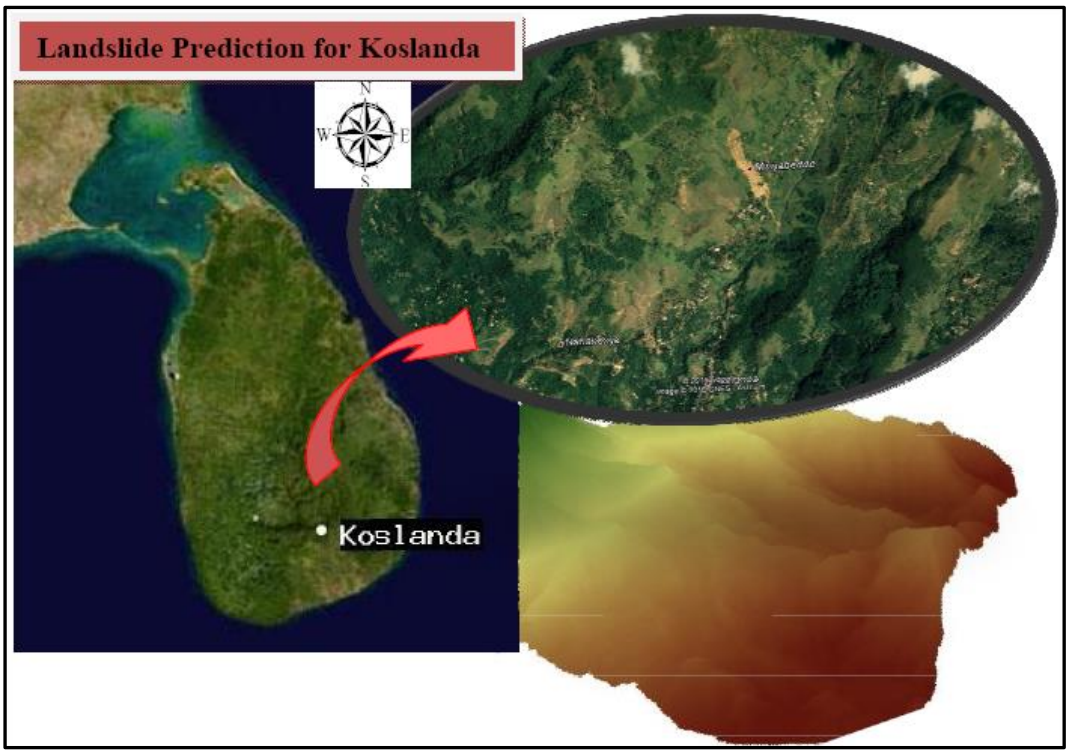

Figure 4-1 : Topographical formation of the selected Koslanda area for Landslide susceptibility analysis

4.2 Data and Methodology

The most important phases in landslide prediction analyses are the collection of data from different sources and the construction of a spatial database for these on a common platform (Lan *et al.*, 2004). The preliminary data acquisition, processing stages for the spatial database, and the methodology followed throughout this work are discussed in the sub sections.

4.2.1 Data

The data utilized for the landslide prediction analysis include the topographical, hydrological, geological, soil and land cover factors. All factors are derived from optical images (Landsat-8, Sentinel-2), radar images (Sentinel-1, TerraSAR-X), DEM derived from aerial triangulation and other available data sources (geology, rainfall). Stereo aerial photographs from 1993 are used to generate the DEM using aerial triangulation. The Imagine photogrammetry tool from ERDAS Imagine 2014 (Earth Resource Data Analysis System) software is used for DEM generation. Camera calibration, interior orientation, and exterior orientation by using 25 GCPs, are performed in order to generate the DEM from aerial triangulation. An inventory map of landslides for the study area was constructed by integrating the interpreted multi-temporal aerial photographs, satellite images, and some temporal images from the Google Earth. Verifications are carried out through field investigations.

4.2.2 Methodology

Landslide inventory map, and the topographical, hydrological, geological, soil and land cover factors are processed in order to gain the landslide susceptible regions from bivariate and multivariate statistical analysis. The general flow chart shown in Figure 18 gives a quick overview into the overall set up of this research to achieve the expected outcomes. Topographical factors, elevation, slope, aspect, planar curvature, and profile curvature are derived from the elevation information using the DEM. Furthermore, the DEM is used to calculate the Topographical Wetness Index (TWI), as a hydrological factor. The NDVI and the thermal information derived from Landsat-8 image are used in conjunction for extracting the surface soil moisture. The lineament density and the recent land cover classes were obtained from the supervised classification of Sentinel-2 image (10 m resolution) of 10th October 2016.

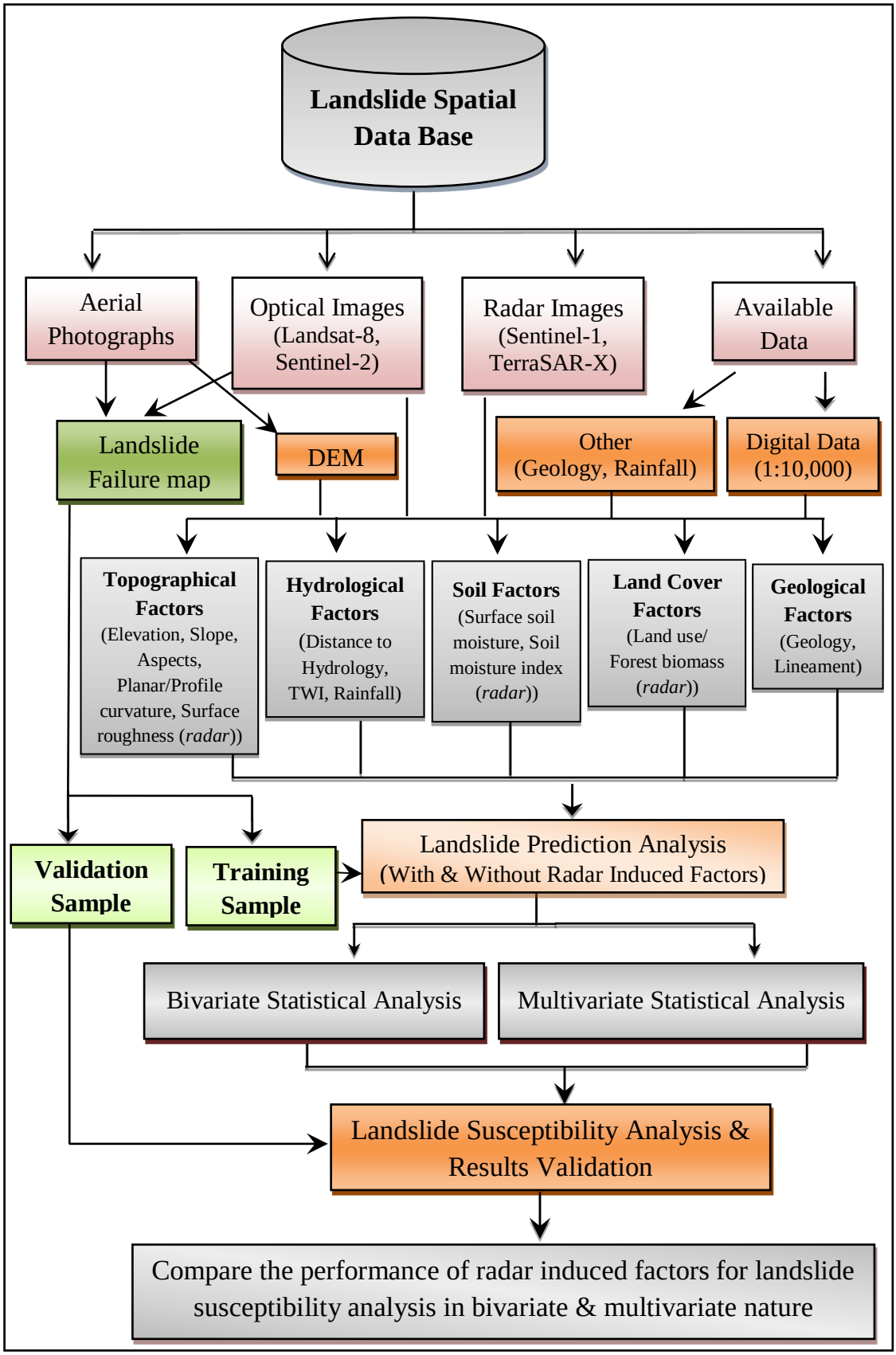

Figure 4-2 : Methodological flow of the Landslide susceptibility analysis using Bivariate and Multivariate approaches

Sentinel-1 radar images with 10 m resolution from wet and dry seasons were used for obtaining the soil moisture index and surface roughness as radar induced factors. Moreover, the TerraSAR-X spotlight image of 02nd November 2014 with a 2 m resolution was used for forest biomass estimation. Geology, rainfall and distance to hydrology were extracted from the available data sources such as geological map from GSMB (Geological Survey Mines Bureau), monthly average rainfall data from the Department of Meteorology, and water bodies as digital vector data layers from the Survey Department of Sri Lanka. Afterwards, the landslide inventory map and the derived causative factors (topographical, hydrological, soil and land cover) are cross-checked to calculate the weight index for the landslide susceptibility analysis.

Validating the results of predictions is of paramount importance to confirm the significance of the analysis and the results. In this research, the landslide failure map derived from previous landslides occurred within the study area are separated in to two independent samples as training and validating. The training samples are used to generate the landslide susceptibility regions while the validation samples are for validating results from the landslide prediction analysis (Remondo *et al.*, 2003; Saha *et al.*, 2005). The same training and validation samples were used of for all the prediction analysis and appropriate validations throughout the entire research.

4.3 Selected Landslide Predisposing Factors

Landslides might occur as a consequence of a number of predisposing and triggering factors. In this research, the predisposing factors were selected from among the most widely considered factors in literature and opinion from experts [Table 4-1]. Most data are derived as primary data from remote sensing techniques for a large area with up-to-date information. As such, fifteen predisposing factors are selected for the landslide susceptibility analysis by using bivariate and multivariate statistical techniques. Of these, twelve factors were derived from optical images, DEM and auxiliary data, while three more factors were derived from radar images. These factors were then combined

in order to analyse the performance of this integration for landslide susceptibility analysis.

Table 4-1: Selected Predisposing Factors for Landslide susceptibility analysis

Factors	
Main Factors	**Sub Factors**
Topographical	Elevation
	Slope
	Aspect
	Planar Curvature
	Profile Curvature
	Surface Roughness (*radar*)
Hydrological	Distance to Hydrology
	TWI
	Rainfall
Soil	Surface Soil Moisture
	Soil Moisture Index (*radar*)
Land cover	Land Cover Type
	Forest Biomass (*radar*)
Geological	Geology
	Lineament

4.3.1 Topographical Factors

The topographical factors include elevation, slope, aspect, planar curvature, profile curvature and surface roughness of the terrain [Figure 4-3, 4-4, and 4-5]. The elevation is important to study the local relief of the terrain and ranges from 446 m -1537 m above MSL (Mean Sea Level) in the study area. Since the area contains high mountains, more than a 1,000 m difference in elevation can be observed. The basic parameter for the slope stability analysis is the slope angle. The slope angle of the study area ranges from 0^0 to 80^0, showing a significant increase of slope angle within

a relatively smaller area. Additionally, the area with steep slopes ranging from 60^0 - 80^0 can be seen in the northern part of Koslanda [Figure 4-3].

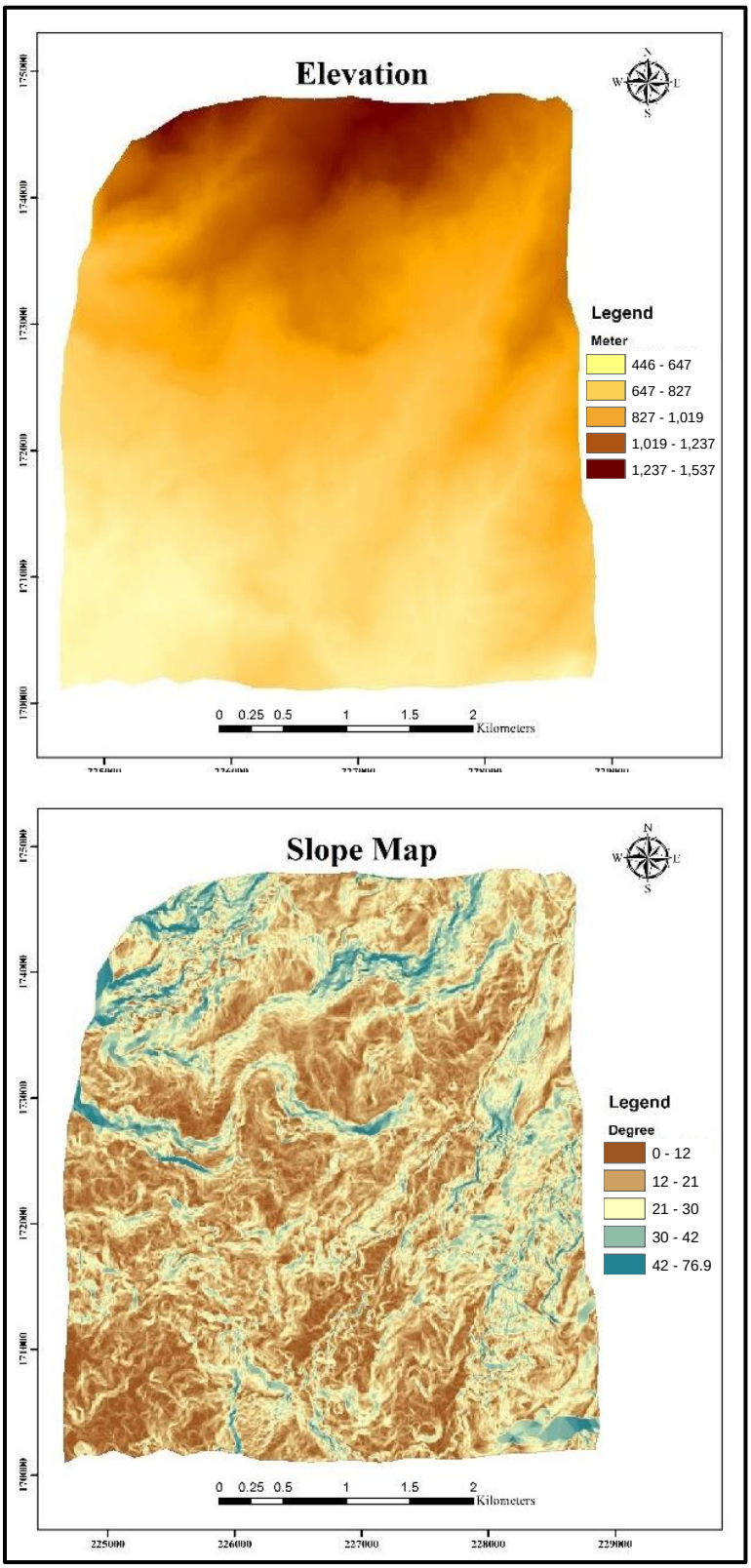

Figure 4-3 : Topographical factors, from top to bottom as Elevation and Slope used in Landslide Susceptibility Analysis

Aspect is defined as the direction of maximum slope of the terrain surface, or the compass direction (one of the eight main directions - N, NE, E, SE, S, SW, W, and NW) of a particular slope. Slopes of many regions on the study area are oriented in SE (South-East) and NW (North-West) directions. The curvature is theoretically defined as the rate of change of slope, or slope, of the focused slope. Planar curvature describes convergence and divergence of the flow across a surface while the profile curvature refers to acceleration or deceleration of the flow across a surface, as discussed in section 6.5.1 [Figure 4-4].

The importance of incorporating these factors for landslide susceptibility analysis is that these factors heavily influence the soil water content. When considering most of the area within the study region, the planar curvature of the South-East and North-West regions are upwardly convex, thereby providing higher convergence (3.68 - 9.37), while the North, South-West and middle regions are upwardly concave, resulting in more divergence of debris. Similarly, the profile curvature defines the South-East and North-West regions as upwardly concave, resulting in more accelerations of debris (8.46 - 21.9) while the North, middle and South-West columns indicate the surfaces as upwardly convex with more decelerations (1.13- (-3.28)) in the study area [Figure 4-4, 4-5].

Under radar configuration, the magnitude of radar backscatter is defined as a function of surface roughness and moisture content. Hence, to estimate the surface roughness without the use of any ancillary field data, a radar image of 12th March 2015 under dry climatic condition is used to reduce the effect of the moisture component from the radar backscatter [Figure 4-5]. The texture is the structure, or appearance, of the surface, and as such, describes the coarseness or the homogeneity of the image structure. One of the most prominent methods for texture analysis is Grey Level Co-occurrence Matrix (GLCM), which is based on the second order probability density function. Hence, the GLCM texture analysis is performed using a window size of 9*9 pixels and the homogeneity or dissimilarity criterion is used to determine the surface

roughness of the study area (Rahman *et al.*, 2008; Rahman *et al.*, 2007; Septiadi and Nasution, 2009).

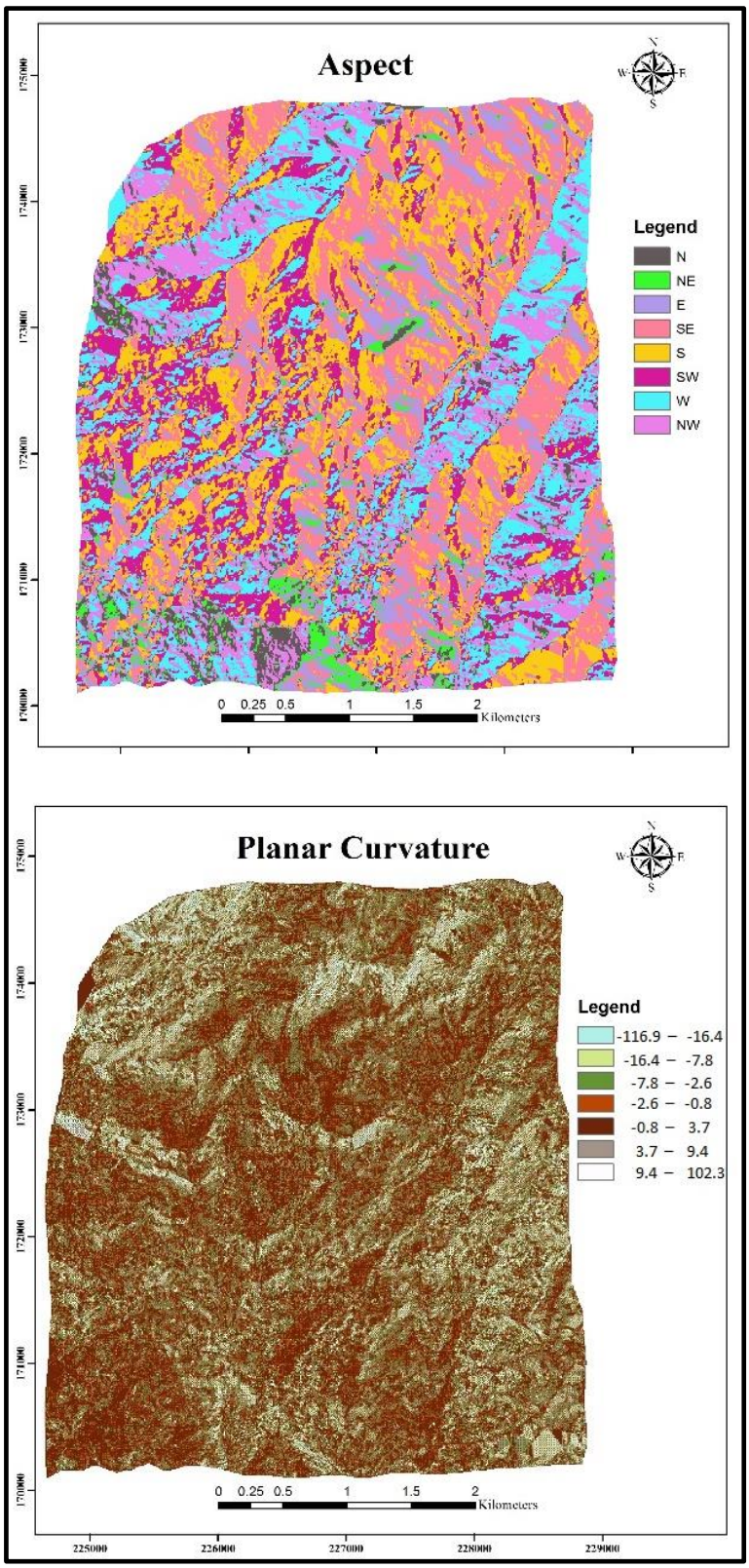

Figure 4-4 : Topographical factors, from top to bottom as Aspect and Planar Curvature used in Landslide Susceptibility Analysis

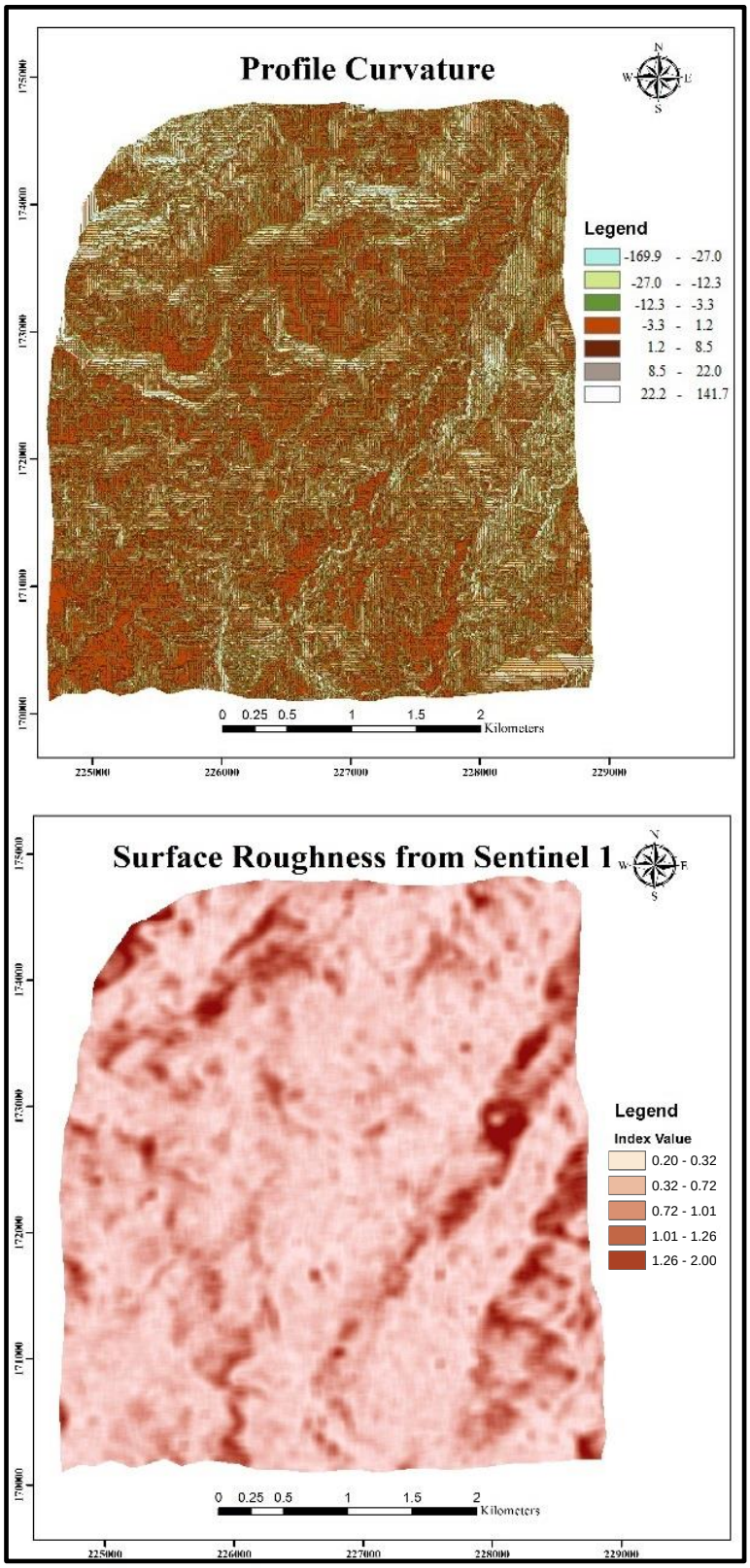

Figure 4-5 : Topographical factors, from top to bottom as Profile Curvature and Surface Roughness used in Landslide Susceptibility Analysis

4.3.2 Hydrological Factors

Distance to hydrology, TWI and rainfall are selected as the hydrological factors for this landslide susceptibility analysis [Figure 4-6]. Proximity to the hydrological features is an important factor when considering the landslide susceptible analyses (Beven and Kirkby, 1979). Hence, through the assigning of weights, this work investigated the effect of this particular parameter for the landslide prediction analysis. The Eruwendumpola Oya is along the valley of the lower slope of the study area, and the debris flow materials from the landslide at Meeriyabedda were finally accumulated in this river. There are many small streams and drainage systems commencing from the top of the mountainous regions. Therefore, the proximity to hydrological features is also considered in the landslide prediction analysis.

TWI is a solid index that is capable of predicting areas susceptible to saturation or wetness of land surfaces, and the areas that have the potential to produce an overland flow. TWI has been used to study the spatial scale effects, or topographic control, on hydrological processes. This index was developed by (Beven and Kirkby, 1979) and can be defined as;

$$\mathrm{TWI} = \ln[\propto/\tan\beta] \qquad (10)$$

where $\propto$ is the local upslope area draining through a certain point per unit of contour length, and β is the gradient of the local slope in degrees. The index is designed for the hill slope catenas and will not be a relevant variable for flat land studies. The best results can be achieved from high resolution DEMs (Kavzoglu *et al.*, 2014; Sørensen *et al.*, 2006).

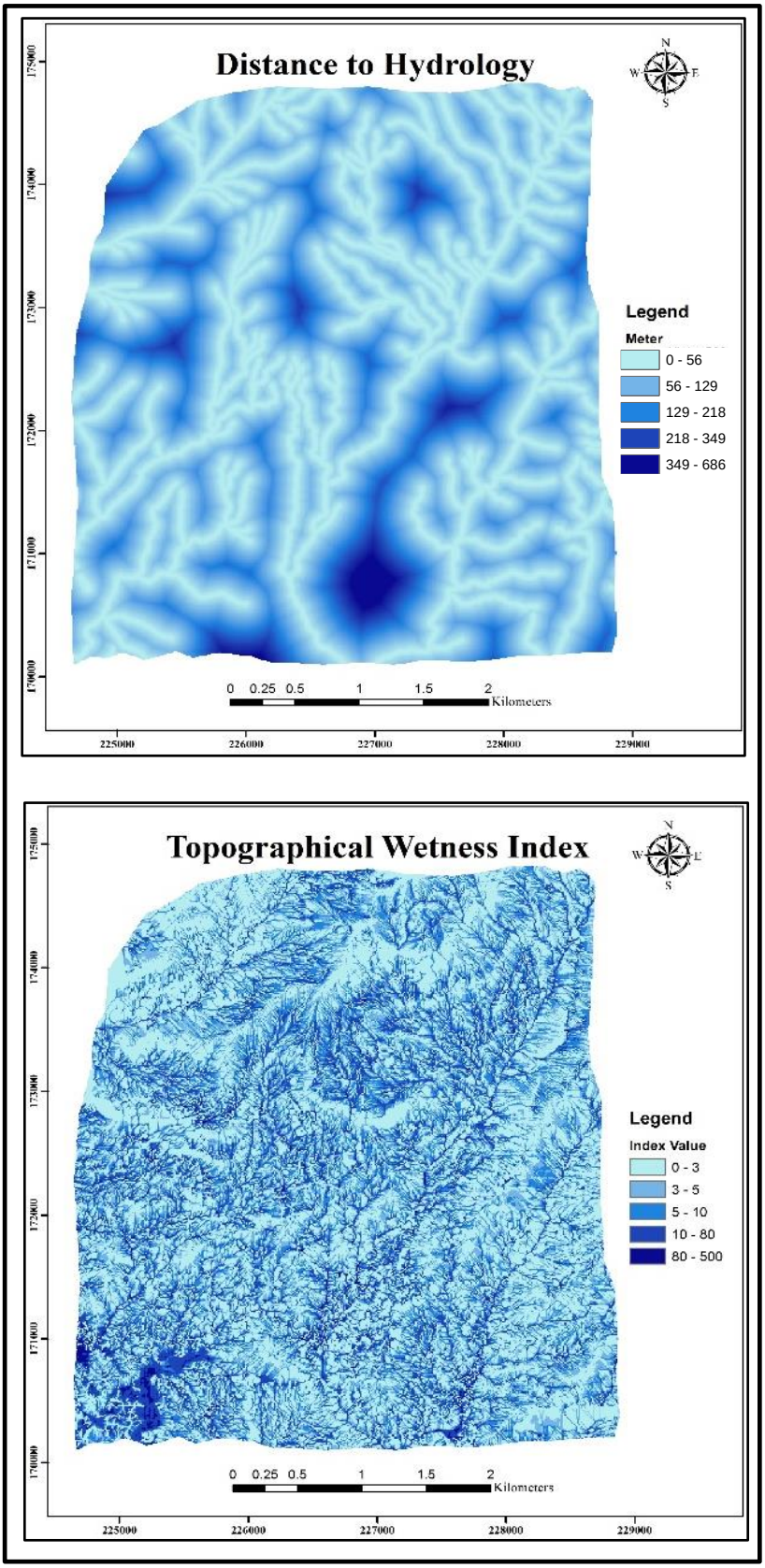

Figure 4-6 : Hydrological factors from top to bottom as Distance to hydrology and Topographical Wetness Index (TWI) used for Landslide Susceptibility Analysis

Within the Sri Lankan context, heavy and prolonged rainfall is the main triggering factor for the landslides. The monthly average rainfall data for the year 2014 from 10 nearby stations to Koslanda as Buttala, Konketiya, Diyatalawa, Badulla, Gangeyaya, Gleanore, Haputale factory, Poonagala, Suriyawewa, Thanamalwila and Wellawaya are used in this study [Figure 4-7]. All of the monthly rainfall data from the above 10 rain gauge stations are averaged, and the average rainfall map for the study area is generated using the IDW (Inverse Distance Weighting) interpolation method within the ArcGIS environment (Sar *et al.*, 2016; Shahabi and Hashim, 2015).

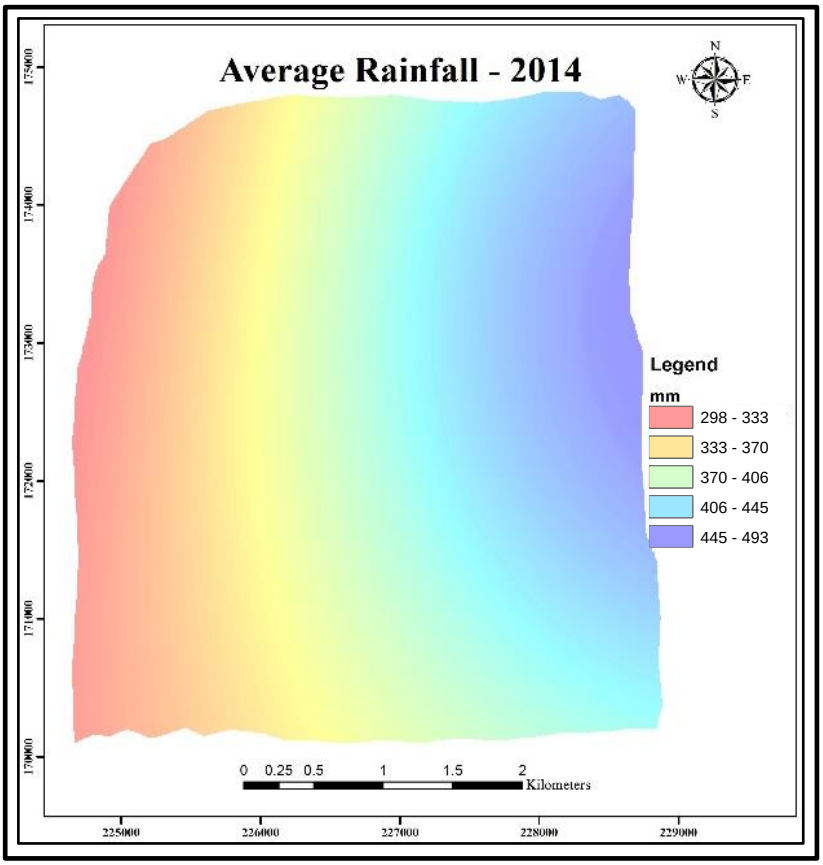

Figure 4-7 : Hydrological factor, Average Rainfall for 2014 used for Landslide Susceptibility Analysis

4.3.3 Soil Factors

The soil factors selected in this study are the SMI (Soil Moisture Index) and Delta Index [Figure 4-8]. Surface soil moisture is the one of most important parameters in land susceptibility analysis. As the soil mass's moisture increases, the pore water pressure rises and increases the shear load while decreasing the shear strength, resulting in landslides. The use of remotely sensed data is potentially of great interest and is prominently used in soil moisture estimation.

Several methods have been proposed to estimate the surface soil moisture conditions accurately with insitu measurements. However, these methods are time consuming and costly with respect to the study of a larger area at a smaller scale. Hence, this research uses the Universal Triangle relationship between Soil Moisture, NDVI and LST (Land Surface Temperature) derived from Landsat-8 image bands as an optical remote sensing approach, and the Delta index derived from two radar images from wet and dry conditions as a radar remote sensing approach (Carlson *et al.*, 1994; Zhan *et al.*, 2002).

Band 5 (Near Infrared (NIR), 30 m resolution), band 4 (Red, 30 m resolution) and band 11 (Thermal, TIR-2, 100 m resolution) of Landsat-8 image of 03rd July 2015 is processed for extracting the soil moisture index in the Thermal-NDVI space. The combination of Thermal-NDVI space is widely used, and has been successfully employed to determine the surface soil moisture information (Hassaballa *et al.*, 2013).

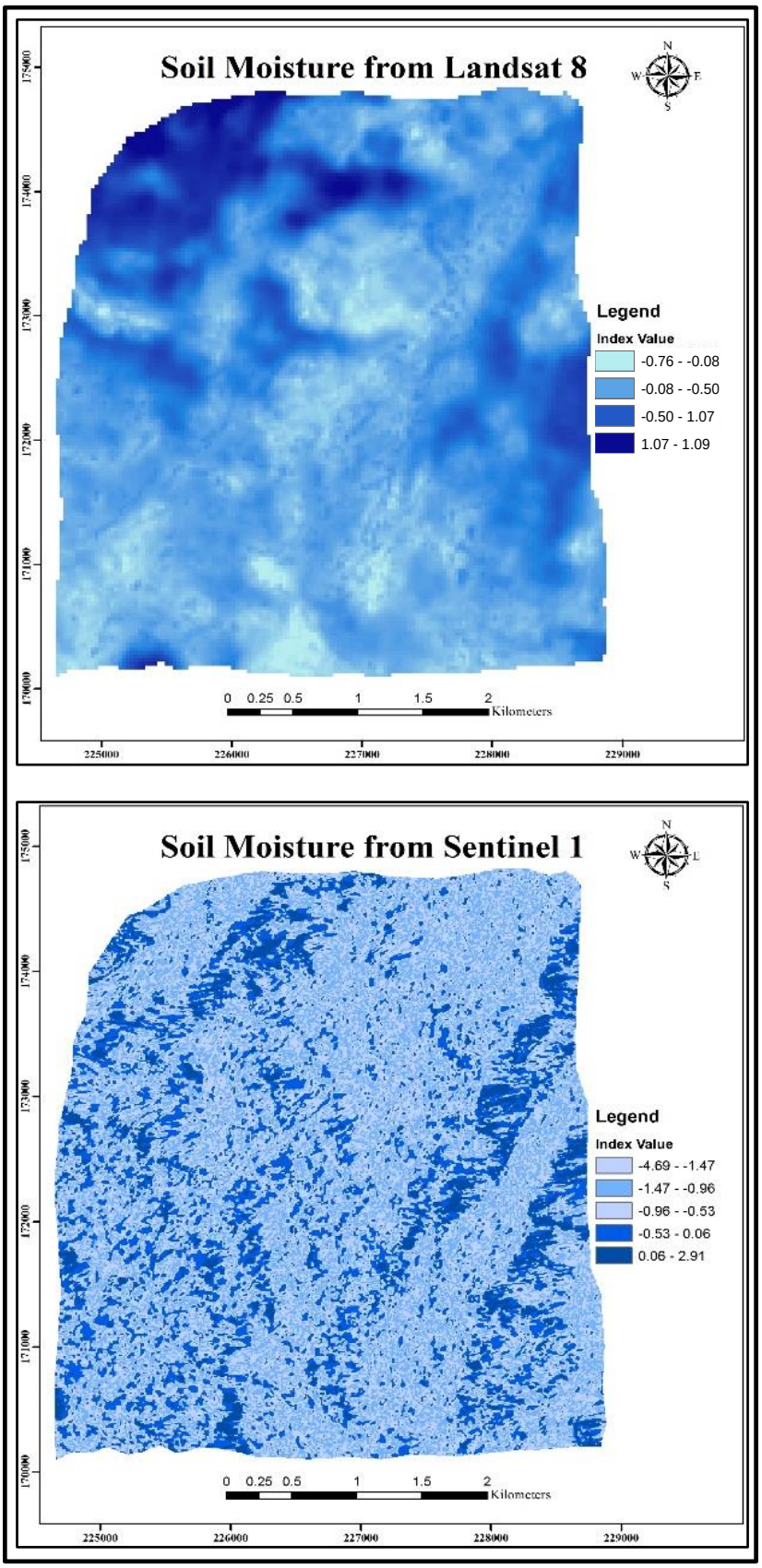

Figure 4-8 : Soil factors top to bottom as Soil Moisture Index (SMI) from optical approach and Delta Index from radar approach used for Landslide Susceptibility Analysis

In this space, the surface temperature is primarily determined by the soil moisture emitted from the land surface, while the vegetation index (NDVI) is determined by the land-surface reflectance. The combination of these two variables (T and NDVI) from remotely sensed measurements apparently carries information about surface soil moisture under different vegetation types expressed by NDVI. The SMI is "0" along the dry edge and "1" is along the wet edge. SMI can be defined as;

$$\text{SMI} = \frac{(T_{max} - T)}{(T_{max} - T_{min})} \quad (11)$$

where T_{max}, T_{min} are the maximum and minimum surface temperature for a given NDVI and T is the remotely sensed data derived surface temperature at a given pixel for a given NDVI (Wang and Qu, 2009; Zenga *et al.,* 2004). The simple regression relationship between T and NDVI is formulated as;

$$T_{max} = a_1 \cdot NDVI + b_1 \quad (12)$$

$$T_{min} = a_2 \cdot NDVI + b_2 \quad (13)$$

where, a_1 = -5.2362, b_1 = 300.14, a_2 = 2.9254, and b_2 = 289.11. Accordingly, the soil moisture index is calculated and the value ranges approximately from 0 to 1. High indices are scattered in the North-West regions of the study area where the area contains thick forest areas at the top of the mountains, and the low soil moisture indices are abundant in the South and South-West regions where the area contains residences, roads, and abundant number of tea estates.

Radar remote sensing provides advantages for extracting near surface soil moisture (0-5 cm) using L band including timely coverage with repeat passes in day and night, under all weather conditions. Technically, the surface roughness and vegetation affect radar backscatter much more than soil moisture. Hence, surface roughness and vegetation have to remain unchanged during the image acquisition for soil moisture estimation (Thoma *et al.,* 2006).

DI (Delta Index) is a modified, image differencing technique, and many studies have proven it to be a good predictor for near surface soil moisture extraction in many studies (Barrett *et al.*, 2009; Moran *et al.*, 2000; Sano *et al.*, 1998; Thoma *et al.*, 2004). This index describes the change of wet scene backscatter relative to the dry scene backscatter. DI require two images, one as the dry reference image and the second a wetter image (when compared with the "dry" image) where the surface roughness and vegetation density of the study area should not change significantly between the image acquisition dates. Delta Index is defined as;

$$Delta\ Index = \left| \frac{\sigma^0_{wet} - \sigma^0_{dry}}{\sigma^0_{dry}} \right| \quad (14)$$

where, σ^0_{wet} is the radar backscatter (decibels) from a pixel in a radar image representing wet soil conditions, and σ^0_{dry} is the radar backscatter (decibels) from a pixel in the same geographic location representing dry soil conditions at a different time. Sentinel-1 images with 10 m spatial resolution and VV polarization is used. Dry reference image was acquired on 12th March 2015 and the wet image was 24th November 2014 after the Meeriyabedda landslide. Hence, the topographical changes as roughness and vegetation density were not significantly changed with in these three months' time. When compared with the near surface soil moisture extracted from radar images with surface soil moisture from optical approach, high and low moisture contents are scattered in similar regions of the study area but in an ad hoc manner.

4.3.4 Land Use

The major land uses existing in this study area are identified as tea, scrub, forest, rock, paddy, water, and residential. Sentinel-2A image from 10th October 2016 is used to extract the desired land uses from the study area by applying supervised classification [Figure 4-9].

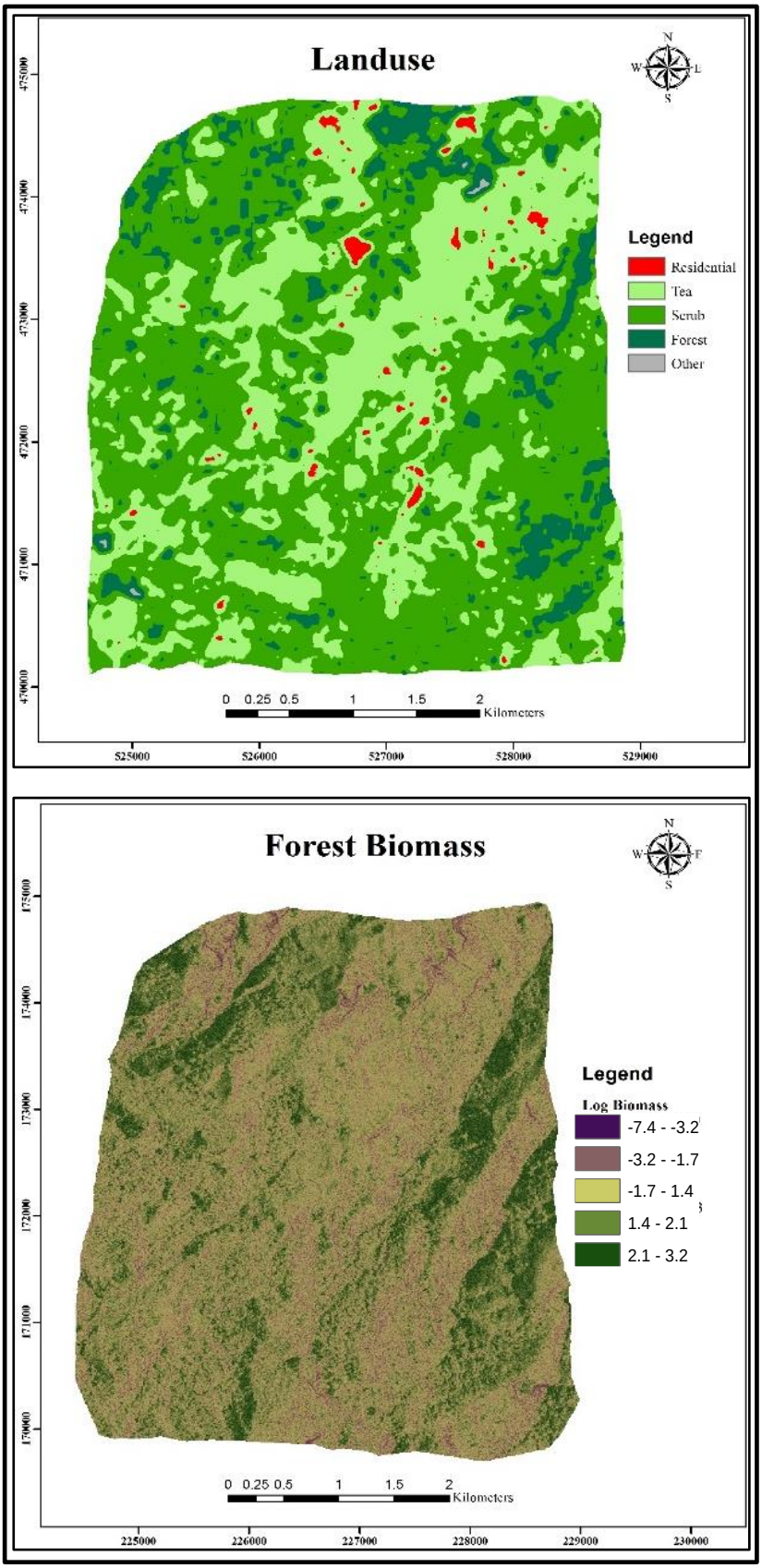

Figure 4-9 : Land use factors top to bottom as Land use from Sentinel – 2A (10 m resolution), and estimated Forest Biomass from TerraSAR-X (3 m resolution) Radar image, which are used in Landslide susceptibility analysis

Tea and scrub areas are prominent in this study region with some forest covers and residential areas. Scrub areas are typically the tea estates that are in abundance, while the residential areas are the rooms of tea workers. It is noted that most of the devastating landslides in this area had occurred in the abundant tea estates. Hence, the main reason for the continuous occurrence of these landslides can be identified as the lack of proper land use management in this study area.

Forest biomass is a significant factor that can control the landmass failures or landslides. Measurements of forest resources are often outdated due to forest degradations, forest fires, intensive logging activities, and natural reforestations on abundant agricultural lands. The main limitations of using optical remote sensing for forest biomass estimation is the near constant tropical cloud cover, and the insensitivity of reflectance to change of the biomass in older and mixed forests. Radar has potential to overcome the above limitations due to its all-weather, day and night capability and mainly with the positive relationship of radar backscatter and forest biomass (Caicoya *et al.*, 2016).

Kuplich *et al.*, (2005) related the radar image texture derived from GLCM to the forest biomass. Field data collections were done from 37 plots to generate allometric regression equations that express the relationship between diameter at breast height, wood density and biomass. JERS-1 (Japanese Earth Resources Satellites), L band in HH polarization data from December 1995 and July 1995 had been used in this work. An experiment was conducted with seven texture measures but only the GLCM derived contrast increased the correlation between the backscatter and the log of biomass. The study concluded that the GLCM derived contrast to backscatter has the potential to increase the accuracy of biomass prediction (Kuplich *et al.*, 2005).

The regression model derived for forest biomass estimation from radar data with the inclusion of textural information (GLCM contrast) are formed as follows,

$$Log\ of\ Biomass = 2.24 + 0.33b + 0.0001c \quad (15)$$

where, b is the radar back scatter and the c is the GLCM contrast texture for the particular radar image.

TerraSAR-X spot light image from 2nd November 2014 with 3m resolution and dual polarization (HH and VV) is used to estimate the forest biomass in this research. The calculated log of forest biomass ranges from -7.43 to 3.19. When comparing the calculated forest biomass from radar with the land use derived from the 10 m resolution Sentinel-2 optical images, forest and scrub land uses are indicated by high indices of forest biomass regions.

4.3.5 Geological Factors

In this research for Landslide susceptibility analysis, two geological factors are considered as geology and lineament density [Figure 4-10]. Geology refers to the physical structure and the substance of the Earth. In order to investigate the land mass failures, the geological structure of that particular area have to be analysed carefully. The geomorphology of Koslanda in section 2.1.3 describes, in detail, the formation of the physical structure of the Earth around the Koslanda study area [Table 4-2].

A combination of geology and improper land uses in the study area has made it more vulnerable for landslides. Hence, the geological information of the particular area is obtained from the available geological map from GSMB at 1:100,000 scale. Seven types of different geological structures are contained in the selected study region.

Lineaments are extractable linear features which are correlated with the geological structures of the earth. When considering the analysis of lineaments with respect to the landslide potentiality, lineaments exhibit the zones of weakness surfaces as faults, fractures, and joints. Lineaments can typically be derived from aerial photographs or satellite images (Mandal and Maiti, 2015). This study uses the Sentinel-2A optical satellite image with 10 m resolution for the extraction of lineaments of the study area. The lineament density is then calculated to use this information for landslide prediction analysis [Figure 4-10].

Table 4-2 : Geological Structures of the Koslanda area obtained from the 1:100,000 Geological Map of GSMB, Sri Lanka

Geological Structures	Description
Pmc	Marble, usually coarse-grained and dolomitic, locally high calcite marble present
Pmgga	Garnet-sillimanite –biotite gness± graphite pelitic schist or gneiss
Pmgga_ga	Garnet-sillimanite –biotite gness± graphite with up to 30% large (1-3cm) red garnet, formerly "khondalite"
Pmgk	Charnockitic gneisses: restricted outcrops, often ridge-forming: typically coarse-grained with characteristic brown or green greasy lustre; may lack hypersthene. Includes patchy in situ charnockites as well as partially retrogressed, bleached "ex-charnockites", stipple indicates local charnockitisation includes Pmgkh hornblende rich charnockitic gneisses with garnet ± graphite
Pmgk_b	Undifferentiated charnockitic biotite gneisses: extensive sequences of charnockitic-looking grey gneisses usually lacking hypersthene, though commonly with boudinaged orthopyroxene-bearing mafic layers; but may include some paragneisses
Pmgqf_ga	Garnetiferousquartzofeldspathic gneiss (formerly "garnet granulite"): leucocratic quartz-feldspar gneiss with abundant pink garnets, often>20%; weathers to iron-rich residual deposits
Pmq	Quartzites: pure coarse-grained ridge-forming quartzites locally with <5% each of sillimanite, kaolinised feldspar or biotite

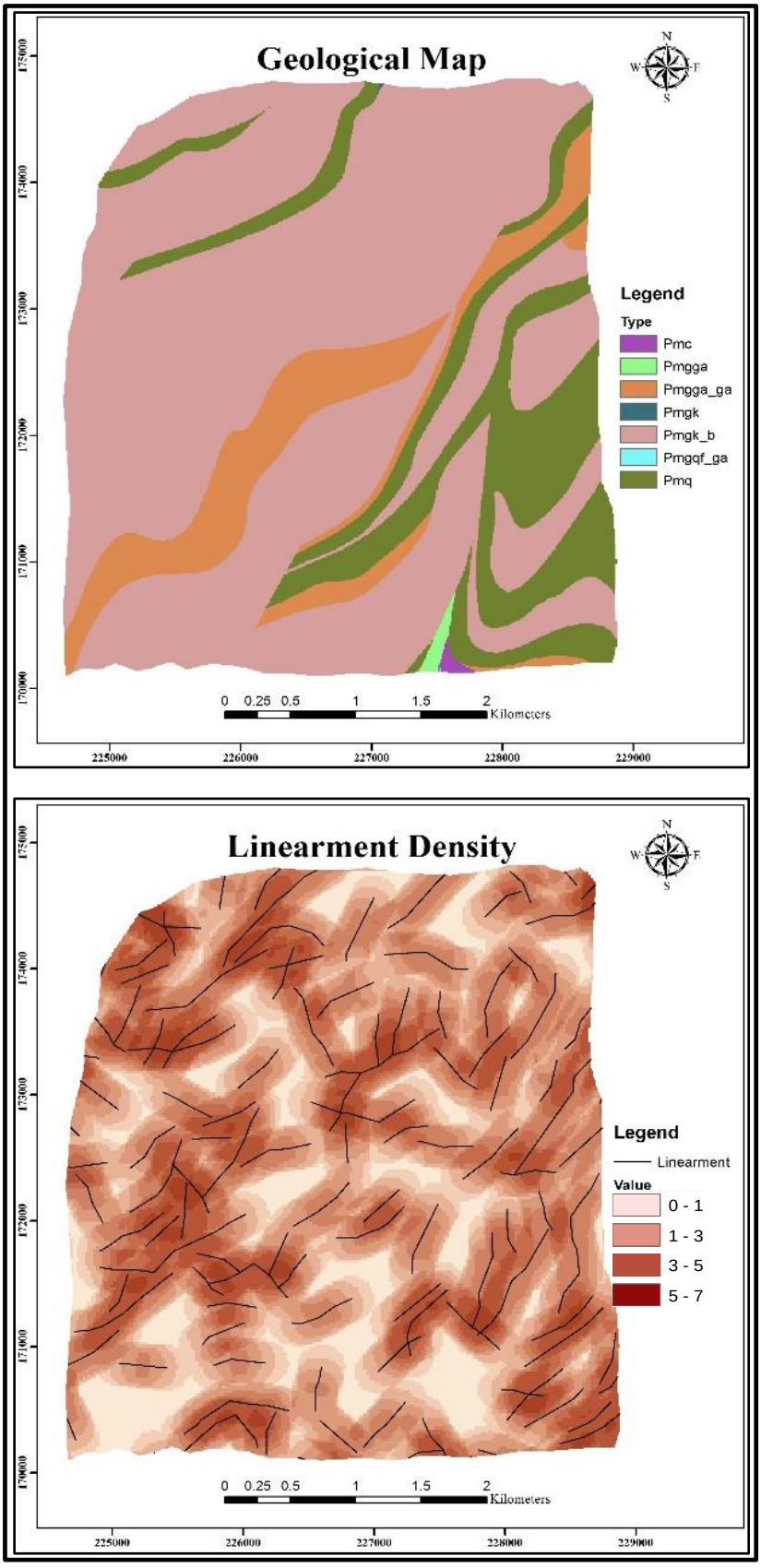

Figure 4-10 : Geological factors top to bottom as 1:100,000 scale Geological map from GSMB, Sri Lanka and Lineament density with the lineaments derived from 10 m resolution Sentinel -2 image used for landslide susceptibility analysis

4.4 Landslide Susceptibility Analysis

Production of landslide maps is an essential tool that can help planners, local administrations, and decision makers in disaster management activities. Accuracy of the landslide maps is crucial for the reduction of negative impacts on human life and property. The prediction models that are available in landslide susceptibility analysis require a combination of various predisposing factors. Many algorithms have been developed and successfully applied, in order to combine these predisposing factors. In recent years, InfoVal method based on simple statistical analysis such as bivariate, and GIS based MCDA as multivariate, have been successfully applied for landslide susceptibility analysis.

After decisive analysis of the types of predisposing factors, present research work aimed to consider fifteen predisposing factors that are derived from optical, radar and other available auxiliary data sources. Three significant causative factors as surface roughness, soil moisture from Delta Index, and forest biomass were estimated by using radar satellite images. Thus, this work investigated the performance of landslide susceptibility analysis from bivariate and multivariate nature with the inclusion of radar induced factors.

4.4.1 Bivariate Statistical Analysis (InfoVal or SI method)

The bivariate statistical analysis determines the susceptibility at each point or pixel, jointly considering the weight of influence of all predisposing factors. The weight of influence is based on the landslide inventory map of the particular area. When constructing a probability model for landslide prediction, it is necessary to assume that the landslide occurrence is determined by landslide-related factors, and that future landslides will also occur under the same, or almost similar, conditions as past landslides. Hence, at the beginning of the analysis, the landslide inventory map was

divided in to two samples as training and validation, enabling the use of this data for landslide susceptibility analysis and results validation respectively.

Information value method as a bivariate approach has been described in detail in section 3.7.2 (a) part (ii). The mathematical analysis for determining the weight of influence for landslide susceptibility analysis is also discussed in Chapter 3, as Equation (2). The Log function is used to control the large variation of weights in calculations. The weight of influence for each factor type is calculated from its relationship to landslide events using training samples of landslide failure map [Table 1-15 of Annexure A]. Larger the weight of influence, the stronger the relationship between landslide occurrence and the given factor's attribute.

Finally, the weight of influence of all thematic maps, with radar induced factors, and without radar induced factors, are added to obtain the contribution of all predisposing factors for landslide susceptibility analysis. The entire study area of each landslide susceptibility map is then discretized in to four classes as 0%, 10%, 30% and 60% of failure regions for very low, low, moderate and high susceptibility classes respectively [Figure 4-11 and 4-12].

Susceptible regions are identified from the bivariate information value method without radar induced factors as 12% for high, 45% for moderate, 38% for low, and 5% for very low. Hence, 57% areas from the total study area are predicted as having high and moderate susceptibility for the landslide hazard. Very steep slope mountains in the North, North West, and East regions are identified as very low susceptibility areas, given that the area was free from historical landslides. The middle regions with 30^0-50^0 slope are detected as having high probability for landslide occurrences with the past experience from Naketiya and Meeriyabedda landslides.

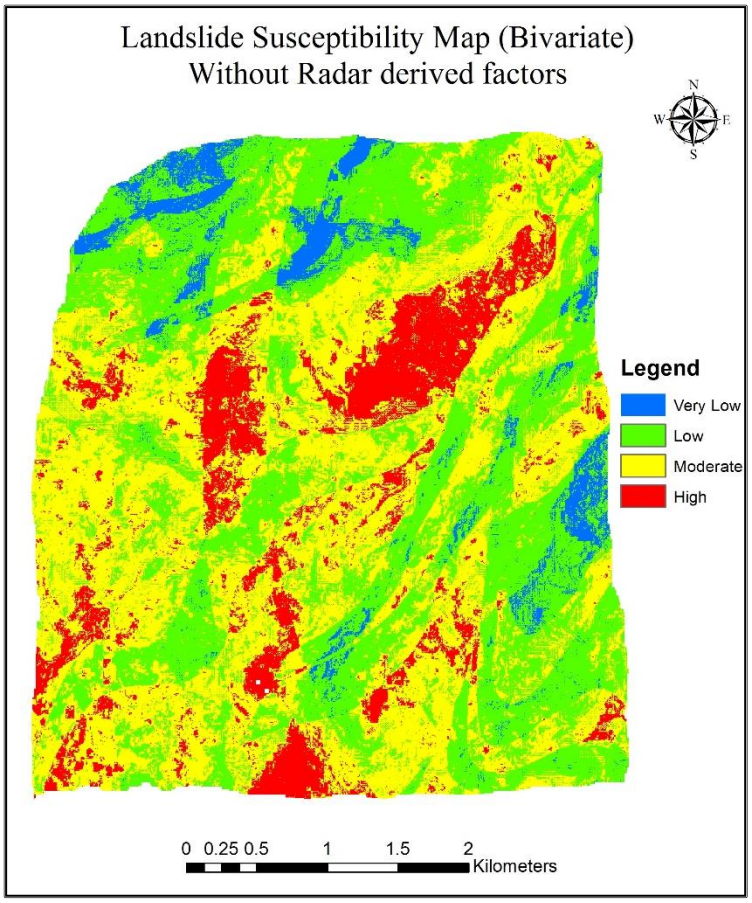

Figure 4-11: Landslide Susceptibility Map from Bivariate, Information Value Method (without Radar Induced Factors)

The bivariate information value method with radar induced factors identified 19% of failure regions for high susceptibility, 39% for moderate, 33% for low, and 9% for very low susceptible regions. Therefore, 58% of the total study area is predicted as having high and moderate susceptibility for landslides. Very steep slope mountains in the North, North West, East, and South East regions, area near to the Eruwendumpola Oya, are identified as having very low susceptibility for landslides. Similar to the bivariate analysis without radar induced factors, the middle regions with 30^0-50^0 slope are detected as having high probability for landslide occurrences.

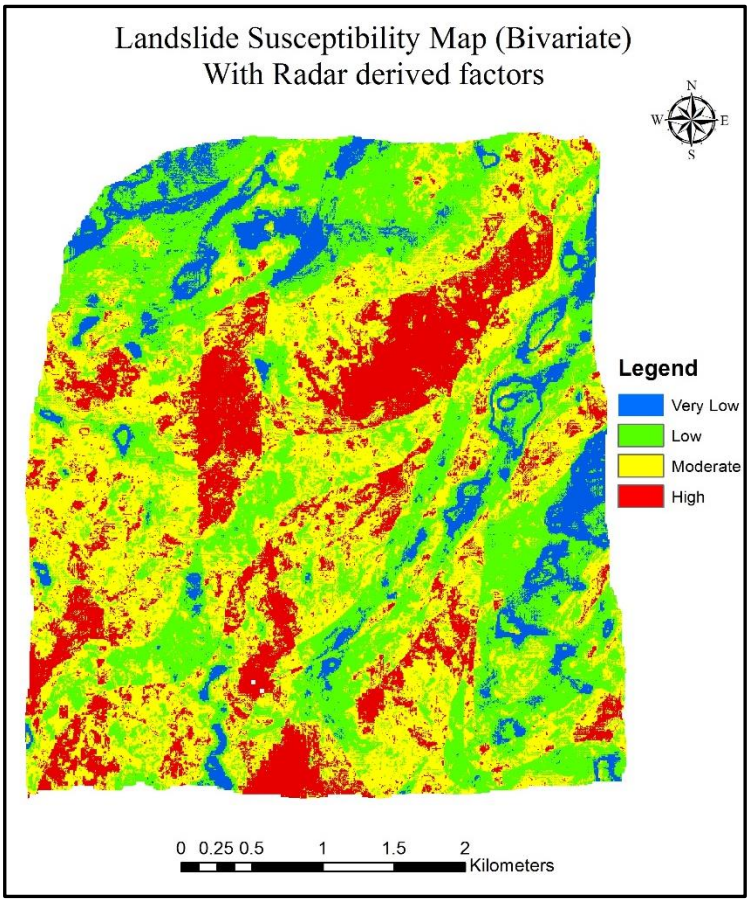

Figure 4-12 : Landslide Susceptibility Map from Bivariate, Information Value Method (with Radar Induced Factors)

4.4.2 Multivariate Statistical Analysis (MCDA based on AHP)

Multivariate methods too, integrate all the independent predisposing factors with the inclusion of relative contribution of each factor by putting more emphasis on the predisposing factors that contribute to landslide occurrence. In multivariate analysis, the same predisposing factors with or without radar, are used to investigate the landslide susceptibility regions from AHP technique within the GIS domain. The AHP provides an effective way to deal with complex decision making. It can assist with identifying and weighting of multi criteria, analysing the collected data, and expediting the decision-making process. Theoretical concepts of Multivariate prediction models and AHP technique are discussed in section 3.7.2 (b).

In AHP, each pair of factors in a particular factor group is examined at one time, in terms of their relative importance. Relative weights for each factor are calculated based on a questionnaire survey from experts in the field [Annexure B]. These relative weights are then used to generate a pair-wise comparison matrix which is the basic measurement mode when applying the AHP procedure. The selected predisposing factors, and relevant relative weights, are used to generate the normalized matrix with final weights by performing the weighted linear combination. Practically, the weight analyses are benefitted from the expert knowledge of causal factors for landslides. However, expert knowledge could be subjective at times, or may cause to assign different weights for each factor, when dealing with a large number of causative factors. Hence, in order to avoid this inconsistency, CR (Consistency Ratio) is calculated. For better predictive models, the CR should be less than 0.1, or else have to be generated weights for each factor with the proper pairwise comparison [Section 3.7.2 (b) part (i)].

All fifteen weighted predisposing factors were grouped as with or without radar induced factors, and weighted overlay is performed separately in order to obtain the landslide susceptibility regions. When considering the twelve predisposing factors without radar, a 12×12 pairwise comparison matrix [Annexure B, Table 16] and the normalized matrix [Annexure B, Table 17] are generated in order to calculate the final weights for each predisposing factor. The calculated weights for elevation, slope, aspect, planar curvature, profile curvature, TWI, land use, lineament density, distance to hydrology, SMI in NDVI-T domain, geology, and rainfall are 0.030, 0.172, 0.022, 0.018, 0.014, 0.074, 0.149, 0.052, 0.045, 0.094, 0.185, and 0.145, respectively. The CR is 0.089, making it less than the 0.1, the value showing the reasonable level of consistency in the pairwise comparison.

Then the fifteen predisposing factors with radar induced factors are selected and, a 15×15 pairwise comparison matrix [Annexure B, Table 18] and the normalized matrix [Annexure B, Table 19] are generated in order to calculate the final weights for each

predisposing factor. The weights for elevation, slope, aspect, planar curvature, profile curvature, TWI, land use, lineament density, distance to hydrology, SMI in NDVI-T domain, geology, rainfall, soil moisture (Delta index), surface roughness, and forest biomass are 0.022, 0.145, 0.016, 0.013, 0.011, 0.053, 0.126, 0.039, 0.033, 0.065, 0.153, 0.124, 0.088, 0.088, and 0.027, respectively. When considering the fifteen predisposing factors, the CR is calculated as 0.092, which is less than the 0.1 thereby showing a realistic level of consistency in the pairwise comparison matrix.

Finally, the multi criteria decision analysis using AHP theories is performed to obtain the landslide susceptibility regions for the study area. As in with the bivariate method, the whole study area is discretized in to four classes as 0%, 10%, 30% and 60% of failure regions for very low, low, moderate and high susceptibility classes, respectively. Figure 4-13 illustrates the landslide susceptibility map from the multivariate method without radar induced factors. Multivariate AHP technique is able to identify 18% for high, 44% for moderate, 36% for low and 2% for very low susceptible regions. Hence, 62% of areas from the total study area are predicted to be of high and moderate susceptibility for landslide hazard.

The tops of the mountains in the North West and East regions are identified as having very low susceptibility for landslides. Similar to the bivariate approaches, the middle regions are detected as having a high and moderate probability for landslide occurrences.

The landslide susceptibility map from the multivariate method with radar induced factors, are illustrated in Figure 4-14. From the total area, 21% of the area having high susceptibility to landslides, 40% of area for moderate, 34% area for low and 5% of area as having very low susceptibility to landslides have been identified from this analysis. Hence, 61% of areas from the study area are predicted as having high and moderate susceptibility for the landslide hazard.

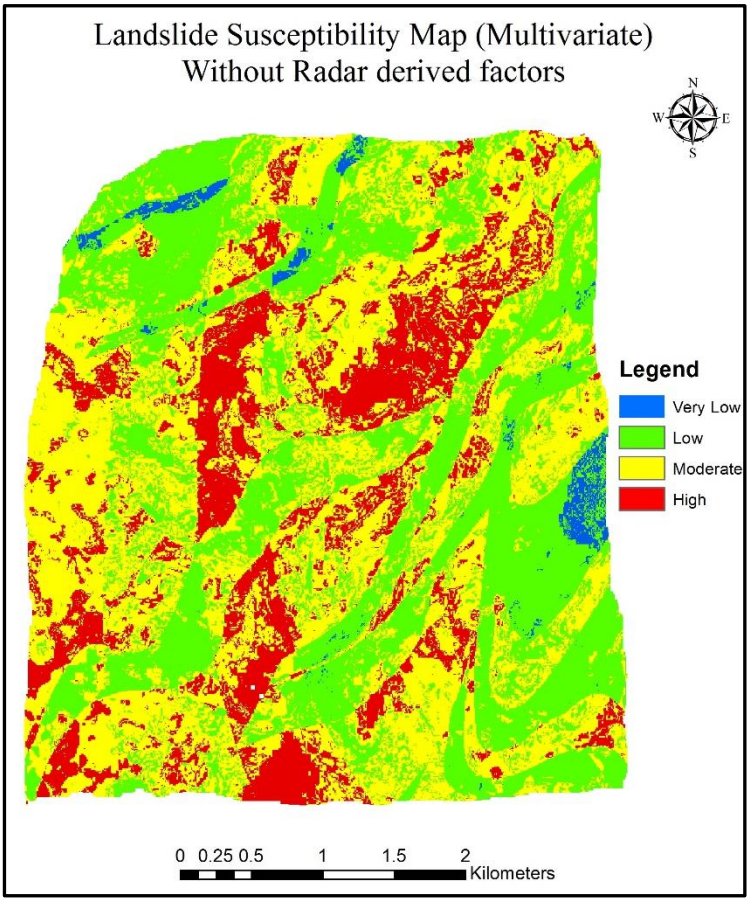

Figure 4-13 : Landslide susceptibility map from Multivariate, AHP based on MCDA (without Radar Induced Factors)

The top of the mountains in the North, North West, East, and South East regions, with area near to the Eruwendumpola Oya, are identified as having a very low susceptibility to landslide hazards. The middle regions with 30^0-50^0 slopes are detected as having high and moderate probability for landslide occurrences.

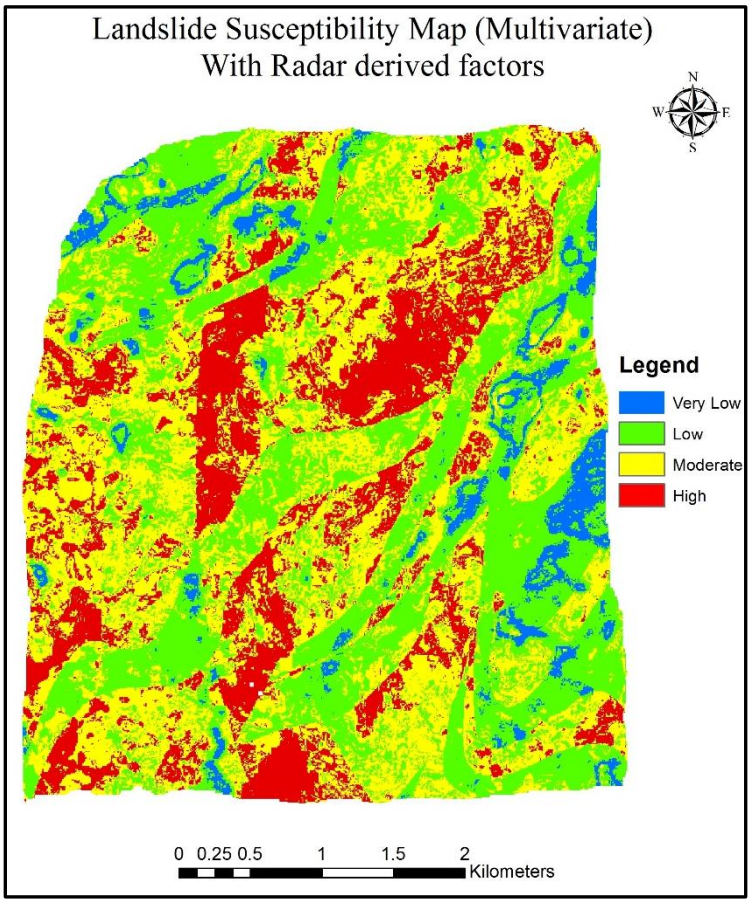

Figure 4-14 : Landslide susceptibility map from Multivariate, AHP based on MCDA (with Radar Induced Factors)

Table 4-3 shows the comparison of landslide susceptibility derived from bivariate and multivariate analysis, and with and without radar induced factors. The following notations are used in the table;

BiNR - Bivariate analysis without radar induced factors

BiWR - Bivariate analysis with radar induced factors

MNR - Multivariate analysis without radar induced factors

MWR - Multivariate analysis with radar induced factors

Table 4-3 : Landslide susceptible area comparison from bivariate and multivariate analysis with and without radar induced factors

	BiNR	BiWR	MNR	MWR
High	**12%**	**19%**	**18%**	**21%**
Moderate	45%	39%	44%	40%
Low	38%	33%	36%	34%
Very Low	**05%**	**09%**	**02%**	**05%**

The area identified as having high and moderate susceptibility classes in these four approaches (57%, 58%, 62%, and 61% respectively in BiNR, BiWR, MNR, and MWR) are approximately similar but shows a slight increase in multivariate analysis when compared with bivariate analysis. Moderate and low landslide susceptibility areas show only some slight changes throughout these four analyses. With the integration of radar induced factors as surface roughness, near surface soil moisture from delta index, and forest biomass in bivariate and multivariate analysis, the high and very low susceptible areas are increased significantly (high: 7% - bivariate, 3% - multivariate and very low: 4% - bivariate, 3%- multivariate). However, when comparing the high and very low susceptibility areas from bivariate and multivariate analysis, high susceptibility areas show a significant increase (without radar: 6% and with radar: 2%) while, very low susceptibility areas have a significant decrease (without radar: 3% and with radar: 4%).

4.5 Results Validation

As the last step, the landslide susceptibility maps derived from the bivariate information value method and multivariate AHP techniques are validated using the validation samples from the landslide failure map. Two of the most commonly used and scientifically recognized validation methods are followed as RFD (Relative Failure Density) and ROC (Receiver Operating Characteristics) curves, and these have been used in the validation stage of this work.

4.5.1 RFD Analysis

RFD is used to quantify the accuracy of the landslide prediction analysis from many years in the literature (Dai and Lee, 2002; Guinau *et al.*, 2007; Remondo *et al.*, 2003).

$$RFDi = 100.(Npix(Si)/Npix(Ni))/\sum_{i=1}^{n}(Npix(Si)/Npix(Ni)) \qquad (16)$$

where, $Npix(Si)$ is the number of failed pixels in the ith factor class, $Npix(Ni)$ is the number of pixels in the ith susceptibility class, and "n" is the number of susceptibility classes. Here, "n" is "4" with the four susceptibility classes as very low, low, moderate, and high. The RFD of the very low susceptibility class is "0" in all prediction models (bivariate and multivariate with and without radar induced factors) as number of failure pixels ($Npix(Si)$) are not available in the particular class. RFD of low, moderate, and high susceptibility classes are having 22.134, 47.755, and 30.111 in BiNR, 19.618, 43.120, and 37.262 in BiWR, 27.933, 40.250, and 31.817 in MNR, and 31.133, 35.278, and 33.589 in MWR.

Figure 4-15 describes the relative failure density in each susceptibility classes from bivariate and multivariate analysis, with and without radar induced factors. The validation results from both techniques imply that the prediction results are in acceptable form with analysed predicted susceptibility classes as "0" RFD in very low susceptibility class, less than 30% in low and more than 70% in moderate and high susceptibility classes providing gradual increase from very low to high susceptibility classes.

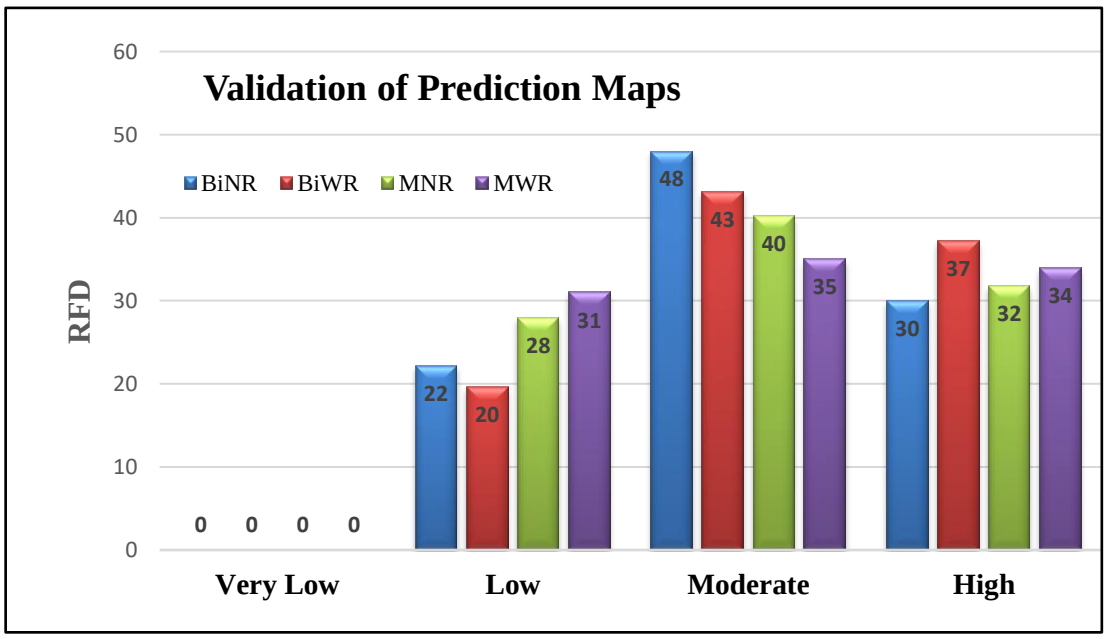

Figure 4-15 : Graphic display of validation results for each landslide susceptibility class from bivariate and multivariate techniques with and without radar induced factors

Validation of prediction maps from RFD for bivariate and multivariate analysis, with and without radar induced factors, indicate that the prediction results from both the bivariate and multivariate techniques are fit with the prediction analysis. This is because, it is observed that the very low susceptible regions from the four statistical predictive analyses are validated as 0%. From RFD analysis more than 70% of the areas are identified as having high and moderate landslide susceptibility areas. The validation results from bivariate and multivariate statistical analysis illustrate the gradual increase of RFD from very low to (moderate + high) susceptibility classes. As a whole, the prediction analysis from the four approaches can be considered as within acceptable range, confirming the careful selection of predisposal factors and suitable methodology for landslide susceptibility analysis.

4.5.2 ROC Curves

ROC is a graphical plot that illustrates the performance of classification, and is considered as a powerful tool for the validation of landslide susceptibility analysis from many years [Section 3.9]. The AUC (Area Under Curves) for the four different approaches, as bivariate and multivariate with and without radar induced factors, are calculated [Figure 4-16, 4-17, 4-18, and 4-19]

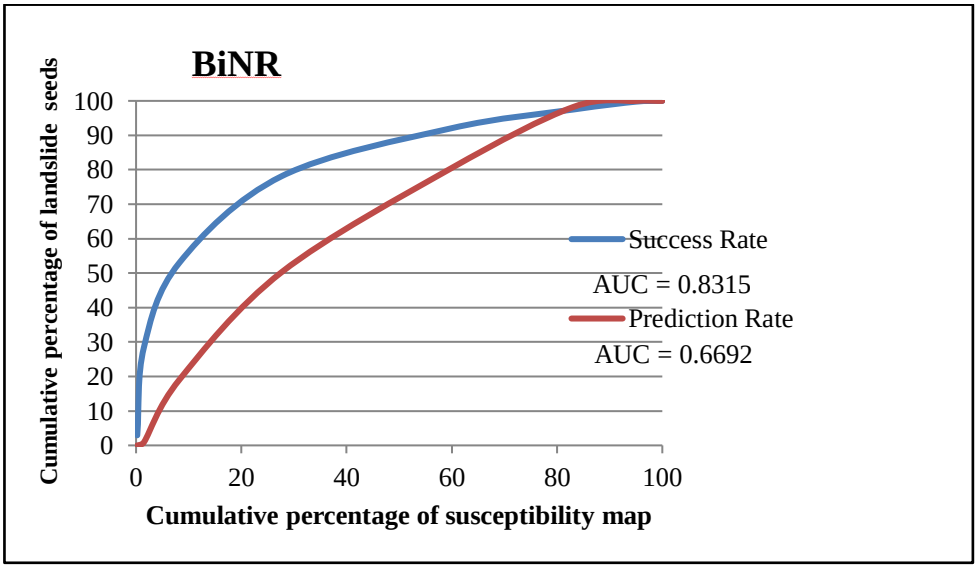

Figure 4-16 : Success rate and Prediction rate curves with AUC for the bivariate analysis without radar induced factors

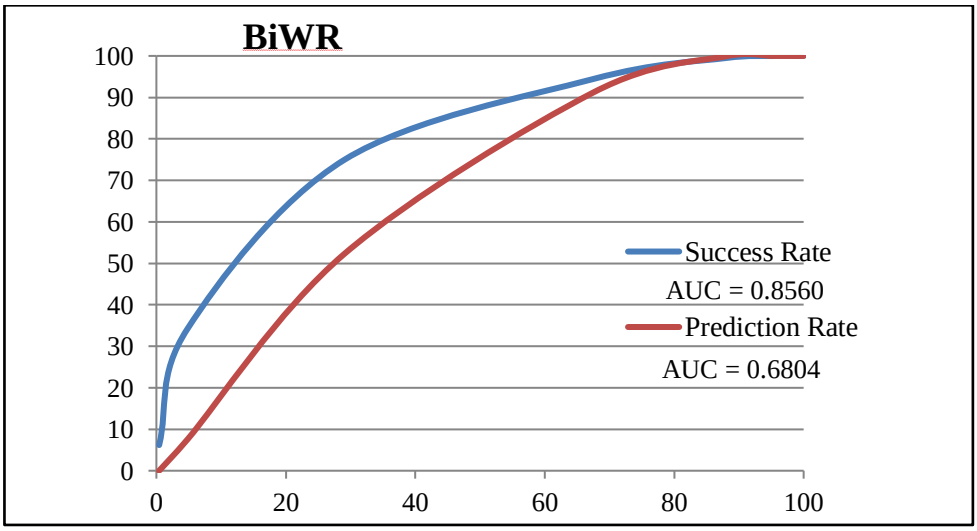

Figure 4-17 : Success rate and Prediction rate curves with AUC for the bivariate analysis with radar induced factors

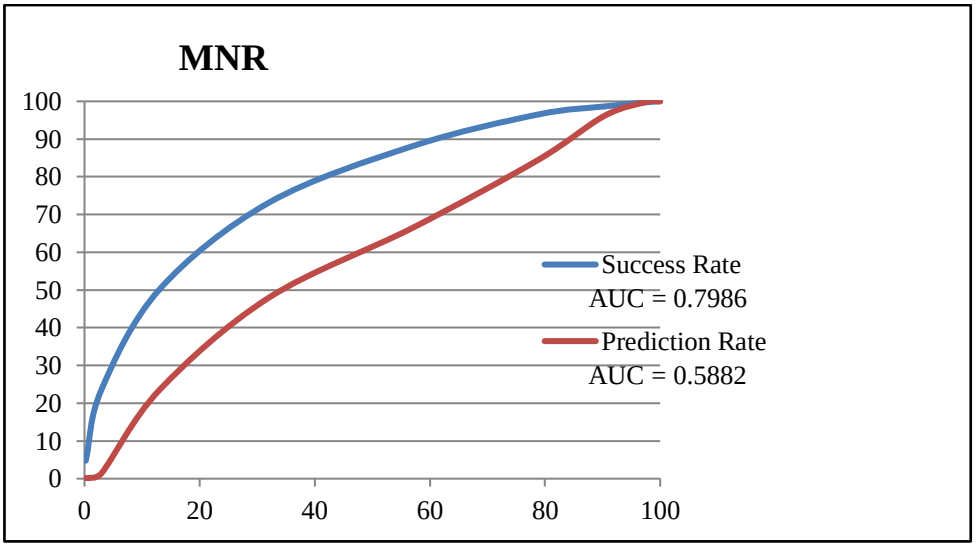

Figure 4-18 : Success rate and Prediction rate curves with AUC for the multivariate analysis without radar induced factors

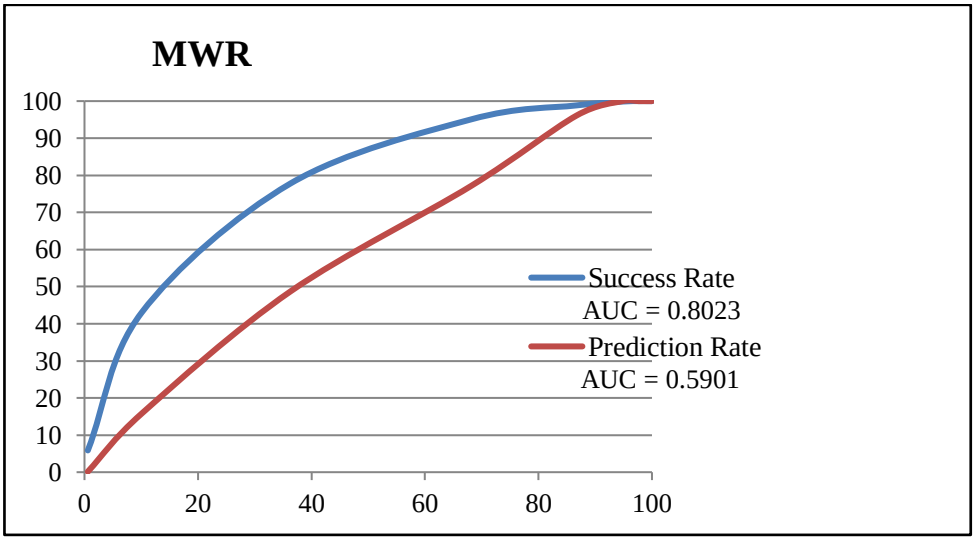

Figure 4-19 : Success rate and Prediction rate curves with AUC for the multivariate analysis with radar induced factors

The areas under the success rate curves measure how the landslide prediction analysis fit with the training data set, while the areas under the prediction rate curves measure how well the landslide prediction models and landslide causative factors predict the landslides. If the area under the ROC curve is closer to 1, the result of the test is

excellent and vice versa, and when AUC is closer to 0.5, the result of the test is fair or acceptable (Kamp *et al.*, 2008).

The AUC of all the success rates are more-or-less near 0.80, indicating good prediction performances according to the definition. The AUC of all the prediction rates are having values above, 0.50 indicating that they are within the acceptable range as per the definition. As such, they indicate that the accuracy of prediction rate of land susceptibility and the selection of land causative factors are somewhat acceptable, but not excellent even though the fit between the landslide prediction and the training data set are excellent [Table 4-4]. The incompleteness of the available landslide inventory map and an insufficient number of validation samples in the study area are reasons for the discrepancy. As a whole, better prediction and validation capabilities are shown by the bivariate analysis when compared with the multivariate approaches.

Table 4-4 : Comparison of area under Success rate and Prediction rate curves for bivariate and multivariate analysis with and without radar induced factors

AUC	BiNR	BiWR	MNR	MWR
Success rate	0.8315	0.8560	0.7986	0.8023
Prediction rate	0.6692	0.6804	0.5882	0.5901

4.6 Discussions and Conclusions

The main difference of bivariate and multivariate analysis is that in multivariate analysis, selected predisposing factors are also weighted by considering how each of them affect for landslide hazard. This study investigated fifteen landslide predisposing factors as elevation, slope, aspect, planar curvature, profile curvature, TWI, land use, lineament density, distance to hydrology, SMI in NDVI-T domain, geology, rainfall, soil moisture (Delta Index), surface roughness, and forest biomass. Most of the factors are derived from radar and optical remote sensing techniques, where smaller scale

studies with up-to-date information allows the work to be done to the meter-level accuracy, and repeated analysis simultaneously.

From the obtained results, it can be concluded that the bivariate and multivariate statistical analysis, with and without radar induced factors, can be used for landslide prediction analysis. However, with the integration of radar induced factors as surface roughness, near surface soil moisture from delta index, and forest biomass, the detection of the boundary between the high and very low susceptibility areas increased. When comparing the bivariate analysis with the multivariate analysis, the area identified as high susceptibility regions are increased when very low susceptibility regions decreased. As a whole, there is a slight improvement of prediction and validation performances of bivariate analysis than multivariate analysis.

4.7 Chapter Summary

InfoVal method as bivariate and MCDA based on AHP as multivariate with (15 factors) and without (12 factors) radar induced factors were considered for landslide prediction analysis. The InfoVal method combines the failure map with each thematic map to determine the weight of influence on terrain susceptibility for each parameter class. Integration of all weights of influences determines the terrain susceptibility levels for the landslides. The AHP is the structured technique for analysing and weighting multi criterions through the pair-wise comparison. Hence, each thematic map was analysed through the MCDA based on the AHP theoretical concepts. The four landslide susceptible maps from InfoVal method and MCDA based on AHP were divided in to four susceptibility classes as having very low, low, moderate, and high susceptibility to landslides.

The validation process was conducted in two methods as RFD calculated from validation samples and AUC of success rate and prediction rate curves generated from training and validation samples of the landslide failure map. Finally, as this chapter

shows that despite their simplicity, bivariate statistical methods have more acceptable precision than multivariate methods, and consequently, they are more compatible with the landslide prediction modelling. With the inclusion of radar induced factors, the discrimination between high and very low susceptibility areas are increased. Therefore, the result of this study can be used in the preliminary hazard mapping and selection of suitable locations for future land use planning.

CHAPTER 5 : PERFORMANCE ASSESSMENT OF RADAR AND OPTICAL REMOTE SENSING FOR LANDSLIDE DETECTION

Landslide detection is an essential requirement in pre and post disaster hazard analysis, and in early times, landslide detection was often achieved through time consuming, cost intensive field surveys and visual orthophoto interpretation. Now, EO (Earth Observation) data offer new opportunities for fast, reliable and accurate landslide identification at smaller scales, and can contribute for effective landslide monitoring and hazard management.

5.1 Introduction

Landslides are a very familiar, yearly event, to the Sri Lankan community. A fairly large number of landslides have occurred in Elapatha (1986), Abepura (2003), Helauda (2003, 2006), Naketiya (1998), Meeriyabedda (2014), Pambahinna (2016), and Aranayaka (2016) which took human lives, and damaged property and infrastructures (NBRO, 2016; Weerawansha *et al.*, 2007). Some highway stretches of A4 in Beragala and Koslanda areas, and Puswellawa on the A5 had to have extensive repair due to landslides in the last couple of decades. Furthermore, due to the Watawala landslide in 1990, the upcountry railway track was damaged and train travel was affected for a considerable period.

Frequently, detail landslide studies are performed by the field-based techniques with the use of aerial photo interpretation. However, most field techniques provide point-based discrete measurements of the landslides but do not consider any past movements. In active landslides, although the ground-based techniques can provide very precise information on displacement or deformation at very specific locations, especially in residential or areas with major infrastructures, they do not provide

information on the changes due to land sliding in wider area. Moreover, the field techniques in preliminary investigations of unstable areas may sometimes not be cost effective and advisable (Javier *et al.*, 2003; Rosin *et al.*, 2000).

Recently, all disaster management phases are becoming dependent on results derived from satellite image analysis when the damage area is large, and the terrain is mostly inaccessible (Tralli *et al.*, 2005; Voigt *et al.*, 2007). With the availability of a large number of Earth Observation satellites with a wide range of spatial, temporal and spectral resolutions, and better organization to share the data in emergency scenarios, the applicability of satellite remote sensing for disaster management is promising. High resolution remote sensing images, especially, have proved their potential for landslide studies in detection of the damages area, and assessment of the damage from the landslides (Guzzetti, 2004; Vinodkumar *et al.*, 2008), preparation of an inventory of landslides (Martha *et al.*, 2010a), estimation of the volume of the landslide (Martha *et al.*, 2010b), and monitoring of landslides for early warning purposes (van Westen and Lulie, 2003).

Optical sensors can provide information about the geographical phenomena that can be interpreted by the human directly. However, optical satellite image techniques are limited given that observations under cloud-cover conditions and during night time are not possible. SAR (Synthetic Aperture Radar) is free from these restrictions and thus becomes more convenient to be used, especially in post-disaster responses (Rathje and Adams, 2008; Yamazaki *et al.*, 2011). Landslides detection using the integration of radar and optical sensors are carried out frequently all over the world. Even though, there most studies to-date have combined the use of radar and optical remote sensing for landslide detections using different change detection techniques with advanced mathematical principles (Afify, 2011; Tsuchida *et al.*, 2015), without comparing and evaluating the performance of radar remote sensing for landslide detection.

Thus, the main objective of this section of the research is to compare the detection of Meeriyabedda landslide from optical and radar remote sensing techniques. The back-scattering characteristics from the C band radar images of Sentinel-1, acquired before and after the landslide event, are examined in order to extract the land use changes due to the landslide. The high resolution Geoeye and Worldview II optical satellite images, pre and post event scenarios, are analysed for detecting the landslide area from change detection techniques.

5.2 Study Area

A severe landslide occurred in Meeriyabedda area in Kotabathma Grama Niladhari division in Haldumulla Divisional Secretariat Division in Badulla District on 29th October 2014 at around 7.30 am [Figure 5-1 and Section 2.1.4]. Immediately after the landslide, JICA (Japan International Co-operation Agency) Technical Co-operation Project for Landslide Mitigation, together with the NBRO and DMC (Disaster Management Center), Sri Lanka, carried an air survey (Landslide, 2014).

5.3 Data and methodology

The information about the radar and optical satellite images that have been utilized and methodological flow followed in order to achieve expected objectives are discussed in this section.

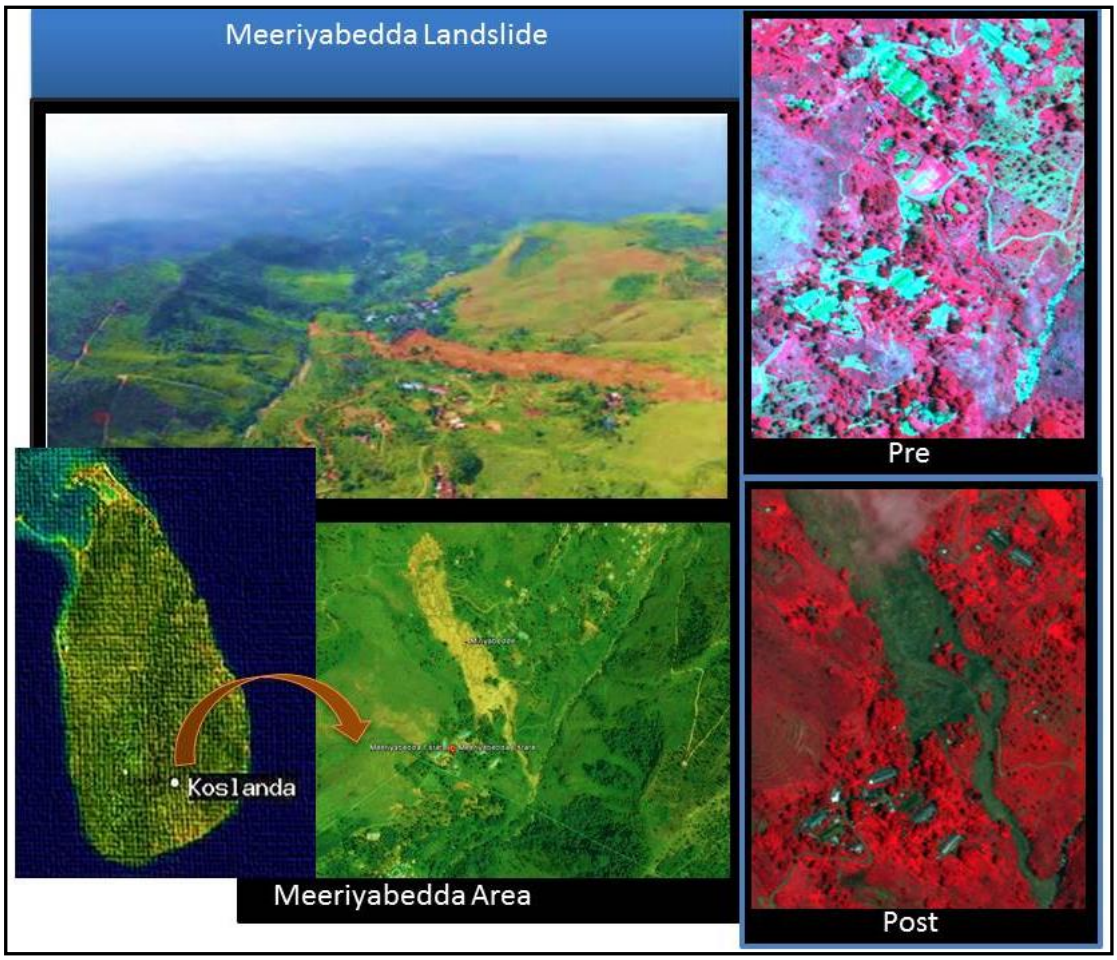

Figure 5-1 : Meeriyabedda Landslide in Koslanda, Sri Lanka and its pre and post high resolution satellite views

5.3.1 Data

Current study depended entirely on optical satellite images from Geoeye and World View II, and the radar images from Sentinel 1, acquired before and after the Meeriyabedda landslide. Optical images before the event were obtained on 16th May 2013 without any cloud cover, and the image after the event was from 06th November 2014 with 0.114 cloud cover. It was a difficult task to find cloud-free images after the event due to the prevailing bad weather conditions. All optical images obtained had the bands Red (R), Green (G), Blue (B), and Near Infrared (NIR) standard colors at a 2 m spatial resolution, and the panchromatic bands at 0.5m resolution. Sentinel-1 radar images before the event were captured on 19th October 2014, and the image after the

landslide was acquired on 31st October 2014 at a 10 m spatial resolution. Though the radar images are independent from the sun illumination and weather conditions, thus providing clear images even in the disaster situation, feature extractions are restricted to the nature of radar imaging and spatial resolution. A 7 m resolution DEM was derived from the method of aerial triangulation using aerial photographs from 1993, as discussed in section 2.2.1.

5.3.2 Methodology

The methodology consisted of two major components depending solely on the data used. The landslide area was detected from both optical and radar images using inherent change detection techniques. In order to extract the ground surface changes following a landslide, the satellite images before and after the event were geometrically co-registered and radiometrically normalized, enabling for pixel-based analysis. The general flow chart shown in Figure 5-2 gives a quick look at the overall set up of this research for delineating the damaged area due to the landslide.

During the pre-processing stage, the DNs (Digital Numbers) were converted into the TOA (Top-Of-Atmosphere) reflectance for both Worldview II and Geoeye images with their own parameters (earth sun distance, solar zenith angle, mean solar atmospheric spectral irradiances, and spectral radiance). Geometrical registration of high-resolution optical images of hilly terrain areas require orthorectification to remove the effects caused by relief displacements. Hence the orthorectification of pre and post images were performed by using the 7 m resolution DEM derived from aerial triangulation (Hervas *et al.*, 2003).

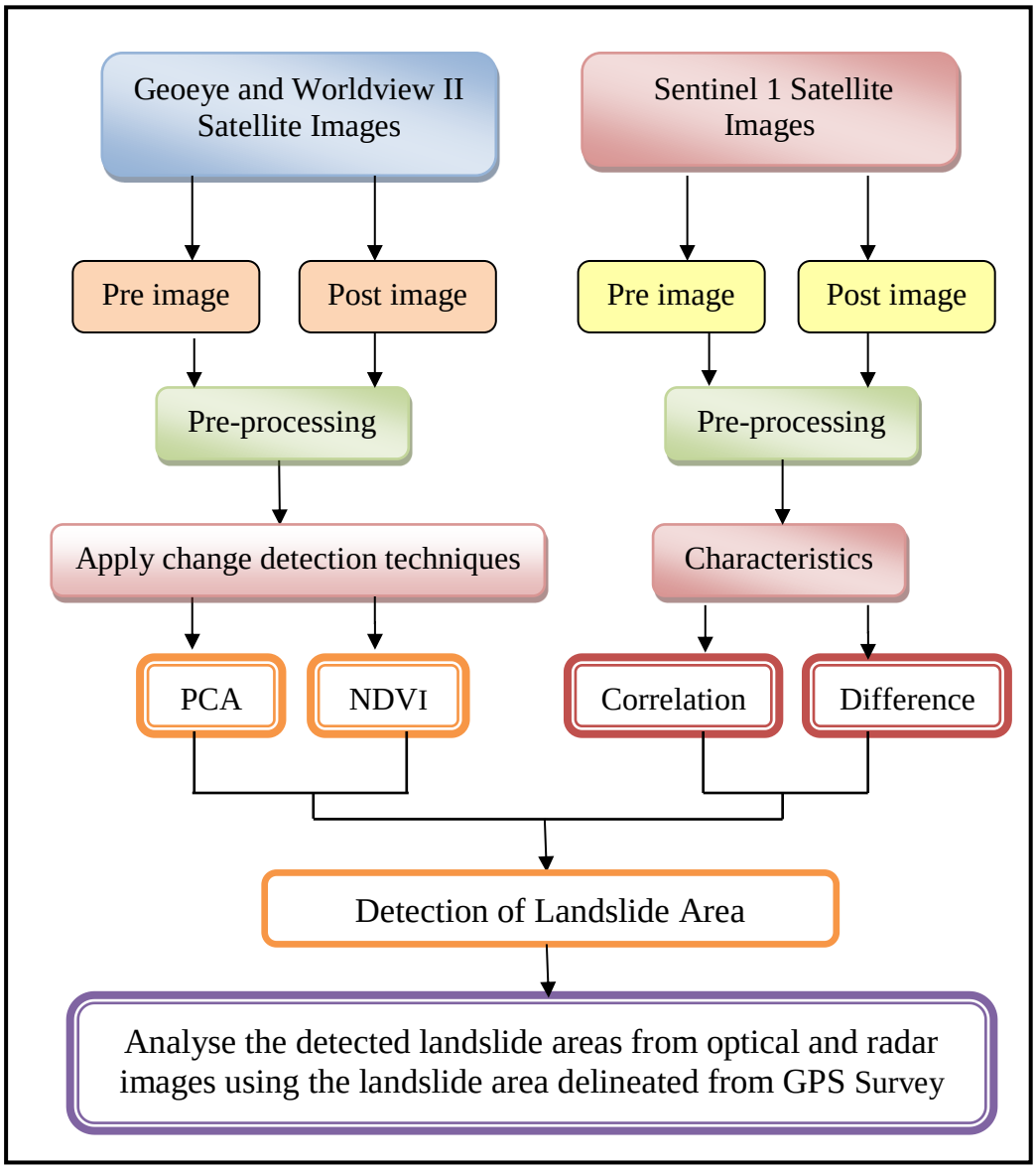

Figure 5-2 : Conceptual methodology for detecting Meeriyabedda Landslide from radar and optical satellite images

In the radar imaging approach, Sentinel-1 images before and after the event were radiometrically calibrated by converting the original DN values pertaining to the intensity data of the C band of the Sentinel-1 satellite to the backscattering coefficients. In order to reduce the speckle noise effect and to obtain the square shaped pixels, using enhanced lee filter, multi look processing and image filtering were performed. In the next step, the two images were corrected for image displacement due to relief, and geometrically registered using SRTM 30 m DEM.

Afterwards, PCA and NDVI change detection analysis for optical images, and with the mathematical relationships for analysing the change, the correlations, and the difference parameters for radar images were calculated for delineating the area of the landslide disaster. Detected landslide areas were then compared with the area extracted from the ground-based GPS surveying.

5.4 Landslide detection from optical images

In most cases, a landslide displaces a significant portion of landmass in mountainous regions. As it causes for changes to some geomorphological settings, identification of such changes is difficult from spectral domain alone, when using either satellite or aerial data sets. The common noticeable element after the occurrence of landslides is the loss of vegetation and exposure of fresh rock and soil. With the high-resolution images used in this study, it can be interpreted that some buildings, roads and part of vegetation with trees have collapsed [Figure 5-3]. This unique property from the nature of landslide is taken in to consideration for the detection of damaged areas when using PCA and NDVI change detection techniques.

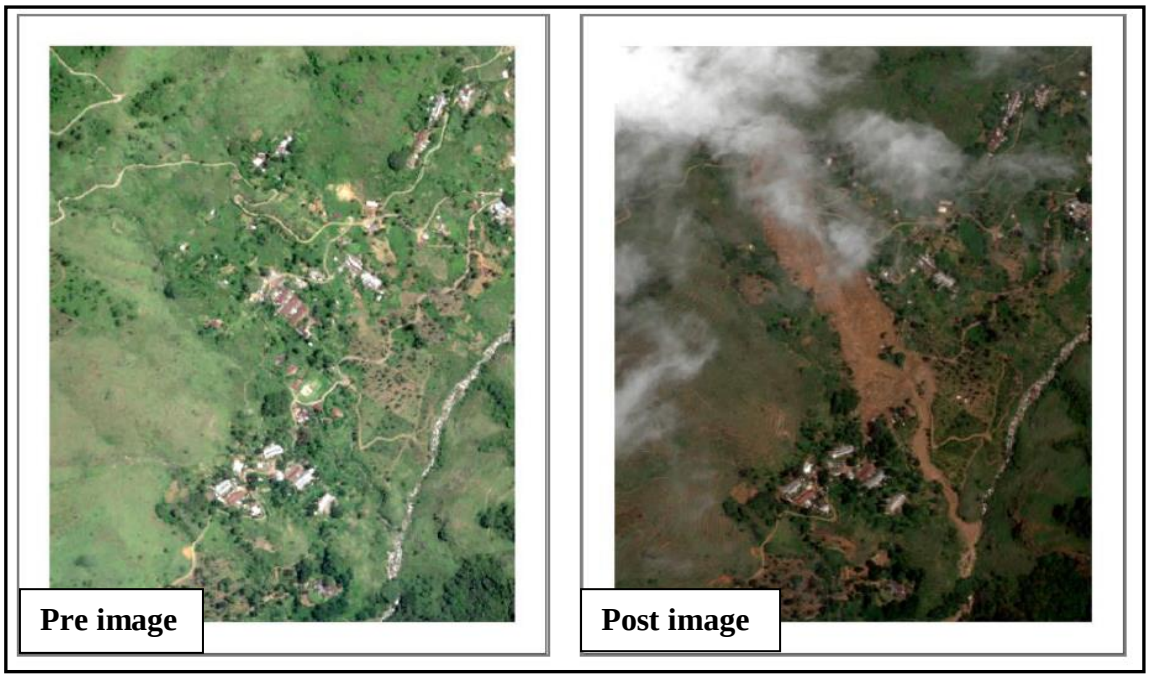

Figure 5-3 : Worldview II satellite image (before) with damaged properties and Geoeye image (after) with Meeriyabedda Landslide

5.4.1 Principle Component Analysis

The PCA is a technique that can be applied to both multispectral and hyperspectral remotely sensed data, as a method of data compression. PCA allows redundant data to be compacted in to lesser bands. The bands of PCA data are non-correlated and independent. Hence, interpretation of such bands, or components, is easier than when using the source data [Figure 5-4].

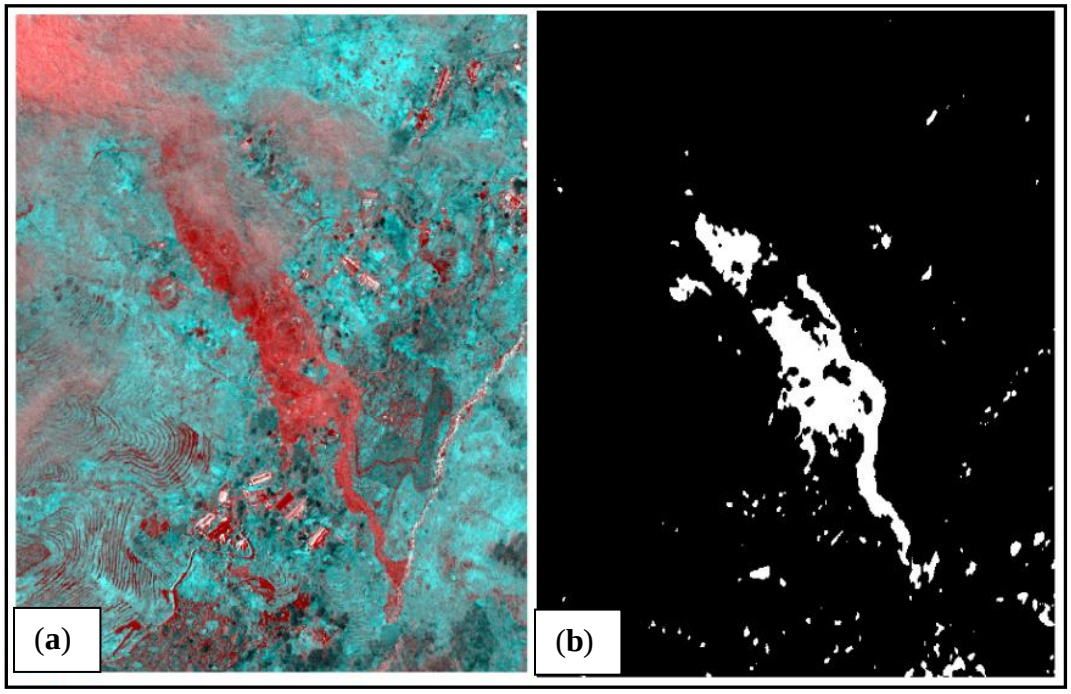

Figure 5-4 : Landslide detection from PCA applied for high resolution optical images. (a) – red colour, (b) – white represent detected change from the pre and post images

In this research, PCA was performed for the post and pre-images of Meeriyabedda separately. All the principle components from the pre and post images were first analysed in order to delineate the landslide area from the surrounding. Then, the colour composite image was generated by assigning Red, Green, and Blue colors for appropriate bands so as to identify the damaged areas from the landslide [Figure 5-4 (a)]. By trial and error, it was found that by assigning Red colour for the PCA2 from the post image and Green and Blue for the PCA1 from the pre-image, the landslide component can be extracted.

The next step was to calculate the principle components for the difference image that were obtained by subtracting the reflectance values of pre-image from the post image. All possibilities for extracting the landslide area as a change from the post image were investigated. The difference between PCA1 and PCA4 gives the better discrimination of reflectance values for the disaster region. Hence, by applying a threshold value (difference > 0) for the PCA1 and PCA4 difference image, it was possible to detect the landslide area from the surrounding [Figure 5-4 (b)].

5.4.2 NDVI

The study area consisted of a combination of buildings, roads and part of vegetation with trees. Thus, it can be noted that, the landslide caused a reduction of NDVI values due to the exposure of bare soil. Since the pre-event image was taken in May 2013, while the post-event was in November 2014, the NDVI is supposed to have increased in most pixels. If the NDVI had decreased, then landslides might have occurred in the corresponding area. Thus, it is correct to assume that pixels with reduced NDVI values after the event can be considered as corresponding to the landslide area. The clouds that existed in the post-event image were a disturbance for better delineation of the landslide area.

In order to extract damages to the vegetation due to the landslide, and the vegetation changes within the time period, NDVI ratio was calculated using the combination of Near Infar Red (NIR) and Red band as [(NIR-Red)/(NIR+Red)] for the post-event image, and the difference image separately. NDVI difference image identified the main change features as cloud patch and the landslide region. However, the boundary was not clearly extracted due to the fact that the buildings inside the landslide damaged area were not recognized as changes by the difference image. This is because the image pixels for buildings in the pre-image and debris flow in the post image were not really different [Figure 5-5 (a)]. The NDVI of the post-event image identified the cloud

patch, the landslide area, and the additional buildings developed within this time period [Figure 5-5 (b)].

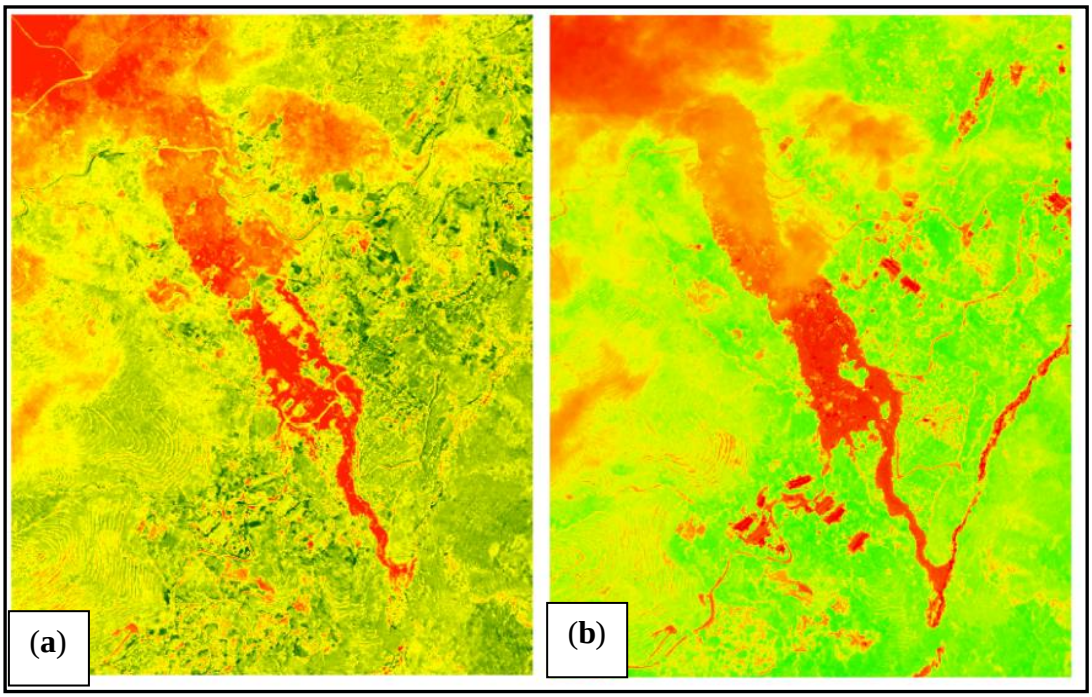

Figure 5-5 : Landslide detection from NDVI analysis for high resolution optical images. Red colour features are detected change from pre and post images

5.5 Landslide detection from radar images

The backscatter values of radar images depend highly on the radar viewing geometry. Due to side looking configurations, the intensity images of radar were highly affected by the incidence angle with the earth surface. Especially in mountainous regions where topographical effects are most prominent, radar intensity images suffer mostly from typical topographic effects of layover, foreshortening, and radar shadow. Hence, careful consideration is needed when selecting appropriate radar images for a mountainous study area, as the slope angle and the orientation of the slope with respect to the radar illumination differ depending on the locations.

The radar images used in this research were mainly the C band and VV polarization from the freely available Sentinel-1 images. While looking at the timely radar images before and after any disaster situations, radar images are independent from the sun illumination and weather conditions, and provide cloud free clear images. Meeriyabedda landslide in Koslanda area occurred on 29th October 2014. It was possible to obtain the free radar images from 19th October 2014 and 31st October 2014 for analysis to detect the landslide area. However, due to limitations of spatial resolution and spectral characteristics of radar images, visual image interpretations for feature extractions were not conclusive [Figure 5-6].

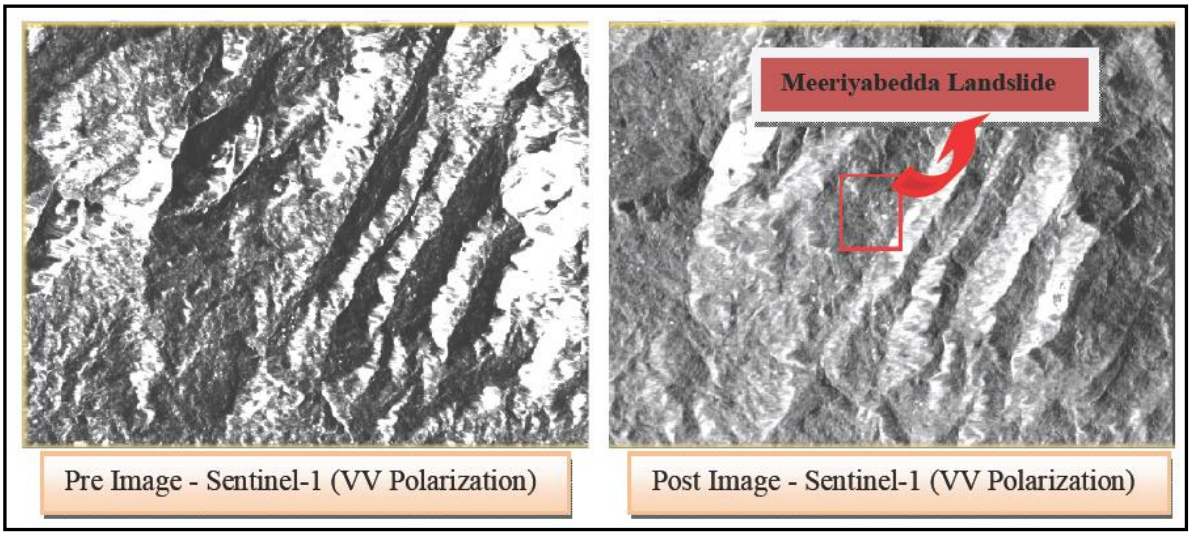

Figure 5-6 : Radar images before and after the Meeriyabedda Landslide in Koslanda area

The two images pertaining to the pre and post disaster events were first radiometrically calibrated, while multi look processing was performed in the second step so as to reduce the speckle noise and obtain square shaped pixels. Speckle noise was reduced again using an enhanced Lee filter. Finally, the radar images were geometrically corrected for the terrain using the 30 m SRTM DEM that were freely available. After completing all the pre-processing stages for correcting the two images that are geometrically co-registered and radiometrically balanced, change detection techniques were applied with the intension of extracting the damaged areas due to the landslide.

5.5.1 Correlation and Difference

In order to extract the changes due to the landslide, the correlation coefficient and the changes between the pre-and post-event radar images were calculated for the landslide area. The reduction of the correlation coefficient was mainly expected from the landslide damaged area, with some radar illumination changes. Seasonal changes of forest canopy and vegetation patches cannot be expected as the temporal difference of two images were only a few days.

With the purpose of examining the characteristics of radar backscatter values in the landslide area, Figure 39 plots the relationship between the correlation and difference of the two radar images before and after the landslide. Theoretically, if any changes of geographical phenomena occurred in-between these two image acquisitions, the smaller correlation (<0) or minus relationships define the change. It can be visually interpreted that the area damaged consisted of some buildings and vegetation. Hence, the backscatter value reduced from the pre-image to the post disaster image [Figure 5-7].

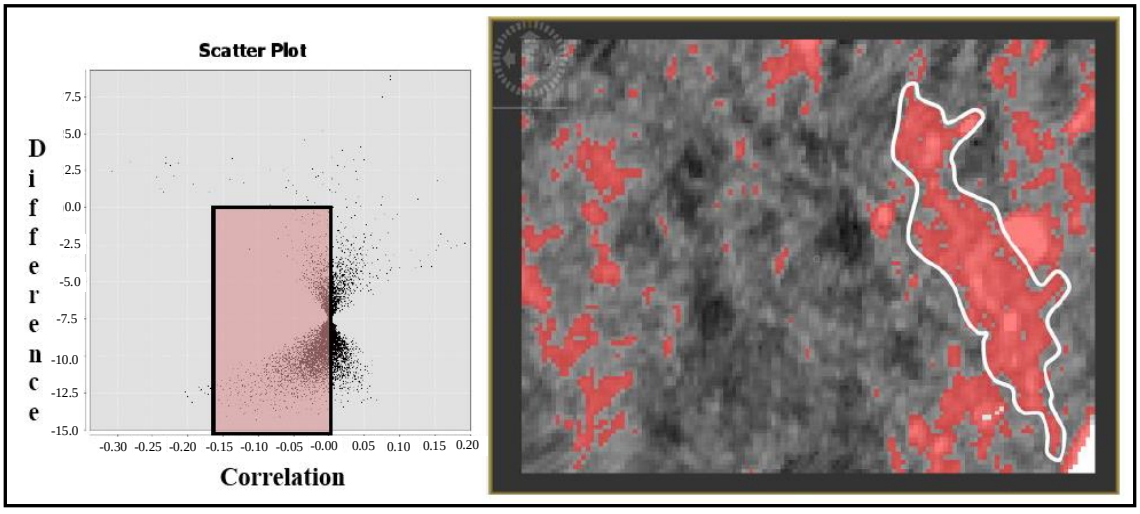

Figure 5-7 : Areas detected as change from 19th - 31st October 2014 from image correlation and difference domain

Additionally, a similar phenomenon was observed even in the difference image (minus values represented the change areas in the scatter plot). By taking all concepts into the consideration, change pixels were extracted by selecting the Region of Interest (ROI) from the minus areas of the scatter plot. The possible range of landslides in the correlation vs. difference plot, and the extracted landslide areas after masking are illustrated in Figure 5-7.

5.6 Results Analysis

In this research, the main objective was to detect the landslide from radar and optical remote sensing techniques by applying different change detection methods. Consequently, the PCA and NDVI change detection techniques used in the optical approach were applied to two high resolution images before and after the event. The correlation and difference theory were applied for the Sentinel-1 radar images in order to extract the change due to the landslide.

The interaction between NIR, Red and Green standard colour bands in optical images with the real earth features as vegetation and manmade features was different. By taking these facts into consideration, PCA and NDVI analysis were performed. Validating the results from analysis were of paramount importance to confirm the significance of the applied methodology. In this process, detected landslide areas were numerically compared with the area derived from GPS field surveying technique. GPS survey was carried using LICA handheld GPS with the positional accuracy of 3m for extracting the landslide boundary in July 2015. At that time, field surveying in the landslide area was possible as the area was free from the risk of disaster. Table 5-1 contains the percentage of the accuracy of area detected as landslide from difference change detection techniques when compared with the area observed through GPS survey.

It is observed that the area detected from optical approaches provide a lesser percentage of accuracy when compared with the radar method. This is mainly because of the cloud effect on optical images, especially due to the prevailing weather conditions during a disaster situation. The damaged area from the GPS survey was 80692 m^2. The accuracy percentages from the optical methods range from 63% to 76%. The colour combination of PCA derived from the two images identified the landslide area damage better than the other optical approaches. By proving the radar capability in the study of disaster, the landslide area detected from Sentinel-1 images showed the higher percentage of accuracy than any optical methods. It was around 86% when compared with the reference area as shown in Table 5-1.

Table 5-1: Comparison of the detected landslide area from optical and remote sensing techniques with the area from GPS survey

Change Detection Techniques		Landslide delineated area (m^2)	Accuracy (%)
GPS Survey		**80692**	-
OPTICAL	Principal Component Difference	50480	63
	Color Combination of Principal Components	61179	76
	Post NDVI	57268	71
	NDVI Difference	52163	65
Radar Images Analysis		69680	86

5.7 Discussion

This research study investigated the capability of radar and high-resolution optical images to extract the landslide from different change detection techniques. The native characteristics of radar and optical images for landslide studies, and the capability of different change detection techniques with respect to an area like Meeriyabedda to determine the change due to landslide, were examined. In an approach of using high

resolution optical images, PCA and NDVI change detection techniques for the Worldview II (pre-event) and Geoeye (post event) were applied.

In the image analysis using PCA, the influence of clouds was reduced when compared with the other optical based methods. The reason is that, most of the cloud pixels and landslide pixels depart to the two different principal components. However, the influence of the total cloud effect was difficult to avoid. The principle behind the NDVI difference technique is also an acceptable method to detect certain changes due to landslides. However, it is limited as this method is more appropriate to identify changes over vegetation or forest covers. In the NDVI difference image, some pixels inside the landslide have been identified as unchanged pixels, even though it is clearly observed that those pixels should be related to the damaged area. The fact that these pixels were covered by buildings before the occurrence of the landslide, can be shown as a reason for this, and as such, higher NDVI differences cannot be expected from those pixels.

However, there are some advantages with the above limitation, as most of the manmade properties which were damaged by the landslide could be clearly identified from the NDVI difference image. Hence, these results would be very useful for rescue efforts like searching for survivors. The post NDVI image clearly extracted most parts of the landslide (71%), but it is difficult to directly state that the post NDVI result is more accurate than the NDVI difference image as it does not indicate any change. However, if there are some prior knowledge about the land use in the area, and if any changes had occurred in a vegetated region, then the post NDVI image provides better clues about changes due to landslide in the study area.

The main difficulty in detecting the change using optical images is having clouds over some areas. This is because clouds hide some important information while getting classified as changes. In the case of SAR images in mountainous regions, the backscatter is highly affected by the incident angle and angle of slopes, more so than

the type surface materials and their conditions. Furthermore, radar back scatter changes with the illumination conditions of the time of data acquisition due to the side looking configurations. Hence, the most appropriate radar images have to be selected very carefully, and then used for the change detection analysis. This research aimed to use freely available, C band images at 10 m resolution from the sentinel-1 with VV polarization for detecting the landslide. It was difficult to perform the pre-processing of radar images in pre and post event with the freely available Sentinel-1 images to better suit the change detection analysis as they covered a much-undulated region with serious geometrical distortions. However, it was possible to obtain more than 80% accuracy for delineating the landslide area by using a subset that included the Meeriyabedda landslide.

According to the validation results, colour combination of PCA had produced better results (76%) than other optical methods because all available bands were utilized in the analysis process. The PCA difference and the NDVI difference gained least accuracy (63% and 65% respectively), for landslide detection as the methods caused some other radiometric changes of land cover and illumination than the change due to landslide in pre and post image acquisitions. Yet, due to the advantages shown by radar in disaster situations (with prevailing bad weather conditions and timely information in smaller scale), radar remote sensing techniques have proven their suitability for disaster studies. As such, it can be concluded that radar remote sensing for landslide detection offer significant advantages. At the same time, detection of the landslide from PCA in optical techniques is also acceptable at more than 75%, even though both techniques have their own limitations.

5.8 Chapter Summary

Two radar and optical images before and after the event are used in order to delineate the landslide area from different change detection techniques. Geometrically registered and radiometrically normalized World View II and Geoeye optical images

were used. Satellite image pixel intensity changes were extracted by calculating the NDVI and PCA. Two pre and post Sentinel-1 images were pre-processed in order to apply pixel-based classifications. Backscatter difference and the correlation coefficient between two images were examined to threshold the image in order to extract the changed pixels or landslide area from non-changed pixels. Due to weather independent capability of radar images, all the landslide regions were detected. However, radar suffers serious geometrical distortions specially when studying the high relief terrain areas. Moreover, when considering the spatial resolution, radar has some limitations to detect small landslides as compared to optical images.

Detected landslide areas from radar and optical images were compared with the area extracted from the GPS field surveying technique. Comparison distinguished that the colour combination of PCA produced better results (76%) than the other methods of using optical images. With the inherent nature of the radar images in disaster situation, radar image analysis has confirmed the suitability for disaster studies by identifying 86% of the area from landside. Finally, it can be concluded that the radar remote sensing can be successfully used for landslide detection, but PCA in optical techniques is also acceptable for the same purpose.

CHAPTER 6 : ENHANCEMENT OF LANDSLIDE SUSCEPTIBILITY ANALYSIS THROUGH THE INTEGRATION OF DEBRIS FLOW

Landslide is a natural disaster which occurs frequently in the mountainous region. Debris flows are most dangerous processes due to their rapid rate of movement and long runout zone. Sudden and rather unexpected impacts produce huge damages to the buildings, infrastructure and human lives. Under intensive rainfall, debris flows tend to travel long distances following the steepest path and merging with the drainage network. This concept has been used to determine the areas that are prone to debris flows.

6.1 Introduction

Landslide susceptibility assessment is necessary for disaster management and planning development activities in mountainous regions. By assessing landslide prone areas, damages to human life and property can be reduced. The term susceptibility defines the location of potential landslides in a region based on the terrain characteristics. Many research studies of landslide hazard susceptibility analysis are accomplished by assuming that future landslides are likely to be produced by the same conditioning factors as the landslides in the past and the present (Carrara *et al.*, 1999; Guinau *et al.*, 2007; Varnes, 1984b). Even if such studies provide information on potentially unstable terrain regions, they do not necessarily supply the direct information on landslide magnitude and frequency. Although it is yet difficult to predict a landslide in space and time, various studies (Chung and Fabbri, 2003; Coe *et al.*, 2004; Dai and Lee, 2002; Guinau *et al.*, 2007; Hurlimann *et al.*, 2006; Kappes *et al.*, 2011) have proven that the integration of terrain failure susceptibility analysis and runout behaviour of the mobilized materials can provide improved end results on landslide susceptibility analysis.

The probability of spatial occurrence can be determined by heuristic, statistic (bivariate or multivariate) or deterministic approaches. Heuristically potential areas can be identified in the field and on aerial photographs. Statistical methods integrate various environmental factors for identification of the terrain failures or source regions at smaller scale. The models are based on the bivariate or multivariate statistics(Carrara *et al.*, 1999; Dai and Lee, 2002; van Westen *et al.*, 2006). After determining the potential source regions, runout behaviour can be analysed by using the empirical, analytical and numerical approaches in order to demarcate the areas that could be reached by the debris (Dai and Lee, 2002; Hurlimann *et al.*, 2006).

Especially in developing countries, scarcity of good quality data, insufficient funds, lack of specialized expertise are some factors that severely affect for proper landslide susceptibility assessments. Hence, there is a necessity of developing a low-cost methodology for landslide susceptibility assessments. With the recent technological developments, even the developing countries tend to use GIS as its tools enable the handling and production of large amount of data. DEM has become very significant in most environmental studies, and has proven its importance in the study of landslides (Guinau *et al.*, 2007). Hence, one aim of this research is to develop a low-cost methodology for landslide susceptibility analysis with acceptable accuracy at a smaller scale as suited to the conditions in most developing countries.

6.2 Study Area

Landslides, earthquakes, tsunami and storms are, of course, natural disasters. Yet, their impact can be minimized by scientific planning and preventative measures. The growing incidence of landslides in Sri Lanka is getting higher with many damages to the economy in the up-country. Parallel to this, unplanned land clearing for tea and other plantations, forest degradation, changing the existing natural drainage patterns and dramatically reduced vegetation covers, make larger areas more vulnerable to

landslides. Koslanda is a remote or hilly area with geographically difficult access, facing many harsh weather conditions [Figure 4-1, Chapter 4].

6.3 Data Acquisition

Two types of data, DEM and landslide inventory map, enabled the development and validation of the terrain failure and debris flow susceptibility analysis in the study area. A 7 m resolution DEM was derived from aerial triangulation methodology, utilizing aerial photographs taken in 1993. The "Imagine photogrammetry" tool from ERDAS Imagine 2014 software was used to generate the DEM from aerial photographs. Camera calibration, interior orientation, and exterior orientation by using 25 GCPs were performed in order to generate the DEM from aerial triangulation.

Three devastating former landslides that occurred in the study area and other landmass failures are delineated from the aerial photographs captured in year 1997 and Geo-eye satellite image acquired on 06th November 2014 with 0.114 cloud cover. All these landslide images from different sources are integrated in to one polygon shapefile with ArcGIS (version 10.1) with the purpose of generating the landslide inventory map. In order to carry out a joint analysis of landslides and DEM data, the landslide regions are rasterized to the DEM resolution.

6.4 Methodology

The methodology of this work contains the terrain failure and the debris flow susceptibility analysis. The flow chart shown in Figure 6-1 illustrates the methodology followed in the terrain failure susceptibility analysis for this study area. Terrain failure susceptibility analysis is performed by using four terrain factors derived from DEM, and the training samples from landslide inventory map in the study area. The resultant

terrain failure susceptibility regions were validated using validation samples from the landslide inventory map from RFD (Relative Failure Density) analysis.

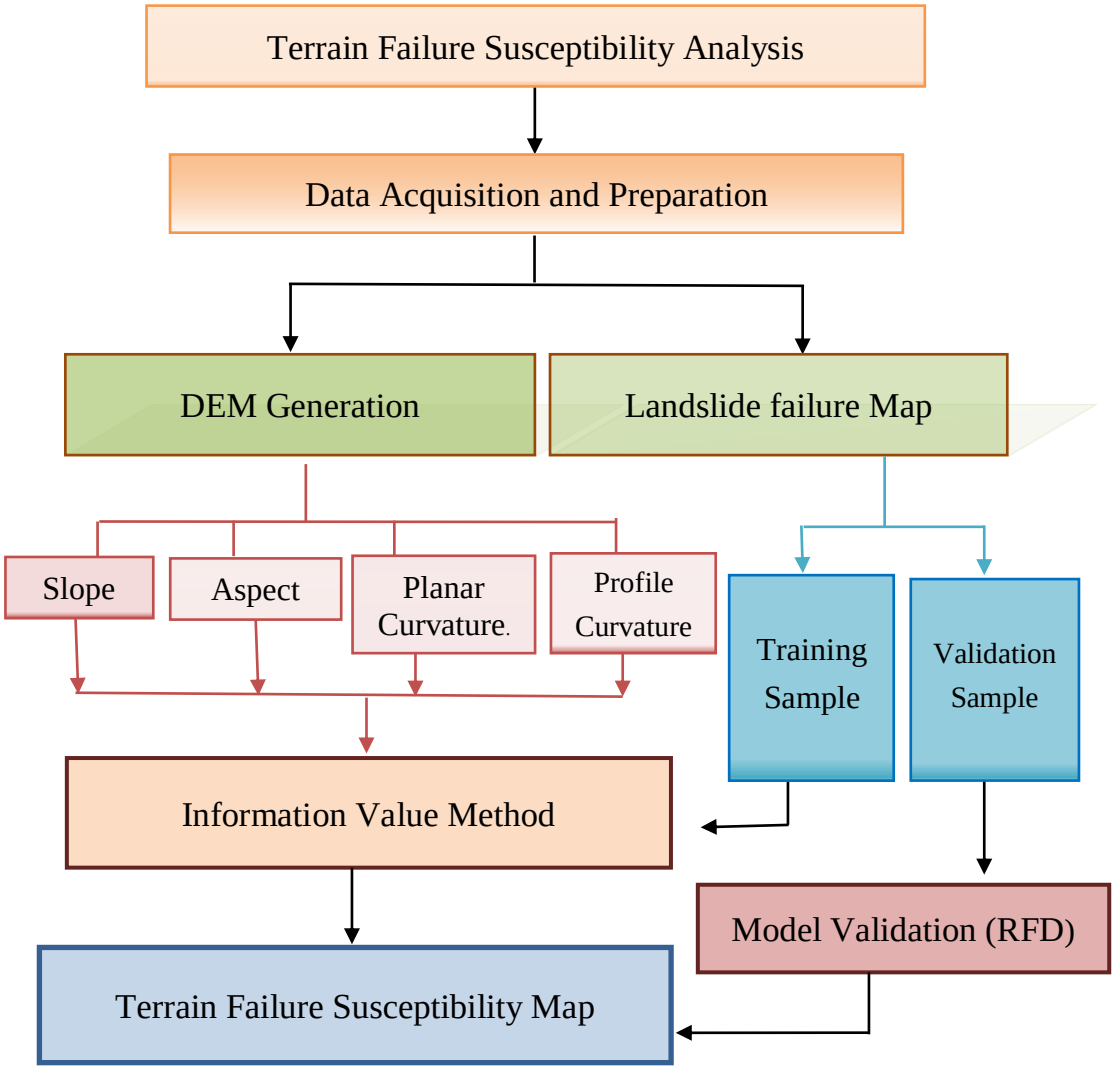

Figure 6-1 : Methodological flow to analyse the terrain failure susceptibility regions

Debris flow analysis considered the fact that under intense rainfall, debris flows tend to travel long distances following the steepest path, and merges with the drainage network (Guinau *et al.*, 2007; Pall`as *et al.*, 2004). In this study, the debris flow susceptibility regions are extracted with the use of the open source TauDEM 5.1 software developed by (Tarboton, 1997), which is electronically available on the internet (http://www.engineering.usu.edu/dtarb/taudem, accessed on 12th February

2016). Figure 6-2 illustrates the methodology followed to extract the debris flow susceptibility regions in the study area. This straight-forward statistical calculation allows determining the contribution of each terrain factor for ground instability assessment by using common GIS tools and simple raster calculations.

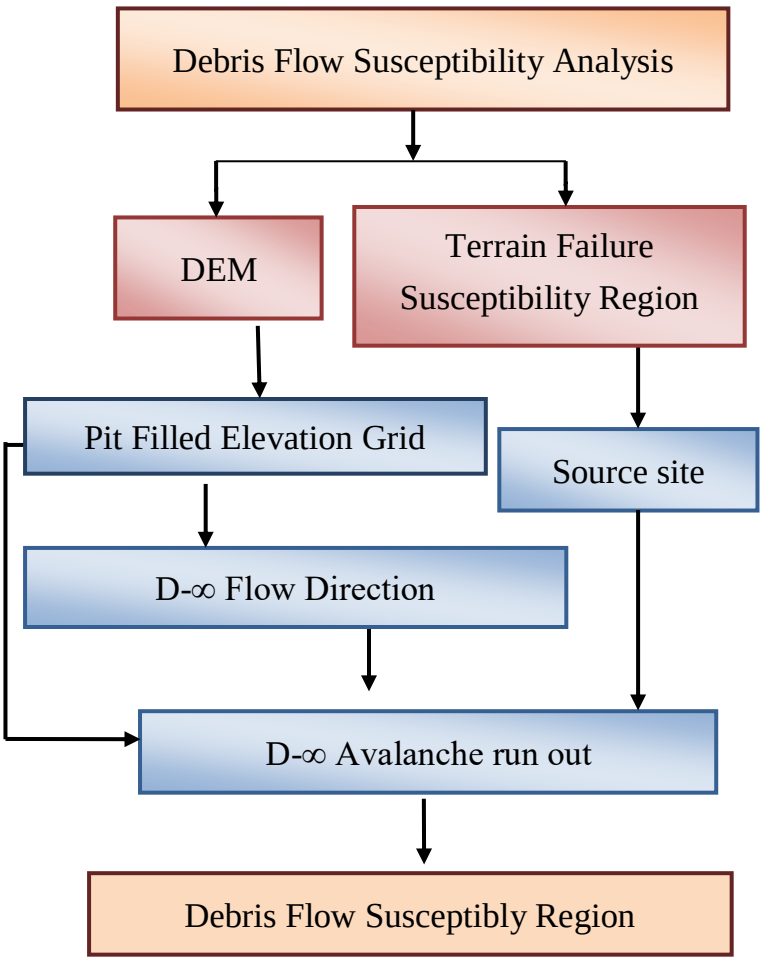

Figure 6-2 : Methodological flow to analyse the debris flow susceptibility regions

TauDEM (Terrain analysis using Digital Elevation Models) is an open source software developed by (Tarboton, 1997) for hydrologic terrain analysis and channel network extraction. This software can be executed as an ArcGIS extension. Three simple tools are utilized as Pit remove, D-∞ flow direction and D-∞ avalanche runout. Pit remove identifies all pits in the DEM and raises their elevation to the level of the lowest pour point around their edge. The D-∞ flow direction is defined as the steepest downward slope on a planar triangular surface encoded as an angle of radians between 0 and 2π.

The D-∞ avalanche runout identifies an avalanche's affected area and the flow path length to each cell in that affected area from a given source pixel.

6.5 Terrain Failure Susceptibility Analysis

Bivariate statistical analysis is simple and is a quantitatively suitable technique for terrain failure analysis (Saha *et al.*, 2005). The aim of this work is to combine instability condition of terrain factors and landslide inventory map so as to determine the weight of influence for each factor class. The weights are then added to obtain the TFSI (Terrain Failure Susceptibility Index) for each pixel (Guinau *et al.*, 2007). Even though continuous variables are more informative than the discrete variables, most end users can understand a map with susceptibility classes than strange numerical values (Begueria, 2006; Chung and Fabbri, 2003). Hence, in order to better visualize the terrain failure susceptibility classes in a map, terrain failure indices are generally classified in to four susceptibility classes as very low, low, moderate, and high.

Validating the results of predictions is of paramount importance to confirm the significance of the model and the model results. In this process, two independent samples as training and validating from the landslide inventory map are utilized. Training samples are used to generate the landslide susceptibility regions, and the validation samples are used for validating the results from the prediction analysis (Remondo *et al.*, 2003; Saha *et al.*, 2005). However, since this work is focused mainly on the contribution of debris flow path for the landslide prediction analysis, debris flow path regions are excluded from the training and validation samples in order to avoid the misclassifications.

6.5.1 Extraction of Terrain Factors from DEM

Terrain factors derived from the DEM are very significant in most environmental studies, and have confirmed the importance in the study of landslides (Guinau *et al.*, 2007). Four terrain factors are derived as slope, aspect, planar curvature and the profile curvature. Slope is the gradient of the elevation and aspect is the compass direction of the slope. Curvature is the second derivative of a surface or the slope of the slope. Planar curvature relates to the convergence and divergence of flow across a surface. The information regarding the degree of concavity or convexity along a line perpendicular to the slope profile can be extracted from the planar curvature. Profile curvature affects the acceleration or deceleration of flow across a surface. The degree of concavity or convexity of the slope profile can be explained from the profile curvature [Figure 6-3].

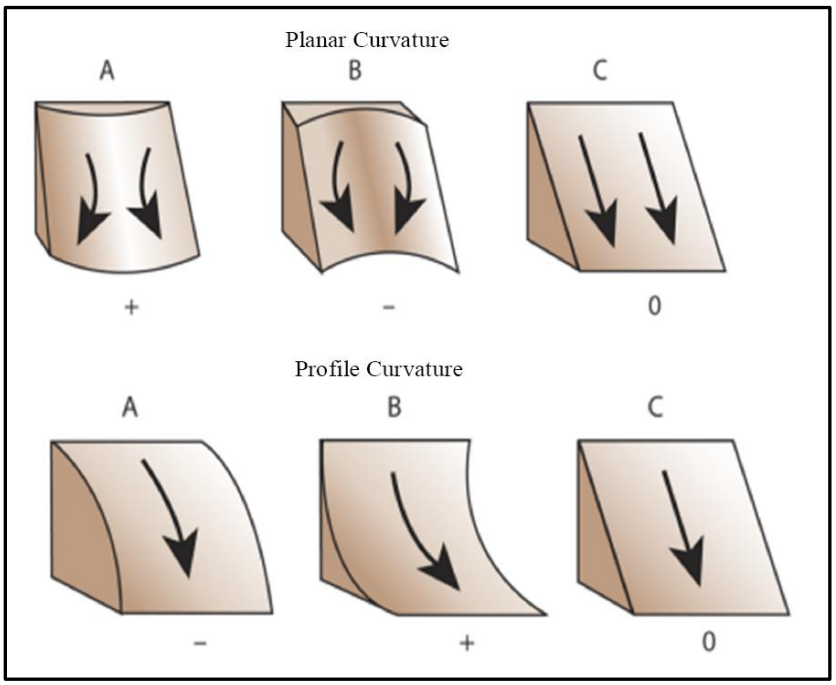

Figure 6-3 : Interpretation of geographical formation through planar and profile curvature. Planar curvature: A – surface is laterally convex and divergence flow across a surface, B – surface is laterally concave and convergence flow across a surface, C – surface is linear
Profile curvature: A- surface is upwardly convex and deceleration across a surface, B- surface is upwardly concave and acceleration across a surface, C- surface is linear. Source :http://desktop.arcgis.com/en/arcmap/10.3/manage-data/raster-and-images/curvature-function.htm

The negative values of planar curvature represent a surface that is laterally concave, and positive values indicate a surface that is laterally convex. For the profile curvature, negative values correspond to a surface that is upwardly convex while positive values characterize a surface that is upwardly concave. Figure 43 describe the thematic maps in which the discretized terrain parameters are represented.

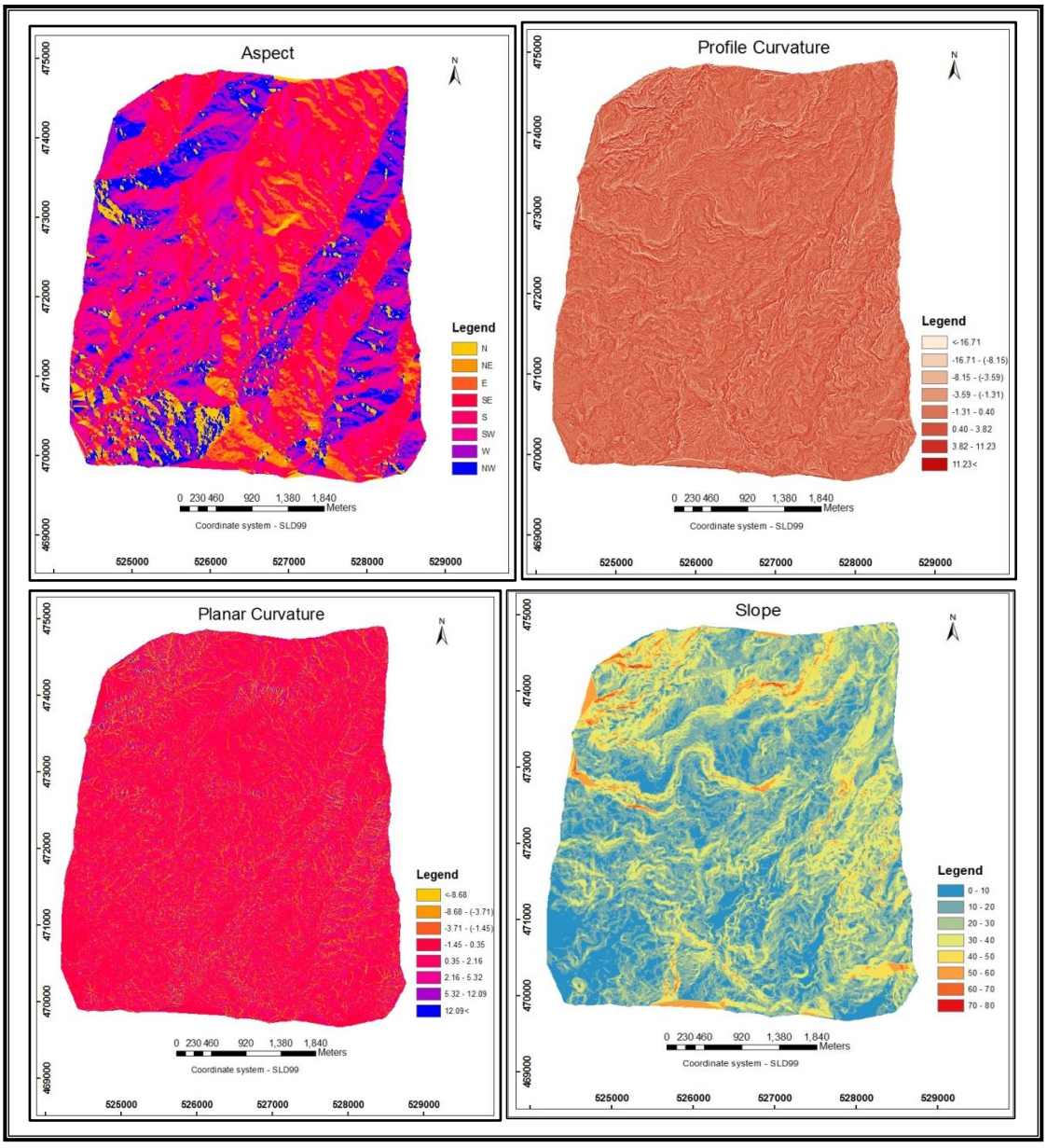

Figure 6-4 : Thematic maps obtained from the DEM. Each thematic map illustrates the generated terrain factors with discretized number of classes. Left to right and top to bottom, aspect, profile curvature, planar curvature and slope.

The basis for selecting these parameters is due to their influence on soil water content, which is responsible for landslide occurrences under heavy rain fall. According to the notions from NBRO, most of the landslides in Sri Lanka occurred due to the heavy and prolonged rainfall in the hilly areas.

6.5.2 Terrain failure susceptibility analysis using Information Value Method

Many research studies proposed the Information value method for terrain failure susceptibility analysis (Guinau *et al.*, 2007; Saha *et al.*, 2005; van Westen, 1997). This method combines the failure map with each thematic map to determine the weight of influence on terrain instability for each parameter class. The failure map consists of only the training samples. Then the weight of influence for landslide susceptibility is calculated by using formula derived in Information value method as described in Section 3.7.2 (ii) and Equation (2).

The information value weights obtained for each factor class and the area represented are tabulated in Table 6-1. It can be observed that the slopes between 30^0 and 50^0 consist of the higher Information Values in the Slope factor class. S, SE and SW factor classes in the aspect terrain factor contain higher information value weights than the other aspects. Once the Information Values of each factor class are calculated for all thematic maps, they are superimposed and added to obtain the TFSI for each pixel in the study area. The value of TFSI defines the landslide susceptibility levels as high TFSI for high susceptibility classes and low TFSI for low susceptibility classes.

Table 6-1 : Computed Information Value weights for each factor class in the four thematic maps

Terrain Factors	Factor Classes	Area (%)	Information Value
Slope	0-10	17	-0.037
	10-20	32	-0.067
	20-30	28	-0.027
	30-40	15	0.131
	40-50	6	0.111
	50-60	2	0.088
	60-70	0	0.022
	70-80	0	0.013
Aspect	N	4	-0.883
	NE	3	-0.502
	E	8	-0.28
	SE	21	0.003
	S	20	0.224
	SW	16	0.224
	W	17	-0.226
	NW	11	-0.687
Planar Curvature	< -8.68	1	-1.037
	-3.71	4	-0.109
	-1.45	13	0.043
	0.35	44	0.016
	2.16	27	0.025
	5.32	9	-0.11
	12.9	2	-0.334
	12.09 <	0	-0.554
Profile Curvature	< -16.71	0	-0.877
	-8.15	1	-0.483
	-3.59	5	-0.222
	-1.31	14	-0.019
	0.4	43	0.016
	3.82	32	0.041
	11.23	5	-0.108
	11.23 <	0	-0.645

6.5.3 Susceptible area discretization

For better understanding of the terrain failure susceptible regions, the area is discretized in to four susceptible classes as very low, low, moderate and high. The class separations are based on the cumulative percentage of failures as: very low susceptibility ($(-2477e^{-3}) < TFSI < (-872e^{-3})$) : interval containing 0% of failures, low susceptibility ($(-872e^{-3}) < TFSI < (-274e^{-3})$) : interval containing 10% of failures, moderate susceptibility ($(-274e^{-3}) < TFSI < (33e^{-3})$) : interval containing 30% of failures and high susceptibility ($(33e^{-3} < TFSI < (439e^{-3})$) : interval containing 60% of failures (Guinau *et al.*, 2007; Saha *et al.*, 2005). The value ranges for each percentage of failure are obtained after performing the equal interval classification for 10 classes in GIS environment. The whole study area is then discretized into four classes as 0%, 10%, 30% and 60% of failure regions for very low, low, moderate and high susceptibility classes respectively [Figure 6-5].

6.5.4 Results Validation

Validation is the most prominent phase in the prediction analysis (Chung and Fabbri, 2003; Guinau *et al.*, 2007; Remondo *et al.*, 2003). Validation is performed using separate validation samples which consist of the Meeriyabedda landslide. RFD analysis is used to quantify the accuracy of the predictions [Section 4.5.1 and Equation 16]. Figure 6-6 illustrates the RFD in each susceptibility class and it can be clearly seen that there is a gradual increase of RFD from very low to the high terrain failure susceptibility classes.

Even if the validation results imply that the prediction model is fit with the validation samples, it does not explain the predictive capability of the failures with temporal information. Figure 6-5 illustrates the terrain failure susceptibility map with the four landslide susceptible classes.

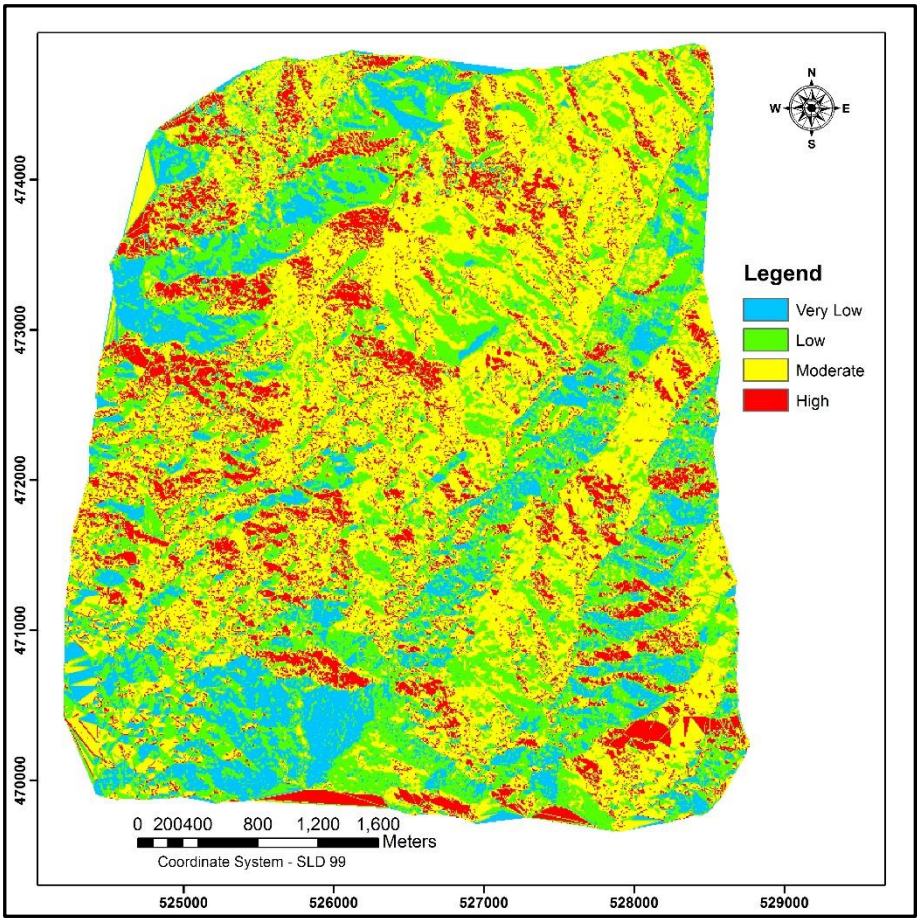

Figure 6-5 : Terrain failure susceptibility map with four landslide susceptibility classes

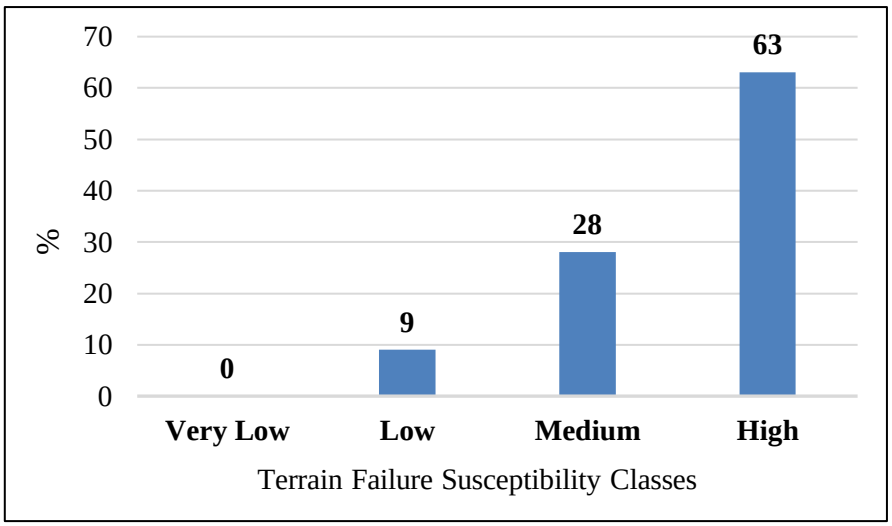

Figure 6-6 : Graphic showing of RFD for each terrain failure susceptibility class

6.6 Debris Flow Susceptibility Analysis

The debris flow behaviour is controlled by topographical structure, land use, soil type, debris volume, and the amount of liquefaction. Characterizing these parameters for debris flow prediction is a complicated task. This can be overcome by considering the debris flow path under intense rainfall that tends to follow the steepest path to connect with the drainage network (Guinau *et al.*, 2007; Pall`as *et al.*, 2004).

6.6.1 Debris Flow Susceptibility Assessment

High susceptibility class in the terrain failure map is used as the source zones to assess the debris flow susceptibility regions in the study area. Pit filled DEM is used to calculate the D-∞ flow direction in order to extract the steepest downward slope regions. With the use of D-∞ flow direction and the terrain failure high susceptibility regions as source points, the D-∞ avalanche runout identify the avalanche's affected area and flow path length from the source points. In order to discretize the avalanche affected area or DFR (Debris Flow Regions) into selected susceptibility classes, the study area is classified as 0% debris flow for very low (DFR<20), 10% debris flow for low (20<DFR<21.35), 30% debris flow for medium (21.35<DFR<23.93), and 60% debris flow for high (DFR>23.93) susceptibility classes.

6.6.2 Results Validation

Validation is performed by overlaying the validation sample on the classified image. At this point, the validation sample consists of the debris flow path as the debris flow analysis is entirely dependent on the way of hydrological modelling (Chung and Fabbri, 2003; Remondo *et al.*, 2003) RDFD (Relative Debris Flow Density) is used to quantify the accuracy of the debris flow analysis [Section 4.5.1 and Equation 16].

Figure 6-7 illustrates the RDFD (Relative Debris Flow Density) for each susceptibility class. There is a gradual increase of a RDFD from the very low to high terrain failure susceptibility classes (2%, 6%, 28%, and 64%). The validation results confirm that the prediction model is fit with the real landslide scenarios (validation samples), and Figure 6-8 shows the debris flow susceptibility map with four landslide susceptibility classes.

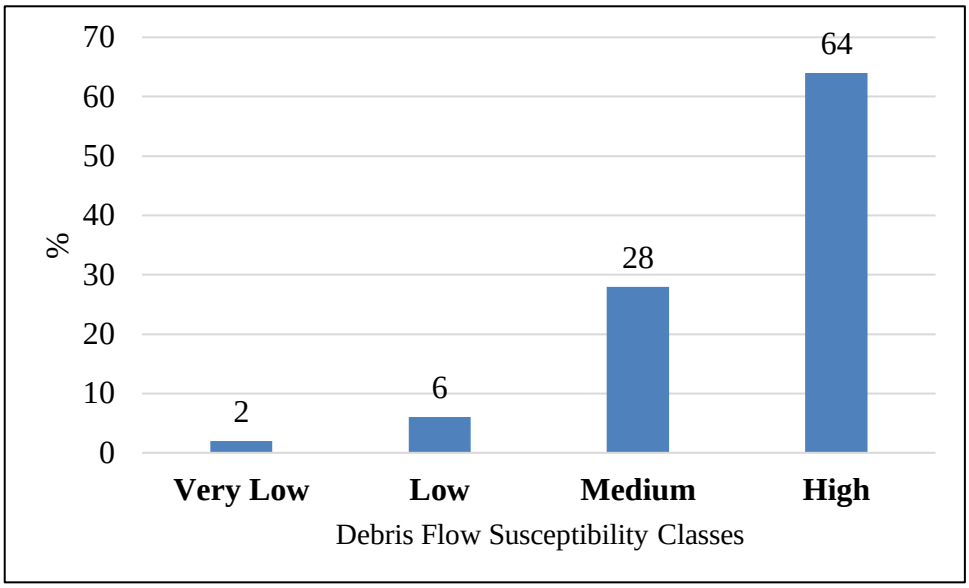

Figure 6-7 : Graphic showing of RDFD for each Debris Flow susceptibility class

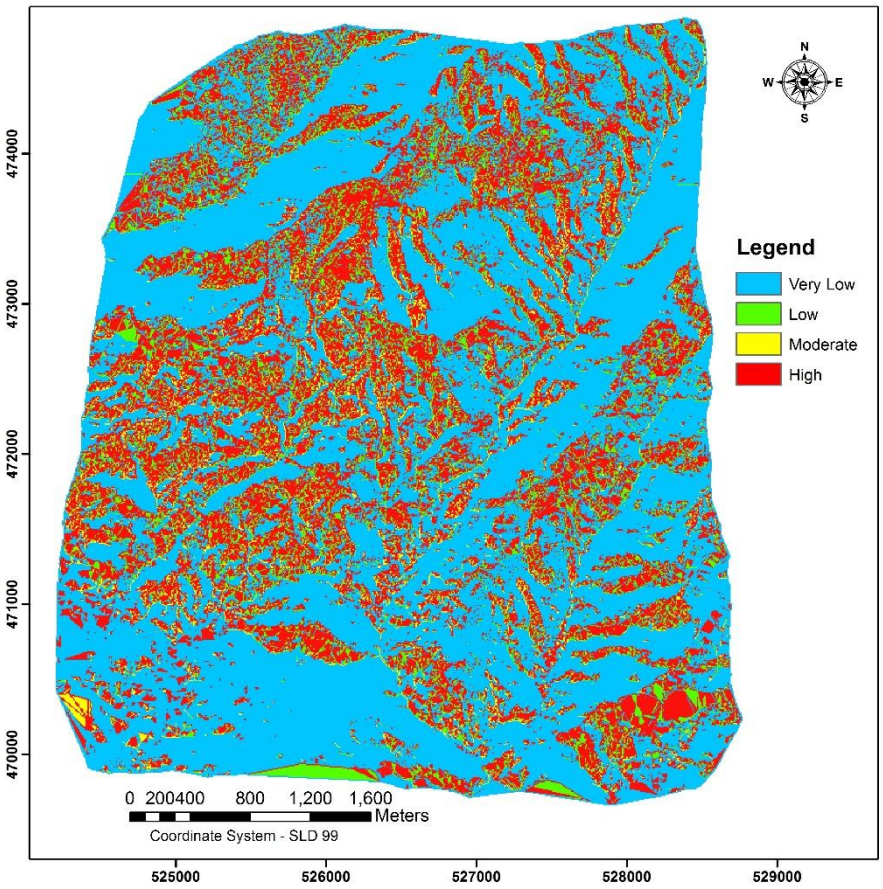

Figure 6-8 : Debris flow susceptibility map with four susceptibility classes

6.7 Integration of Terrain Failures and Debris Flow Susceptibility Regions

In order to map the landslide susceptibility regions, two independent studies are performed as terrain failure susceptibility analysis and debris flow susceptibility analysis by considering only the terrain parameters extracted from a DEM. The integration of these two concepts can provide far more realistic prediction results and is done through a comparison matrix. Figure 6-9 illustrates the comparison matrix and Figure 6-10 shows the final results from this integration. It is observed that 35% of the study area is highly susceptible, 18% is medium susceptible, 33% is low susceptible, and 14% is very low susceptible for landslide disasters.

Terrain / Debris	High (H)	Medium (M)	Low (L)	Very Low (VL)
High (h)	Hh	Mh	Lh	VLh
Medium (m)	Hm	Mm	Lm	VLm
Low (l)	Hl	Ml	Ll	VLl
Very Low (vl)	Hvl	Mvl	Lvl	VLvl

Figure 6-9 : Matrix with terrain susceptibility classes in the columns and debris flow susceptibility classes on the rows

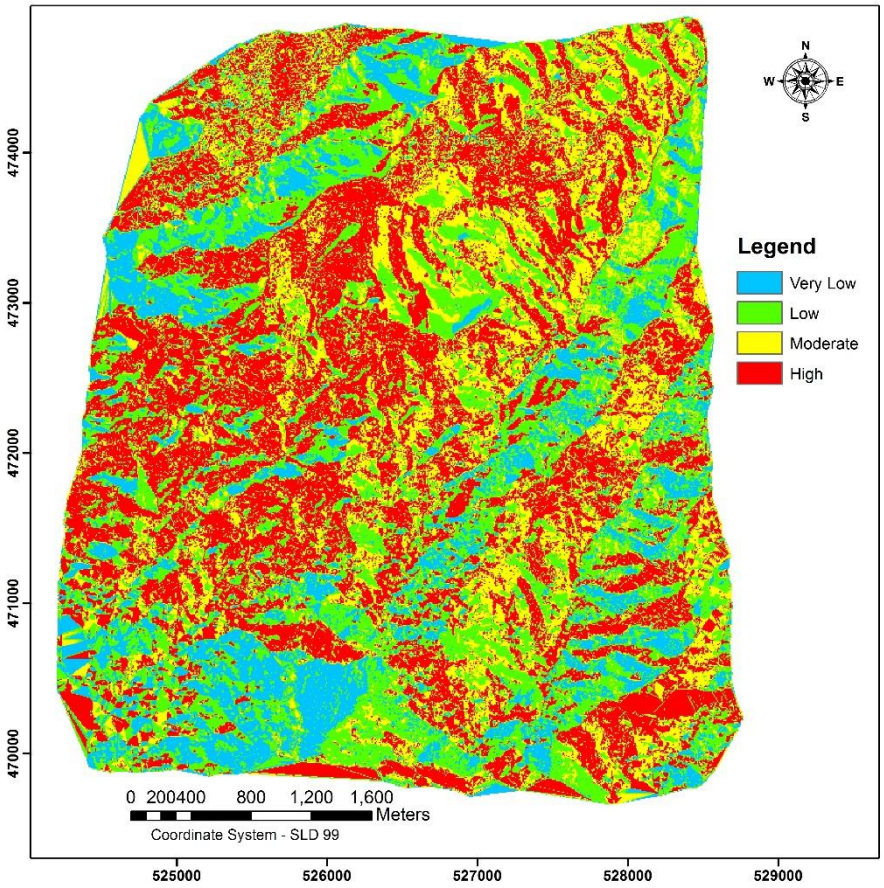

Figure 6-10 : Landslide susceptibility map with integration of terrain failure and debris flow susceptibility analysis

6.8 Discussions and Conclusions

Landslide prediction is of utmost importance in all phases of disaster management and development activities in a country. Within the recent years, Koslanda in Sri Lanka, has been found to be significantly prone to the landslide disaster [Figure 6-11].

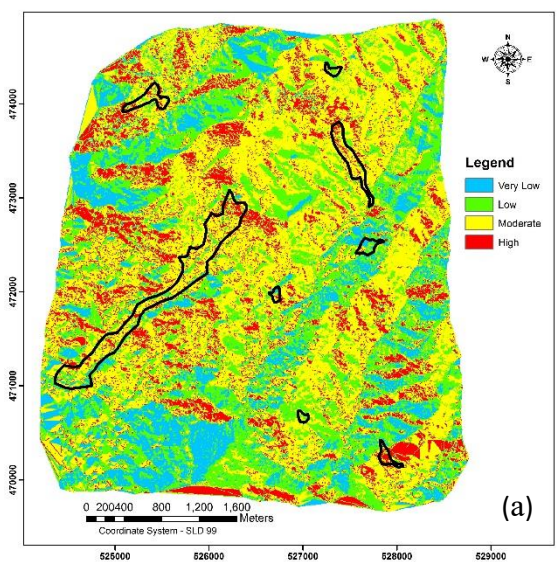

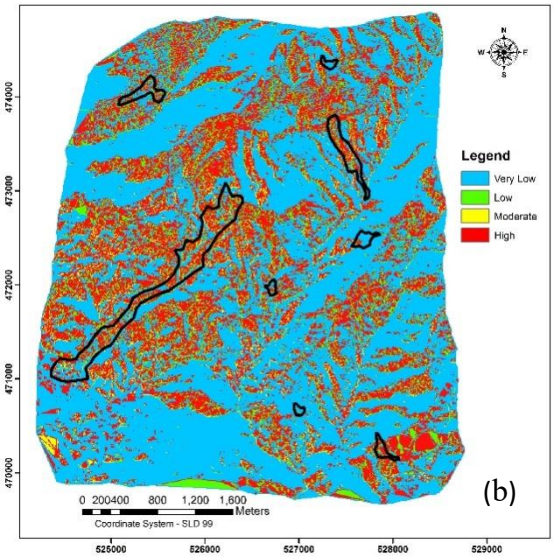

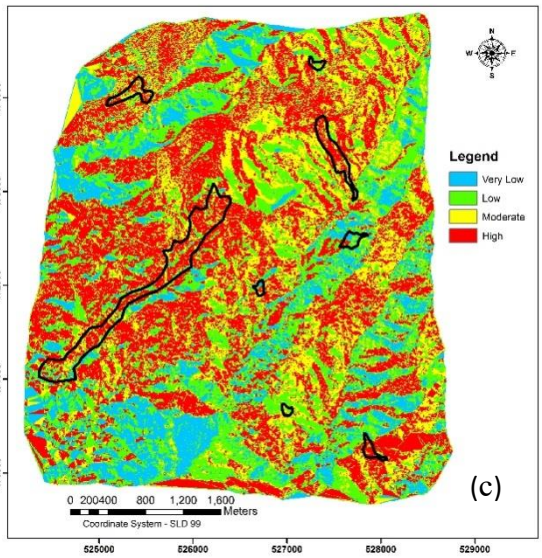

	Failure	Debris	Integration
High	17%	70%	78%
Moderate	71%	08%	11%
Low	05%	03%	07%
Very Low	07%	19%	04%

(d)

Figure 6-11:Susceptibility maps from terrain failure (a) debris flow analysis (b) and their integration (c) overlaid with the prominent landslides occurred in the study area and (d) number of landslide failure pixels in the terrain failure, debris flow, and integrated map.

Naketiya landslide in year 1997 and Meeriyabedda landslide in 2014 record the most severe losses of human life and damages to properties so far. The investigations by NBRO, Sri Lanka, have revealed that the area closer to Naketiya is still active with slow land movements. Hence, a reliable study with available data for landslide studies is of utmost importance.

Even though the multivariate statistical methods consider various parameters simultaneously, the process is complex and time consuming. Thus, the low-cost bivariate methodology is more helpful to obtain terrain failure susceptibility regions using terrain factors derived from DEM data due to the lack of detailed information about the bedrock, geology and soil structure in this study area [Figure 6-11].

Debris flow motion depends on the debris volume, amount of fluids and terrain morphology. The TauDEM extension allowed for determining the flow paths following the steepest tracks from the source points to the drainage network. The validation results confirm the suitability of the selection of terrain parameters and methodology. Figure 6-11 illustrates the performance of landslide prediction analysis with the integration of debris flow path by overlaying the landslide inventory map on each prediction analysis.

High and moderate susceptibility pixels in the landslide inventory map from the terrain failure analysis are 17% and, 71% (88%), and from debris flow path analysis is 70%, and 08% (78%), and from the integrated analysis is 78%, and 11% (89%) respectively. Thus, it can be concluded that the integration of debris flow path with the landslide susceptibility analysis can provide far more realistic landslide prediction analysis as compared to taking those individually.

The high and moderate landslide susceptibility areas in landslide failure analysis are14% and 44%, from debris flow analysis 29% and 04%, and from integrated analysis 35% and 18%, covering a considerable area showing the limitations of land for planning developments and human settlements in this area [Figure 6-11, Table 6-2]. Areas having a high susceptibility, can be used for forestation, while medium susceptibility areas can be utilized for agriculture. The areas showing low and very low susceptible regions (33% and 14%) from integrated analysis can be reserved for settlements, schools and religious places. The buildings located in areas with very low susceptibility can be used as the shelters in the case of emergencies.

Table 6-2 : Landslide susceptibility classes in the Terrain Failure, Debris Flow and the Integrated analysis

	Failure	**Debris**	**Integration**
High	14%	29%	35%
Moderate	44%	04%	18%
Low	30%	09%	33%
Very Low	14%	58%	14%

6.9 Chapter Summary

This research work utilizes the landslide inventory map for tracing the selected predisposing factors from DEM as slope, aspect, planar curvature and profile curvature. Simple and comprehensive bivariate information value method has been used to obtain the weight of influence of landslide disaster for each topographical factor. The highest weights are used as the source points for debris flow analysis. By integrating terrain failure regions and debris flow susceptibility regions, final landslide susceptibility classes can be generated. Validation results emphasize the better

estimations of landslide susceptibility classes by considering the integration of terrain failure and debris flow path for landslide susceptibility analysis as a low-cost approach.

CHAPTER 7 : CONCLUSIONS AND RECOMMENDATIONS

The work presented in this research focuses on developing a versatile approach for landslide prediction and detection through the integration of radar and optical satellite data. Both optical and radar data have their own merits, and the integration of these two would complement each other, especially in disaster studies.

7.1 Fundamental Contribution of this Research to the Field of Landslide Studies

The main focus after a landslide disaster is to carry out relief and rescue operations, and afterwards for monitoring and mapping of the landslide. These are often disturbed by lack of timely information under the prevailing bad weather conditions, particularly in inaccessible mountainous areas. Though field surveys can provide accurate and reliable data, it is not capable of satisfying all of the requirements of landslide studies at a smaller scale, and for active sliding. The present practice in Sri Lanka is to use aerial photographs for landslide investigations other than the field surveys. Hence, by proving the significance of a remote tool for landslide investigations, this research work highlighted the use of remote sensing techniques for landslide investigations with freely available satellite images at high spatial, spectral, and temporal resolutions with ample area coverage.

Radar is both revolutionary, and considered to be unique among the remote sensing systems as it is all-weather, independent of the time of day, and is able to penetrate into objects. Hence, only radar can offer timely information for landslide investigations for immediate disaster management activities remotely. Moreover, radar images are capable of extracting several natural surface parameters such as the surface soil moisture, forest biomass, and surface roughness which are major causative

factors for landslide prediction analysis. Hence, this research proves the significance of radar in landslide investigations through landslide detections, and landslide predictions with the radar induced predisposing factors.

Optical remote sensing is traditionally used in disaster management as it can provide high spatial, spectral, and temporal information about the earth surface that can be directly and easily interpreted by humans. Optical satellite images are significant data sources for extracting predisposal factors for landslide susceptibility analysis, such as land use and lineament. However, optical satellite images are limited by observations under cloud-cover conditions and during night time. In landslide detection using PCA, the influence of clouds was reduced when compared with the other change detection techniques. This is because most of the cloud pixels and landslide pixels depart to two different principal components. The principle behind the NDVI is also an acceptable method for detecting changes due to landslides as vegetation is reduced due to most landslides. Hence, this research evaluated the use of optical remote sensing for improved landslide investigations by filling the existing gap with radar.

Unexpected landslides with debris flows result in damages either over a period of time, or rapidly, destroying property and human lives suddenly. Yet, most landslide studies ignore the debris flow path in landslide susceptibility analysis. Especially in developing countries, timely information, scarcity of good quality data, insufficient funds, lack of specialized expertise are some factors that severely affect proper landslide investigations. Hence, there is a necessity of developing a low-cost methodology for improved landslide investigations as better suited for developing countries. DEM has become very significant in the study of landslides by providing some of the most prominent predisposing factors such as slope, aspect, planar, and profile curvature. Moreover, DEMs are freely available worldwide, with medium resolution (example – 30 m SRTM and ASTER), but most recently at high resolution (example–10 m TanDEM-X). Hence, this research developed a low-cost methodology

for landslide susceptibility analysis, maintaining an acceptable accuracy at a smaller scale as suited with the conditions in most developing countries.

The main reason for landslides in Sri Lanka is improper land use management and as a result, landslide occurs frequently in mountainous regions. Hence, the selected main pre-disposal factors such as land use, slope, aspect, elevation, lineament, geology, soil moisture, surface roughness, rainfall, hydrology, and forest biomass are so common for any type of landslide studies in Sri Lanka. Moreover, the comparison of bivariate and multivariate statistical analysis for landslide susceptibility analysis with the inclusion of radar induced factors for improved analysis can be easily applied for any landslide as the methodology is site independent. Furthermore, the same methodology applied in landslide detections can also be applied for any landslides as most of the limitations (clouds, vegetation, and weather) are common to any landslide.

7.2 Conclusions of the Research

Following conclusions can be derived from this research work:

1. Integration of optical and radar remote sensing could be used to quite satisfactorily predict Meeriyabedda landslide. Integration of radar images improve the predictability achieved by optical remote sensing alone. Inclusion of radar induced factors (soil moisture, surface roughness, and forest biomass) in a landslide prediction model can improve the prediction of high and low susceptibility areas.
2. Selection of pre-disposing factors for landslide prediction is highly dependent on the specific geographic area, and no universal rule can be laid down for such selection. Care and intuition are needed in this matter.
3. In landslide prediction models, bivariate approach shows better prediction and validation capabilities than multivariate approach.

4. Radar for landslide detection is promising with the advantages of radar imaging in the disaster situation and simultaneously, with PCA from optical under their own limitations
5. Landslide prediction analysis are improved by integrating debris flow analysis with DEM derived topographical factors, as applicable for a developing country with data scarcity for fine scale studies.

7.3 Discussions on Conclusions

This research first produces and compares the landslide prediction models derived from bivariate and multivariate statistical analysis with and without inclusion of the radar induced factors. Then it carries out the detection of the Meeriyabedda landslide in Sri Lanka by using different change detection techniques and evaluate their performances with respect to the field measurement. As the last step, the study develops a feasible methodology for landslide susceptibility analysis, which can be readily tested and implemented, under the prevailing conditions of most developing countries like Sri Lanka, where there exists a scarcity of timely data for fine scale studies.

7.3.1 Main Objective – Investigate the integration of radar and optical remote sensing for landslide prediction through a detailed study of landslides

To achieve the main objective of the research, Landslide prediction models from bivariate and multivariate statistical analysis with and without the inclusion of radar induced factors were developed (Chapter 4). The main focus of this work was to analyse the importance of landslide predisposing factors in an equal and weighted environment, and to analyse the influence of radar induced factors for landslide susceptibility analysis. Most developing countries, like Sri Lanka, have difficulties in timely access to complementary data needed for fine scale landslide prediction and analysis work. Further, the damages due to debris flow path are not considered in most

of the landslide susceptibility analysis. As such, the work in Chapter 6 produced, and tested, a low cost, timely analysis of landslide susceptibility by incorporating the debris flow path. The capability of detecting a landslide from different change detection techniques using radar and optical data was investigated (Chapter 5) using the Meeriyabedda landslide, and it was observed that the radar was more capable of detecting landslide damaged area than optical, under the weather conditions of the disaster situations.

7.3.2 Detection of Meeriyabedda landslide using different change detection techniques inherent to radar and optical

This work examined the capability of radar and high-resolution optical images for landslide detection by considering native characteristic of satellite images and the performance of change detection techniques. In the optical approach, high resolution satellite images were analysed by using PCA and NDVI. The influence of the cloud effect is reduced by PCA as most of the cloud pixels are separated into different principal components. Landslide area can be recognized from NDVI difference and post NDVI image due to elimination of vegetation cover from the landmass failures. Most of the manmade properties which were damaged due to landslide could be clearly identified from the NDVI difference image. Even though the post NDVI image detected 71% of the affected area, it is difficult to conclude that the post NDVI result is more accurate than the NDVI difference image as it does not specify any change, and reduction could be the result of either landslide or drop of vegetation. However, with prior knowledge of the land use, and if any changes had occurred in a vegetated region, then the post NDVI image can provides better detections about the landslide damaged areas.

In change detection analysis, clouds hide some important information while getting classified as changes. This can be overcome with the use of radar images, which is most important in disaster studies. However, in radar image analysis of hilly regions,

radar backscatter is highly affected by incident angle and angle of fore slopes, more so than the type of surface materials and their conditions. Moreover, radar back scatter changes with the illumination conditions of the time of image acquisition due to side looking configurations. Hence, most appropriate radar images have to be selected for change detection analysis. Freely available Sentinel-1, C band radar images at 10 m resolution with VV polarization is used. Pre-processing of radar images in pre and post event was challenging as they covered much undulated region with serious geometrical distortions. Yet, it was possible to obtain 86% of accuracy for landslide damaged area for Meeriyabedda landslide.

Validation results highlighted the colour combination of PCA gained better results (76%) as all available image bands were used in image analysis. PCA and NDVI difference obtained least accuracy (63% and 65% respectively), as it was affected by other radiometric and illumination changes than the change due to landslide in pre and post image. Hitherto, due to the advantages of radar images in disaster situations, it has proven the suitability for disaster studies. Hence, it can be concluded that the radar for landslide detection is promising, simultaneously with PCA as optical is at 76% under their own limitations.

7.3.3 Identification of the most prominent landslide pre-disposing factors from remotely sensed sources, i.e. DEM, Optical and Radar

Landslides may occur as consequences of complex predisposing and triggering factors. Long term topographical, geological, and land use predisposing factors, together with local climatic conditions, trigger landslide occurrences. There are no universal strategies for the selection of predisposing factors in landslide susceptibility analysis. Thus, determining of appropriate causal factors is a difficult task, and no specific rule exists to define how many factors are sufficient for a specific landslide susceptibility analysis. Hence, the selections of predisposing factors are dependent on the nature of the study area, opinions of the experts, and the availability of data for generating the

appropriate spatial and thematic information. Furthermore, selection of these factors, and preparation of corresponding thematic data layers, are vital for landslide susceptibility analysis.

Selection of predisposing factors were based on the careful investigations of the study area, literature recommendations, and the expert opinions. Fifteen topographical, hydrological, geological, land cover, and soil factors were considered, including three radar induced factors. All factors were derived from optical images (Landsat-8, Sentinel-2), radar images (Sentinel-1, TerraSAR-X), and DEM derived from aerial triangulation and other available data sources (Geology, Rainfall). Twelve factors were derived from optical images, DEM and auxiliary data. Three more factors (surface roughness, soil moisture index, and forest biomass) derived from radar images were incorporated in order to analyse the performance of this integration for landslide susceptibility analysis.

7.3.4 Building landslide prediction models from bivariate and multivariate statistical methods

Prediction models combine various predisposing factors through a predefined algorithm in landslide susceptibility analysis. Information Value method based on simple statistical analysis as bivariate and AHP based MCDA as multivariate have been applied for landslide susceptibility analysis. Bivariate analysis calculates the susceptibility at each point with the equally joined weight of influence of all predisposing factors. The weight of influence is estimated based on the landslide inventory map of the study area. Multivariate analysis integrates all the predisposing factors with relative contribution of each factor by putting more emphasis on landslide occurrences. AHP calculate the relative importance by using questionnaire survey from the experts in the field of geology and decision makers in DMC, UDA, and NBRO. The expert knowledge could be subjective or may assign different weights for each factor when analysing a large number of predisposing factors. Hence, in order to

minimize this inconsistency, CR is calculated. For better predictive models, the CR should be less than 0.1, and otherwise, weights for each factor have to be regenerated.

7.3.5 Investigation of the performance of landslide prediction model, with the inclusion of landslide causal factors derived from radar images

High and moderate susceptibility classes in bivariate and multivariate analysis with and without radar induced factors are approximately identical but showslight increase in multivariate analysis than bivariate. However, with the inclusion of radar induced factors, as surface roughness, near surface soil moisture from delta index, and forest biomass, the high and very low susceptible areas are increased significantly (high: 7%, 3%, and very low: 4%, 3% bivariate and multivariate respectively). However, when comparing high and very low susceptibility areas from bivariate and multivariate analysis, high susceptibility areas have significant increase (without radar - 6% and with radar - 2%) while, very low susceptibility areas have significant decrease (without radar - 3% and with radar - 4%). Hence, it can be noted that with the inclusion of radar induced factors, the discrimination between high and very low susceptibility areas are increased.

Validation was conducted from two different approaches as RFD and AUC of success rate and prediction rate curves to minimize the inconsistency. The regions predicted as very low are validated as 0% in RFD analysis. More than 70% areas are identified as high and moderate susceptibility areas. The validation results illustrate the gradual increase of RFD from very low to (moderate + high) susceptibility classes. The success rate curves measure prediction performance while, the prediction curves measure validation performance. If the AUC is closer to 1, the result of the test is excellent and AUC is closer 0.5, the result of the test is fairer. Even if the AUC of prediction rates are more than 0.5 which, are in acceptable range, they are closer to the 0.5 predicting fairer performance in validation. The main reason could be the incompleteness of the available landslide inventory map with insufficient validation samples in the study

area. However, with the inclusion of radar induced factors, AUC of success rate and prediction rate curves are increased from 0.8315 to 0.8560, 0.7986 to 0.8023, 0.6692 to 0.6804, and 05882 to 0.5901 in bivariate and multivariate respectively.

7.3.6 Comparing the performance of differently built landslide prediction models

Four landslide prediction models, (i) BiWR, (ii) BiNR, (iii) MWR, and (iv) MNR (bivariate and multivariate, and with and without radar induced factors) are developed and their performances were investigated by using RFD analysis and AUC of success and prediction rate curves. RFD analysis investigate the number of pixels in validation sample in each landslide prediction classes. By observing the correct performance of prediction analysis in all prediction models, very low susceptible areas from prediction analysis are validated as 0% while high and moderate susceptibility areas are above 70% from all these four statistical analyses. However, from RFD analysis the performance of each prediction model could not be distinct as all prediction models perform in similar mode.

The AUC of prediction rate and success rate curves investigate the prediction and validation performances separately. Theoretically, if AUC is closer to 1, the prediction result is “excellent” and on the contrary, if AUC is closer 0.5, the prediction result is “fair”. In these analyses, AUC of all the success rates are closer to or more than 0.80, thereby providing better prediction performances, though the prediction rates predict less performance in validation. The most possible reason would be the incompleteness of the available landslide inventory map with insufficient validation samples. All success and prediction rate analysis in bivariate and multivariate analysis perform well with the inclusion of radar induced factors (Success rate – BiNR – 0.8315, BiWR-0.8560, MNR – 0.7986, MWR – 0.8023 and prediction rate -- BiNR – 0.6692, BiWR-0.6804, MNR – 0.5882, MWR – 0.5901). All in all, the better prediction and validation capabilities are shown by bivariate when compared with the multivariate approaches.

7.3.7 Investigation the post disaster effects from debris flow due to landslide failures

The post disaster effect from debris flows is harmful process due to the rapid rate of movement and long runout zone throughout the hilly terrain by destroying everything they meet. Recent landslide studies have identified that the Koslanda area in Sri Lanka is significantly prone to landslide disaster (Naketiya – 1997, and Meeriyabedda –2014) causing higher losses to human life and severe damages to properties. NBRO investigations have revealed that the area near to Naketiya is still in active with slow land movements.

The multivariate analysis considers several parameters simultaneously, the process is complex and time consuming. Thus, the low-cost bivariate approach is more supportive to categorize terrain failure susceptibility regions using the factors derived from DEM, if there is a lack of detailed information about the study area. Debris flow depends on the debris volume, amount of fluids and terrain morphology. TauDEM determine the flow paths that follow the steepest route from the source points to the drainage network. Two independent studies of susceptibility for terrain failures and debris flow analysis were integrated to obtain more realistic prediction results using a comparison matrix.

The high and moderate susceptible areas (58%) in terrain failure analysis, and debris flow susceptible areas (33%), and the integrated susceptible areas (53%), covered a significant percentage of the study area, showing limitations of land for planning developments and human settlements. High susceptible areas have to be used for forestation while medium areas can be utilized for agriculture. Low and very low regions, obtained as 33% and 14%, from integrated analysis, can be reserved for the settlements, schools and religious places. The buildings in very low susceptible areas can be used as potential shelters in the case of emergencies. The validation results confirm the selection of terrain parameters and suitable methodology.

7.4 Future Works

Remote sensing techniques for disaster investigations have been emerging fields of research in the last decade. In landslide investigations, landslide detections, predictions, monitoring, damage, and risk assessments using spatial predictors and statistical analysis can go a long way in establishing the scientific research in these fields. However, there are some issues that have emerged from this research that need to be addressed in future studies.

The first and foremost step is that the national programme for landslide inventory mapping should be carried out in optimal ways by introducing time and scale dimensions. Time dimensions involve landslide records over time for properly addressing the reactivation history and scale dimensions should be able to change the representation of landslide at different scales from a single point to a set of polygons.

Data about the damages due to landslides are usually scares in landslide inventories and more attention should be taken to link the magnitude of landslides with the damages. Hence, an up-to-date landslide inventory map is recommended for proper landslide studies.

Landslide inventory mapping should be web-based and allow for collaborative mapping, and reporting of landslide occurrences in a simple way by local authorities. In that sense, event-based landslide inventory maps can be produced by using remote sensing or semi-automated techniques of landslide inventory mapping. The demand for query facilities and visualization information through public domain is increasing in geographical information users. Hence, the development of WebGIS on a scientific platform allows integration of data from various sources, means, and methods, and data dissemination through geographical information user.

The increasing availability of free data through the worldwide web can be used for landslide studies where the data scarcity is ultimately a main challenge. At the moment, most data that is freely available is only applicable in smaller scales (SRTM 30 m and 90 m), even though more detailed data with higher resolution (TanDEM 10 m resolution) are gradually increasing in future.

Many landslide predisposal factors are considered in literature for landslide susceptibility mapping, but it is not certain which factor combination provides best results for susceptibility analysis. Though several research studies examine the effects of predisposal factors on landslide susceptibility analysis, as yet, there does not exist a well-established framework exists for the selection of optimum factors for landslide susceptibility analysis.

In addition, a fully polarimetric multi bands system could further improved the radar image analysis than single polarized C band radar images in change detection and soil moisture studies. The present generation of spaceborne SAR sensors operating in fully polarimetric mode at different frequencies (L, X, C) with future planned sensors offer a potential for land surface studies even under highly dense forest.

REFERENCES

Abella, E. A., Jong, S. M., van Westen, C. J., & van Asch, W. J. (2008). *Multi-scale landslide risk assessment in Cuba.* (PhD Thesis), Faculty of Geo-Information and Earth Observation,

Afify, H. A. (2011). Evaluation of change detection techniques for monitoring land-cover changes: A case study in new Burg El-Arab area. *Alexandria Engineering Journal, 50*, pp 187–195.

Akbarimehr, M., Motagh, M., & Haghshenas-Haghighi, M. (2013). Slope stability assessment of the sarcheshmeh landslide, Northeast Iran, investigated using InSAR and GPS observations. *Remote Sensing, 5*, pp 3681–3700.

Akgun, A., Dag, S., & Bulut, F. (2008). Landslide susceptibility mapping for a landslide-prone area (Findikli, NE of Turkey) by likelihood-frequency ratio and weighted linear combination models. *Environmental Geology, 54*, pp 1127–1143.

Aleotti, P., & Chowdhury, R. (1999). Landslide hazard assessment: summary review and new perspectives. *Engineering Geology and the Environment, 58*(1), pp 21-44.

Antonini, G., Ardizzone, F., Cardinali, M., Galli, M., Guzzetti, F., & Reichenbach, P. (2002). Surface deposits and landslide inventory map of the area affected by the 1997 Umbria–Marche earthquakes. *Bollettinodella Societa Geologica Italiana, 121*(2), pp 843-853.

Armas, I. (2012). Weights of evidence method for landslide susceptibility mapping. Prahova Subcarpathians. Romania. *Natural Hazards, 60*, pp 937–950.

Ayalew, L., Yamagishi, H., & Ugawa, N. (2004). Landslide susceptibility mapping using GIS-based weighted linear combination, the case in Tsugawa area of Agano River. Niigata Prefecture, Japan. *Landslide, 1*(1), pp 73-81.

Baker, S., Scharstein, D., Lewis, J. P., Roth, S., Black, M. J., & Szeliski, R. (2011). A database and evaluation methodology for optical flow. *International Journal of Computer Vision, 92*, pp 1-31.

Ballabio, C., & Sterlacchini, S. (2012). Support Vector Machines for Landslide Susceptibility Mapping: The Staffora River Basin Case Study, Italy, (2012) 44: 47. *Mathematical Geosciences, 44*(47), doi:10.1007/s11004-11011-19379-11009.

Bandara, R. M. S. (2005). Landslides in Sri Lanka. *VIDURAVA, 22*(2), pp 9-13.

Baroň, I., Bečkovský, D., & Míča, L. (2014). Application of infrared thermography for mapping open fractures in deep-seated rockslides and unstable cliffs. *Landslides, 11*, pp 15-27.

Barredol, J. I., Benavidesz, A., Herhl, J., & van Westen, C. J. (2000). Comparing heuristic landslide hazard assessment techniques using GIS in the Tirajana basin, Gran Canaria Island, Spain. *International Journal of Applied Earth Observation and Geoinformation, 2*(1), pp 9-23.

Barrett, B. W., Dwyer, E., & Whelan, P. (2009). Soil Moisture Retrieval from Active Spaceborne Microwave Observations: An Evaluation of Current Techniques. . *Remote Sensing, 1*, pp 210-242. doi: doi: 10.3390/rs1030210.

Begueria, S. (2006). Validation and evaluation of predictive models in hazard assessment and risk management. *Natural Hazards, 37*, pp 315-329.

Beven, K. J., & Kirkby, M. J. (1979). A physically based, variable contributing area model of basin hydrology. *Hydrology, 24*, pp 43-69.

Bignami, C., Chini, M., Pierdicca, N., & Stramondo, S. M. (2004). *Comparing and combining the capability of detecting earthquake damages in urban areas using SAR and optical data.* Paper presented at the Proceedings of IEEE/IGARSS 2004, Anchorage, USA.

Bonachea, J., Remondo, J., deTeran, J. R. D., Gonazalez-Diez, A., & Cendrero, A. (2009). Landslide Risk Models for Decision Making. *Journal of Risk Analysis, 29*(11), pp 1629-1643.

Breiman, L., Friedman, J. H., Olshen, R. A., & Stone, C. J. (1984). *Classification and regression trees*. Wadsworth: Belmont.

Bui, D. T., Lofman, O., Revhaug, I., & Dick, O. (2011). Landslide susceptibility analysis in the HoaBinh province of Vietnam using statistical index and logistic regression. *Natural Hazards, 59*, pp 1413–1444.

Bui, D. T., Pradhan, B., Lofman, O., & Revhaug, I. (2012). Landslide susceptibility assessment in Vietnam using support vector machines, decision tree, and naive Bayes models. *Mathematical Problems in Engineering volume 2012*, Article ID 974638, doi:974610.971155/972012/974638.

Caicoya, A. T., Kugler, F., Hajnsek, I., & Papathanassiou, K. P. (2016). Large Scale Biomass Classification in Borel Forests with TanDEM-X Data. . *IEEE Transactions on Geoscience and Remote Sensing, 54*(10), pp 5935-5951.

Canuti, P., Casagli, N., Ermini, L., Fanti, R., & Farina, P. (2004). Landslide activity as a geo indicator in Italy: Significance and new perspectives from remote sensing. *Environmental Geology, 45*, pp 907–919.

Cardinali, M., Galli, M., Guzzetti, F., Ardizzone, F., Reichenbach, P., & Bartoccini, P. (2006). Rainfall induced landslides in December 2004 in south-western Umbria, central Italy: types, extent, damage and risk assessment. *Journal of Natural Hazards and Earth System Sciences, 6*, pp 237-260.

Carlson, T., Gillies, R., & Perry, E. (1994). A method to Make use of Thermal Infrared Temperature and NDVI Measurements to Infer Surface Soil Water Content and Fractional Vegetation Cover. *Remote Sensing Review, 9*, pp 161-173.

Carrara, A., Guzzetti, F., Cardinali, M., & Reichenbach, P. (1999). Use of GIS technology in the prediction and monitoring of landslide hazard. *Natural Hazards, 20*(2-3), pp 117-135.

Cevik, E., & Topal, T. (2003). GIS-based landslide susceptibility mapping for a problematic segment of the natural gas pipeline, Hendek (Turkey). *Environmental Geology, 44*, pp 949–962.

Chalkias, C., Ferentinou, M., & Polykretis, C. (2014). GIS-Based Landslide Susceptibility Mapping on the Peloponnese, Peninsula, Greece. *Geosciences, 4*, pp 176-190, doi:110.3390/geosciences4030176.

Che, V. B., Kervyn, M., Suh, C. E., Fontijn, K., Ernst, G. G. J., Del Marmol, M. A., Jacobs, P. (2012). Landslide susceptibility assessment in Limbe (SW Cameroon): A field calibrated seed cell and information value method. *Journal of Catena, 92*, pp 83-98, DOI: 10.1016/j.catena.2011.1011.1014.

Chen, J., Gong, P., He, C., Pu, R., & Shi, P. (2003). Land-use/land-cover change detection using improved change-vector analysis. *Photogrammetric Engineering & Remote Sensing, 69*, pp 369–379.

Chen, X., Vierling, L., & Deering, D. (2005). A simple and effective radiometric correction method to improve landscape change detection across sensors and across time. *Remote Sensing of Environment, 98*, pp 63–79.

Cheng, P. (2007). Automated High-Accuracy Orthorectification and Mosaicking of PALSAR Data without Ground Control Points. *Geoinformatics, 6*(10), pp 36-38.

Cho, J. H., & Kurup, P. U. (2011). Decision tree approach for classification and dimensionality reduction of electronic nose data. *Sensors and Actuators B: Chemical, 160*(1), pp 542–548.

Chung, C. F., & Fabbri, A. G. (2003). Validation of spatial prediction models for landslide hazard mapping. *Natural Hazard, 30*, pp 451–472.

Coe, J. A., Godt, J. W., Baum, R. L., Bucknam, R. C., & Michael, J. A. (2004). *Landslides: Evaluation and stabilization*. London, 1: Taylor & Francis Group, pp 69–78 T4 - Landslide susceptibility from topography in Guatemala

Colesanti, C., & Wasowski, J. (2006). Investigating landslides with space-borne Synthetic Aperture Radar (SAR) interferometry. *Engineering Geology, 88*, pp 173-199.

Conforti, M., Robustelli, G., Muto, F., & Critelli, S. (2011). Application and validation of bivariate GIS-based landslide susceptibility assessment for the Vitravo river catchment (Calabria, south Italy). *Natural Hazards*, DOI 10.1007/s11069-11011-19781-11060.

Corominas, J., van Westen, C., Frattini, P., Cascini, L., Malet, J. P., Fotopoulou, S., Agliardi, F. (2014). Recommendations for the quantitative analysis of landslide risk. *Engineering Geology and the Environment, 73*, pp 209-263.

Costanzo, D., Rotigliano, E., Irigaray, C., Jimenez-Peralvarez, J. D., & Chacon, J. (2012). Factors selection in landslide susceptibility modelling on large scale

following the GIS matrix method: application to the river Beiro basin (Spain). *Natural Hazards Earth System, 12*, pp 327–340.

Cruden, D. M. (1991). A Simple Definition of a Landslide. *Engineering Geology, 43*, pp 27-29.

Cruden, D. M., & Varnes, D. J. (1996). *Landslides types and processes. In Landslides: Investigation and Mitigation; Transportation Research Board Special No. 247*. Washington, DC, USA: National Academy Press, pp 36–75.

Dahal, R. K., Hasegawa, S., Nonomura, A. Y. M. M. T., & Nishino, K. (2008). GIS-based weights-of-evidence modelling of rainfall-induced landslides in small catchments for landslide susceptibility mapping. *Environmental Geology, 54*, pp 311-324.

Dai, F. C., & Lee, C. F. (2002). Landslide characteristics and slope instability modelling using GIS, Lantau Island, Hong Kong. *Geomorphology, 42*, pp 213–228.

Delacourt, C., Allemand, P., Berthier, E., Raucoules, D., Casson, B., Grandjean, P., Varel, E. (2007). Remote-sensing techniques for analysing landslide kinematics: A review. *Bulletin De La Societe Geologique De France, 178*, pp 89-100.

Demir, G., Aytekin, M., Akgun, A., Ikizler, S. B., & Tatar, O. (2013). A comparison of landslide susceptibility mapping of the eastern part of the North Anatolian Fault Zone (Turkey) by likelihood-frequency ratio and analytic hierarchy process methods. *Natural Hazards, 65*, pp 1481–1506.

Devi, R. N., & Jiji, G. W. (2015). Change Detection Techniques – A Survey. *International Journal on Computational Sciences & Applications (IJCSA), 5*(2), DOI:10.5121/ijcsa.2015.5205.

DMC. (2010). *Sri Lanka National Report on Disaster Risk, Poverty and Human Development Relationship. Disaster Management Center, Ministry of Disaster Management: Disaster Information Management System in Sri Lanka*.

Dubois, P. C., van Zyl, J., & Engman, T. (1995). Measuring soil moisture with imaging radars. *IEEE Transactions on Geoscience and Remote Sensing, 33*(4), pp 915-926.

Farina, P., Colombo, D., Fumagalli, A., Marks, F., & Moretti, S. (2006). Permanent scatters for landslide investigations: Outcomes from the ESA-SLAM project. *Engineering Geology, 88*, pp 200-217.

Fawcett, T. (2006). An introduction to ROC analysis. *Pattern Recognition Letters, 27*, pp 861–874.

Fiorucci, F., Cardinali, M., Carlà, R., Rossi, M., Mondini, A. C., Santurri, L., Guzzetti, F. (2011). Seasonal landslide mapping and estimation of landslide mobilization rates using aerial and satellite images. *Geomorphology, 129*, pp 59-70.

Frattini, P., Crosta, G., & Carrara, A. (2010). Techniques for evaluating the performance of landslide susceptibility models. *Engineering Geology, 111*, pp 62–72.

Guinau, M., Vilajosana, I., & Vilaplana, J. M. (2007). GIS-based debris flow & runout susceptibility assessment from DEM data. *Natural hazards and earth system sciences, 7*, pp 703-716.

Guzzetti, F. (2004). Landslides triggered by the 23 November 2000 rainfall event in the Imperia Province, Western Liguria, Italy. *Engineering Geology, 79*, pp 229–245.

Guzzetti, F., Carrara, A., Cardinalli, M., & Reichenbach, P. (1999). Landslide hazard evaluation: a review of current techniques and their application in a multi-scale study Central Italy. *Geomorphology, 31*(1-4), pp 181-216.

Guzzetti, F., Mondini, A. C., Cardinali, M., Fiorucci, F., Santangelo, M., & Chang, K. T. (2012). Landslide inventory maps: New tools for an old problem. *Journal of Earth Science Revision, 112*, pp 42-66.

Hasekiogullari, G. D., & Ercanoglu, M. (2012). A new approach to use AHP in landslide susceptibility mapping: a case study at Yenice (Karabuk, NW Turkey). *Natural Hazards, 63*, pp 1157–1179.

Hassaballa, A. A., Matori, A. N. B., & Shafri, H. Z. B. M. (2013). Surface Moisture Content Retrieval from Visible/Thermal Infrared Images and Field Measurements. *Caspian Journal of Applied Sciences Research*, pp 182-189.

Hervas, J., I., B. J., Rosin, P. L., Pasuto, A., Mantovani, F., & Silvano, S. (2003). Monitoring Landslides from Optical Remotely Sensed Imagery: the case history of Tessina Landslide, Italy. . *Geomorphology, 54*, pp 63-75. doi:doi: 10.1016/S0169-555X(03)00056-4.

Hurlimann, M., Copons, R., & Altimir, J. (2006). Detailed debris flow hazard assessment in Andorra: A multidisciplinary approach. *Geomorphology, 78*, pp 359-372.

Ilsever, M., & Unsalan, C. (2012). *Two Dimensional Change Detection Methods – Remote Sensing Applications, ISBN: 978-1-4471-4254-6*.

Im, J., & Jensen, J. R. (2005). A change detection model based on neighbourhood correlation image analysis and decision tree classification. *Remote Sensing of Environment, 99*, pp 326–340.

Ioannidis, C., & Vassilaki, D. M. (2008). *Combined use of Spaceborne Optical and SAR Data – Incompatible Data Sources or a Useful Procedure?* Paper presented at the Integrating Generations FIG Working Week 2008, TS 1H - Developments in Scanner and Sensor Technologies, Stockholm, Sweden.

Iverson, R. M., & Denlinger, R. P. (2001). Flow of variably fluidized granular masses across three-dimensional terrain, Coulomb mixture theory. *Journal of Geophysical Research, 106*, pp 537-552.

Jaafari, A., Najafi, A., Pourghasemi, H. R., Rezaeian, J., & Sattarian, A. (2014). GIS-based frequency ratio and index of entropy models for landslide susceptibility assessment in the Caspian forest, northern Iran. *International Journal of Environmental Science and Technology*, *11*(4), pp 909–926.

Jaafari, A., Najafia, A., Rezaeianc, J. S. A., & Ghajare, I. (2015). Planning road networks in landslide-prone areas: A case study from the northern forests of Iran. *Journal of Land Use Policy, 47*, pp 198–208.

Jakob, M., Holm, K., Lango, O., & Schwab, J. (2006). Hydrometeorological threshold for landslide initiation and forest operation shutdowns on the north coast of British Columbia. *Landslides, 3*, pp 228-238.

Javier, H., Jose, I. B., Paul, L. R., Alessandro, P., Franco, M., & Sandro, S. (2003). Monitoring landslides from optical remotely sensed imagery: the case history of Tessina landslide, Italy. *Geomorphology, 54*, pp 63-75.

Joyce, K. E., Belliss, S., Samsonov, S., McNeill, S., & Glassey, P. J. (2009). A review of the status of satellite remote sensing image processing techniques for mapping natural hazards and disasters. *Progress in Physical Geography, 33*(2), pp 1-25.

Kamp, U., Growley, B. J., Khattak, G. A., & Owen, L. A. (2008). GIS-based landslide susceptibility mapping for the 2005 Kashmir earthquake region. Geomorphology. *101*(4), pp 631–642.

Kanungo, D. P., Arora, M. K., Sarkar, S., & Gupta, R. P. (2009). Landslide susceptibility zonation (LSZ) mapping, Journal of South Asia Disaster Studies. *Journal of South Asia Disaster Studies*, *2*, pp 81-105.

Kappes, M. S., Malet, J. P., Remaitre, A., & Bell, R. (2011). Assessment of debris-flow susceptibility at medium-scale in the Barcelonnette Basin, France. *Natural hazards and earth system sciences, 11*, pp 627-641.

Kavzoglu, T., Sahin, E. K., & Colkesen, I. (2014). Landslide susceptibility mapping using GIS-based multi-criteria decision analysis, support vector machines, and logistic regression. *Landslides, 11*(3), pp 425-439.

Kavzoglu, T., Sahin, E. K., & Colkesen, I. (2015). An assessment of multivariate and bivariate approaches in landslide susceptibility mapping: a case study of Duzkoy district. *Natural Hazards, 76*, pp 471–496, DOI 410.1007/s11069-11014-11506-11068.

Klose, M., Highland, L., & Damm, B. T. B. (2014). *Estimation of direct landslide costs in industrialized countries: Challenges, concepts, and case study. In Landslide Science for a Safer Geo-environment*. Berlin, Germany: Springer, pp 661-667.

Kouli, M., Loupasakis, C., Soupios, P., & Vallianatos, F. (2010). Landslide hazard zonation in high risk areas of Rethymno Prefecture, Crete Island, Greece. *Natural Hazards, 52*, pp 599-621.

Kseneman, M., Gleich, D., & Potoˇcnik, B. (2012). Soil-moisture estimation from TerraSAR-X data using neural networks. *Machine Vision and Applications, 23*, pp 937–952, DOI 910.1007/s00138-00011-00375-00133.

Kumar, V. K., & Tapas, R. M. (2007). *Remote Sensing Applications*: National Remote Sensing Centre, pp 331-338 T4 - 14 - Landslides.

Kuplich, T. M., Curran, P. J., & Atkinson, P. M. (2005). Relating SAR image texture to the biomass of regenerating tropical forests. *International Journal of Remote Sensing, 26*(21), pp 4829-4854.

Lan, H. X., Zhou, C. H., Wang, L. J., Zhang, H. Y., & Li, R. H. (2004). Landslide hazard spatial analysis and prediction using GIS in the Xiaojiang watershed, Yunnan, China. *Engineering Geology, 76*(1-2), pp 109–128.

Landsat–8 (2016). Landsat – 8, Data Users Hand Book.

Landslide (2014). Landslide, Wikipedia free encyclopedia.

Lee, S., Hong, S. M., & Jung, H. S. (2017). A Support Vector Machine for Landslide Susceptibility Mapping in Gangwon Province, Korea. *Journal of Sustainability, 9*(48), doi:10.3390/su9010048.

Lillesand, T. M., Kiefer, R. W., & Chipman, J. W. (2008). *Remote Sensing and Image Interpretation, sixth edition*. Hoboken, NJ: John Wiley & Sons.

Lu, D., Mausel, P., Brondízio, E., & Moran, E. (2004). Change detection techniques. *International Journal of Remote Sensing*(25), pp 2365–2400.

Lunetta, R. S., Johnson, D. M., Lyon, J. G., & Crotwell, J. (2004). Impacts of imagery temporal frequency on land-cover change detection monitoring. *Remote Sensing of Environment, 89*, pp 444–454.

Malamud, B. D., Turcotte, D. L., Guzzetti, F., & Reichenbach, P. (2004). Landslide inventories and their statistical properties. *Earth Surface Processes, 29*, pp 687-711.

Mandal, S., & Maiti, R. (2015). Semi-quantitative Approaches for Landslide Assessment and Prediction. Geo-spatial Variability of Physiographic Parameters and Landslide Potentiality. *Springer Natural Hazards*.

Mantovani, F., Soeters, R., & van Westen, C. J. (1996). Remote sensing techniques for landslide studies and hazard zonation in Europe. *Geomorphology, 15*, pp 213-225.

Mapa, R. B., Dassanayake, A. R., & Nayakekorale, H. B. (2005). *Soils of the Intermediate Zone of Sri Lanka, Special publication number 4*: Soil Sciences Society of Sri Lanka.

Martha, T., Jetten, V., & Kerle, N. (2011). *Detection of landslides by object - oriented image analysis.* (PhD Thesis), Faculty of Geo-Information and Earth Observation,

Martha, T. R., Kerle, N., Jetten, V., van Westen, C. J., & Vinodkumar, K. (2010a). Characterising spectral, spatial and morphometric properties of landslides for automatic detection using object-oriented methods. *Geomorphology, 116*(1-2), pp 24–36.

Martha, T. R., Kerle, N., Jetten, V., van Westen, C. J., & Vinodkumar, K. (2010b). Landslide volumetric analysis using Cartosat-1-derived DEMs. *IEEE Geosciences Remote Sensing Letters, 7*(3), pp 582–586.

Metternicht, G., Hurni, L., & Gogu, R. (2005). Remote sensing of landslides: An analysis of the potential contribution to geo-spatial systems for hazard assessment in mountainous environments. *Remote Sensing of Environment, 98*, pp 284-303.

Moran, M. S., Hymer, D. C., Qi, J., & Sano, E. E. (2000). Soil Moisture Evaluation using Multi-Temporal Synthetic Aperture Radar (SAR) in semiarid rangeland. . *Agriculture and Forest Metereology, 105*, pp 69-80.

Murdopo, A. (2013). Distributed Decision Tree Learning for Mining Big Data Streams, MSc thesis.

Muthu, K., Petrou, M., Tarantino, C., & Blonda, P. (2008). Landslide possibility mapping using fuzzy approaches. *IEEE Transactions on Geo-science and Remote Sensing, 46*, pp 1253-1265.

Myles, A. J., Feudale, R. N., Liu, Y., Woody, N. A., & Brown, S. D. (2004). An introduction to decision tree modelling. Journal of Chemometrics. *18*(6), pp 275–285.

Naghibi, S. A., Pourghasemi, H. R., Pourtaghi, Z. S., & Rezaei, A. (2015). Groundwater qanat potential mapping using frequency ratio and Shannon's entropy models in the Moghan watershed, Iran. *Earth Science Informatics, 8*, pp 171–186.

Nandi, A., & Shakoor, A. (2009). A GIS based landslide susceptibility evaluation using bivariate and multivariate statistical analyses. *Engineering Geology, 110*, pp 11-20.

Nandi, A., & Shakoor, A. M. (2006). *Preparation of a Landslide Susceptibility Map of Summit County, Ohio, USA, Using Numerical Models. Paper No. 660.* Paper presented at the In Proceedings of the 10th IAEG Congress, Nottingham, UK.

NBRO (2011). Landslide Research & Risk Management Division, National Building Research Organization, Ministry of Disaster management.

NBRO (2016). Landslide Research & Risk Management Division, National Building Research Organization, Ministry of Disaster management.

Neuhäuser, B., Damm, B., & Terhorst, B. (2012). GIS-based assessment of landslide susceptibility on the base of the weights-of-evidence model. *Landslides, 9*(4), pp 511–528.

Niuniu, X., & Yuxun, L. M. (2010). *Review of decision trees. Computer science and information technology (ICCSIT).* Paper presented at the 3rd IEEE International Conference.

OFDA/CRED (2016). EM-DAT International Disaster Database. - University of Catholique de Louvain, Brussels, Belgium, 2016.

Onagh, M., Kumra, V. K., & Kumar Rai, P. K. (2012). Landslide susceptibility mapping in a part of Uttarkashi District (India) by multiple linear regression method. *International Journal of Geology, Earth and Environmental Sciences, 2*(2), pp 102-120.

Orsomando, F., Lombardo, P., Zavagli, M., & Costantini, M. (2007). SAR and Optical Data Fusion for Change Detection. *Urban Remote Sensing Joint Event 11-13 April 2007, Paris, France*, pp 1-9.

Pall`as, R., Vilaplana, J. M., Guinau, M., Falg`as, E., Alemany, X., & Mu˜noz, A. (2004). A pragmatic approach to debris flow hazard mapping in areas affected by Hurricane Match. *Engineering Geology, 72*, pp 57-72.

Parise, M. (2002). Landslide hazard zonation of slopes susceptible to rock falls and topples. *Natural hazards and earth system sciences, 2*, pp 37-49.

Park, S., Choi, C., Kim, B., & Kim, J. (2013). Landslide susceptibility mapping using frequency ratio, analytic hierarchy process, logistic regression, and artificial neural network methods at the Inje area, Korea. *Environmental Earth Sciences, 68*, pp 1443–1464, DOI 1410.1007/s12665-12012-11842-12665.

Peng, L., Niu, R. Q., Huang, B., Wu, X. L., Zhao, Y. N., & Ye, R. Q. (2014). Landslide susceptibility mapping based on rough set theory and support vector machines: a case of the Three Gorges area, China. *Geomorphology, 204*, pp 287–301.

Pesci, A., Teza, G., Casula, G., Loddo, F., Martino, P., Dolce, M., Pingue, F. (2011). Multi-temporal laser scanner-based observation of the Mt. Vesuvius crater: Characterization of overall geometry and recognition of landslide events". *ISPRS Journal of Photogrammetry and Remote Sensing, 66*, pp 327-336.

Pourghasemi, H. R., Jirandeh, A. G., Pradhan, B., Xu, C., & Gokceoglu, C. (2013). Landslide susceptibility mapping using support vector machine and GIS at the Golestan Province. *Iran Journal of Earth System Sciences, 122*(2), pp 349–369.

Pourghasemi, H. R., Pradhan, B., Gokceoglu, C., Mohammadi, M., & Moradi, H. R. (2012). Application of weights-of-evidence and certainty factor models and their comparison in landslide susceptibility mapping at Haraz watershed, Iran. *Arabian Journal of Geosciences, 6*(7), pp 2351–2365.

Pradhan, B. (2013). A comparative study on the predictive ability of the decision tree, support vector machine and neuro-fuzzy models in landslide susceptibility mapping using GIS. *Computer Geosciences, 51*, pp 350-365, https://doi.org/310.1016/ j.cageo.2012.1008.1023.

Pradhan, B., Xu, C., & Gokceoglu, C. (2013). Landslide susceptibility mapping using support vector machine and GIS at the Golestan Province. *Journal of Earth System Science*, DOI: 10.1007/s12040-12013-10282-12042.

Rahman, M. M., Moran, M. S., Thoma, D. P., Bryant, R., Holifield-Colins, C. D., & Jackson, T. (2008). Mapping Surface Roughness and Soil Moisture using Multi-angular radar imagery without ancillary data. *Remote Sensing of Environment, 112*, pp 391-402.

Rahman, M. M., Moran, M. S., Thoma, D. P., Bryant, R., Sano, E. E., & Holifield-Colins, C. D. (2007). A derivation of roughness correlation length for parameterizing radar backscatter models. . *International Journal of Remote Sensing*, pp 1-18. doi:DOI: 10.1080/01431160601075533.

Raouf, A., & Lichtenegger, J. (1997). Integrated Use of SAR and Optical Data for Coastal Zone Management from ESA Earthnet Online.

Rathje, E., & Adams, B. J. (2008). The role of remote sensing in earthquake science and engineering, Opportunities and Challenges. *Earthquake Spectra, 24*(2), pp 471–492.

Regmi, N. R., Giardino, J. R., & Vitek, J. D. (2010). Modelling susceptibility to landslides using the weight of evidence approach: western Colorado, USA. *Geomorphology, 115*, pp 172-187.

Reis, S., Yalcin, A., Atasoy, M., Nisanci, R., Bayrak, T., Erduran, M., Ekercin, S. (2012). Remote sensing and GIS-based landslide susceptibility mapping using frequency ratio and analytical hierarchy methods in Rize province (NE Turkey). *Environmental Earth Sciences, 66*, pp 2063–2073.

Remondo, J., Gonz´alez-D´ıez, A., D´ıaz de Ter´an, J. R., Cendrero, A., Fabbri, A., & Chung, C. F. (2003). Validation of landslide susceptibility maps; examples and applications from a case study in Northern Spain. *Natural Hazards, 30*, pp 437–449.

Rignot, E. J. M., & van Zyl, J. J. (1993). Change detection techniques for ERS-1 SAR data. *IEEE Transactions on Geoscience and Remote Sensing, 31*, pp 896–906.

Rosin, P. L., Hervas, J., & Barredo, J. I. M. (2000). *Remote sensing image thresholding for landslide motion detection.* Paper presented at the 1st International Workshop on Pattern Recognition Techniques in Remote Sensing.

Rosso, R., Rulli, M. C., & Vannucchi, G. (2006). A physically based model for the hydrologic control on shallow landsliding. *Water Resource Research, 42*, doi:10.1029/2005WR004369.

Rupke, J., Cammeraat, E., Seijmonsbergen, A. C., & vanWesten, C. J. (1988). Engineering geomorphology of the widentobel catchment, appenzell and sankt-gallen, gallen, Switzerland: a geomorphological inventory system applied to geotechnical appraisal of slope stability. *Engineering Geology*, *26*, pp 33-68.

SAARC. (2010). *Report on Landslide Risk Management in South Asia, Thimpu, Bhutan*.

Saaty, T. L. (1980). *The Analytical Hierarchy Process, pp 287*. New York: McGraw Hill, 350.

Saaty, T. L. (2000). *Fundamentals of decision making and priority theory with the analytic hierarchy process*: 6.Rws Publications.

Saha, A. K., Gupta, R. P., Sarkar, I., Arora, M. K., & Csaplovics, E. (2005). An approach for GIS-based statistical landslide susceptibility zonation – with a case study in the Himalayas, Landslides. *2*, pp 61-69.

Sano, E. E., Huete, A. R., Troufleau, D., Moran, M. S., & Vidal, A. (1998). Relation between ERS-1 Synthetic Aperture Radar data and Measurements of Surface Roughness and Moisture Content of Rockey Soils in a semiarid rangeland. . *Water Resource Research, 34*(6), pp 1491-1498.

Santangelo, M., Cardinali, M., Rossi, M., Mondini, A. C., & Guzzetti, F. (2010). Remote landslide mapping using a laser rangefinder binocular and GPS. *Journal of Natural Hazards and Earth System Sciences, 10*, pp 2539–2546, doi: 2510.5194/nhess-2510-2539-2010.

Santurri, L., Carlà, R., Fiorucci, F., Aiazzi, B., Baronti, S., Cardinali, M., & Mondini, A. (2010). Assessment of very high resolution satellite data fusion techniques for landslide recognition. *International Archives of the Photogrammetry, Remote Sensing and Spatial Information Sciences, 38/B7*, pp 492-496.

Sar, N., Khan, A., Chatterjee, S., Das, A., & Mipun, B. S. M. (2016). *Coupling of analytical hierarchy process and frequency ratio based spatial prediction of soil erosion susceptibility in Keleghari river basin, India.* Paper presented at the International soil and water conservation research.

Sarkar, S., & Kanungo, D. P. (2004). An integrated approach for landslide susceptibility mapping using remote sensing and GIS. *Photogrammetric Engineering & Remote Sensing, 70*, pp 617–625.

Sarkar, S., Kanungo, D. P., & Mehrotra, G. S. (1995). Landslide Hazard Zonation: a case Study in Garhwal Himalaya, India. *Mountain Research and Development, 15*, pp 301–309.

Scaioni, M. (2013). Remote sensing for landslide investigations: From research into practice. *Remote Sensing, 5*, pp 5488–5492.

Scaioni, M., Longoni, L., Melillo, V., & Papini, M. (2014). Remote Sensing for Landslide Investigations: An Overview of Recent Achievements and Perspectives. *Remote Sensing, 6*(1), doi: 10.3390/rs3360x3000x.

Schicker, R., & Moon, V. (2012). Comparison of bivariate and multivariate statistical approaches in landslide susceptibility mapping at a regional scale. Geomorphology. *161*, pp 40-57.

Schuster, R. L. (1996). *Socioeconomic significance of landslides. In Landslides: Investigation and Mitigation*. Washington, DC, USA: National Academy Press, pp 12–35.

Sentinel_1 (2016). Sentinel-1 User Handbook.

Sentinel_2 (2016). Sentinel-2 User Handbook.

Septiadi, D., & Nasution, A. M. T. (2009). Determine Surface Roughness Level Based on Texture Analysis. (ICACSIS-09. University of Indonesia, Jakarta, Indonesia, 7 - 8 December. International Conference on Advanced Computer Science and Information Systems.).

Shahabi, H., Ahmad, B. B., & Khezri, S. (2013). Evaluation and comparison of bivariate and multivariate statistical methods for landslide susceptibility mapping (case study: Zab basin). *Arab Journal of Geosciences, 6*, pp 3885–3907, DOI 3810.1007/s12517-12012-10650-12512.

Shahabi, H., & Hashim, M. (2015). *Landslide susceptibility mapping using GIS based statistical models and Remote sensing data in tropical environment. Scientific report*.

Singh, A. (1989). Review article: Digital change detection techniques using remotely-sensed data. *International Journal of Remote Sensing, 10*(6), pp 989–1003.

Singhroy, V., Mattar, K., & Gray, A. (1998). Landslide Characterisation in Canada Using Interferometric SAR and Combined SAR and TM Images. *Advances in Space Research, 21*(3), pp 465-476.

Singhroy, V., & Mattar, K. M. (2000). *SAR image techniques for mapping areas of landslides.* Paper presented at the Proceedings XIXth ISPRS Congress, Amsterdam.

Sithamparapillai, P. M. T. U. N. (1994). *A Compendium of known Landslides in the Hill Country of Sri Lanka.* Paper presented at the National Symposium on landslides in Sri Lanka.

Soergel, U., Thiele, A., Gross, H., & Thoennessen, U. M. (2007). *Extraction of bridge features from high-resolution InSAR data and optical images.* Paper presented at the Urban Remote Sensing Joint Event, Paris, France.

Soeters, R., & van Westen, C. J. (1996). *Slope instability recognition, analysis, and zonation, In Landslides: investigation and mitigation. Transport Research Board Special Report*. 247, pp 129– 177.

Somaratne, M. (2016). Challenges to Overcome: An Overview of Koslanda Landslide.

Song, C., & Woodcock, C. E. (2003). Monitoring forest succession with multi-temporal Landsat images: factors of uncertainty. *IEEE Transactions on Geoscience and Remote Sensing, 41*, pp 2557–2567.

Sørensen, R. U., Zinko, U., & Seibert, J. (2006). On the calculation of the topographic wetness index: evaluation of different methods based on field observations. *Hydrology and Earth System Sciences, 10*, pp 101–112.

Speight, J. G. (1977). Landform pattern description from aerial photographs. *Journal of Photogrammetry, 32*, pp 161-182.

Sportouche, H., Tupin, F., & Denise, L. M. (2009). *Building Detection by Fusion of Optical and SAR Features in Metric Resolution Data.* Paper presented at the International Geoscience & Remote Sensing Symposium, IGARSS 2009, University of Cape Town, Cape Town, South Africa.

Stilla, U., Soergel, U., Thoennessen, U., & Brenner, A. (2005). *Potential and limits for reconstruction of buildings from high resolution SAR data of urban areas.* Paper presented at the 28th General Assembly of International Union Radio Science (URSI), New Delhi, India.

Stramondo, S., Bignami, C., Chini, M., & Pierdicca, N. (2006). Satellite radar and optical remote sensing for earthquake damage detection: results from different case studies. *International Journal of Remote Sensing, 27*(20), pp 4433–4447.

Suzen, M. L., & Kaya, B. S. (2012). Evaluation of environmental parameters in logistic regression models for landslide susceptibility mapping. *International Journal of Digital Earth, 5*, pp 338–355.

Takahashi, T. (2007). *Debris flow: Mechanics, Prediction and Countermeasures*. Leiden, 448p: Taylor & Francis.

Takahashi, T. (2009). A Review of Japanese Debris Flow Research. *International Journal of Erosion Control Engineering, 2*(1).

Tarboton, D. G. (1997). A new method for the determination of flow directions and upslope areas in grid digital elevation models. *Water Resource Research, 33*, pp 309–319.

TerraSAR_X (2016). TerraSAR-X image product guide.

Thoma, D., Moran, M., Bryant, R., Holifield-Colins, C., Rahman, M., & Skirvin, S. (2004). Comparison of Two Methods for Extracting Surface Soil Moisture from C-band Radar Imagery. *IEEE Transactions on Geoscience and Remote Sensing, 4*, pp 827-830.

Thoma, D. P., Moran, M. S., Bryant, R., Rahman, M., & Holifield-Colins, C. D. (2006). Comparison of four models to determine surface soil moisture from C-band radar imagery in a sparsely vegetated semiarid landscape. . *Water Resource Research, 42*. doi:doi:10.1029/2004WR003905.

Tralli, D. M., Blom, R. G., Zlotnicki, V., Donnellan, A., & Evans, D. L. (2005). Satellite remote sensing of earthquake, volcano, flood, landslide and coastal inundation hazards. *ISPRS Journal of Photogrammetry and Remote Sensing, 59*(4), pp 185-198.

Tsuchida, R., Liu, W., & Yamazaki, F. M. (2015). *Detection of landslides in the 2015 Gorkha, Nepal earthquake using satellite imagery.* Paper presented at the 36th Asian Conference on Remote Sensing, Metro Manila, Philippines.

Tupin, F., & Roux, M. (2003). Detection of building outlines based on the fusion of SAR and optical features. *Journal of Photogrammetry and Remote Sensing, 58*(1-2), pp 71–82.

USGS (2004). Landslide Types and Processes, from Fact Sheet 2004-3072.

van Westen, C., van Asch, T., & Soeters, R. (2006). Landslide hazard and risk zonation – why is it still so difficult", B. Eng. Geol. Environ. *Engineering Geology and the Environment, 65*, pp 167-184.

van Westen, C. J. (1993). *Application of geographic information systems to landslide hazard zonation*.

van Westen, C. J. (1997). *Statistical landslide hazard analysis. In: Application guide, ILWIS 2.1 for Windows, ITC, Enschede, The Netherlands, pp 73-84*. ITC, Enschede, The Netherlands.

van Westen, C. J., Castellanos, E., & Kuriakose, S. K. (2008). Spatial data for landslide susceptibility, hazard, and vulnerability assessment: An overview. *Engineering Geology, 102*, pp 112-131.

van Westen, C. J., & Lulie, G. F. (2003). Analyzing the evolution of the Tessina landslide using aerial photographs and digital elevation models. *Geomorphology, 54*(1-2), pp 77-89.

van Westen, C. J., Rengers, N., & Soeters, R. (2003). Use of geomorphological information in indirect landslide susceptibility assessment. *Natural Hazards, 30*, pp 399–419.

Varnes, D. J. (1984a). *Landslide Hazard Zonation: A Review of Principles and Practice, IAEG Commission on landslides and other mass-movements*. Paris, France: The UNESCO Press, p 63.

Varnes, D. J. (1984b). *Landslides: Analysis and Control, Slope movements types and processes*. Washinton DC: Transportation Research Board, National Academy of sciences.

Vieira, M. A., Formaggio, A. R., Rennó, C. D., Atzberger, C., Aguiar, D. A., & Mello, M. P. (2012). Object based image analysis and data mining applied to a remotely sensed Landsat time-series to map sugarcane over large areas. *Remote Sensing of Environment, 123*, pp 530–562.

Vinodkumar, K. V., Lakhera, R. C., Martha, T. R., Chatterjee, R. S., & Bhattacharya, A. (2008). Analysis of the 2003 Varunawat landslide, Uttarkashi, India using earth observation data. *Environmental Geology, 55*, pp 789-799.

Vohora, V. K., & Donoghue, S. L. M. (2004). *Application of remote sensing data to landslide mapping in Hong Kong, 35/B4.* Paper presented at the ISPRS, Turkey.

Voigt, S., Kemper, T., Riedlinger, T., Kiefl, R., Scholte, K., & Mehl, H. (2007). Satellite image analysis for disaster and crisis-management support. *IEEE Transactions on Geosciences and Remote Sensing, 45*(6), pp 1520–1528.

Wang, L., & Qu, J. J. (2009). Satellite Remote Sensing applications for Surface Soil Moisture Monitoring: A review. *Front. Earth Sciences China, 3*(2), pp 237-247. doi:doi: 10.1007/s11707-009-0023-7.

Wasowski, J., & Bovenga, F. (2014). Investigating landslides and unstable slopes with satellite multi-temporal interferometry: Current issues and future perspectives. *Engineering Geology, 174*, pp 103-138.

Weerasinghe, K., Malalasekara, A., & Dahanayake, K. (2008). *Learning to live with LANDSLIDES, Educational Booklet on Landslides*. Natural Hazards and Disasters: Department of Institutional Development, National Institute of Education.

Weerawansha, G., Peiris, H. A. A., Kulatunga, A. K., Ekanayake, S. B., & Dissanayake, P. B. R. M. (2007). *Basic methodology for Landslides related disaster preparedness in Sri Lanka.* Paper presented at the International Conference of the International Institute for Infrastructure Resilience and Reconstruction (IIIRR), Kandy, Sri Lanka.

WorldView_2 (2016). WorldView-2 product guide, Digital Globe.

Yalcin, A. (2008). GIS-based landslide susceptibility mapping using analytical hierarchy process and bivariate statistics in Ardesen (Turkey): comparison of results and confirmations. *Journal of Catena, 72*, pp 1-12.

Yamazaki, F., Inoue, H., & Liu, W. (2011). *Characteristics of SAR backscattered intensity and its application to earthquake damage detection. Computational Stochastic Mechanics*: pp 602-606, ISBN 978-981-08-7619-7.

Yawen, M. (2011). *Regional Scale Multi-hazard Susceptibility Assessment: a case study in Mtskheta-Mtianeti, Georgia.* (MSc Thesis), Faculty of Geoinformation Science and Earth Observation, University of Twente, The Netherlands.

Yilmaz, C., Topal, T., & Suzen, M. L. (2012). GIS-based landslide susceptibility mapping using bivariate statistical analysis in Devrek (Zonguldak-Turkey). *Environmental Earth Sciences, 65*, pp 2161–2178.

Yilmaz, I. (2009). Landslide susceptibility mapping using frequency ratio, logistic regression, artificial neural networks and their comparison: a case study from Kat landslides (Tokat-Turkey). *Computers and Geosciences, 35*, pp 1125–1138.

Yin, K. J., & Yan, T. Z. M. (1988). *Statistical prediction model for slope instability of metamorphosed rocks.* Paper presented at the Proceedings of the 5th international symposium on landslides, Lausanne, Switzerland 2.

Youssef, A. M., Pourghasemi, H. R., El-Haddad, B. A., & Dhahry, B. K. (2015). Landslide susceptibility maps using different probabilistic and bivariate statistical models and comparison of their performance at Wadi Itwad Basin, Asir Region, Saudi Arabia. *Bulletin of Engineering Geology and the Environment*, http://dx.doi.org/10.1007/s10064-10015-10734-10069.

Zenga, Y., Fengb, Z., & Xianga, N. M. (2004). *Assessment of soil moisture using Landsat ETM+temperature/vegetation index in semiarid environment.* Paper presented at the IEEE International Geoscience and Remote Sensing Symposium, IGARSS 04, Anchorage, AK, 06.

Zezere, J., Trigo, R., & Trigo, I. (2005). Shallow and deep landslides induced by rainfall in the Lisbon region (Portugal): assessment of relationships with the North Atlantic Oscillation. *Natural hazards and earth system sciences, 5*, pp 331-344.

Zhan, X., Miller, S., Chauhan, N., Di, L., Ardanuy, P., & Running, S. (2002). Soil Moisture Visible/Infrared Imager/Radiometer Suite Algorithm Theoretical Basis Document. Version 5.

APPENDIX A – Weight of Influence for Landslide predisposing factors

Following tables show the calculation procedure of the weight of influence for the fifteen selected predisposing factors

Table 1: Weight of influence for Topographical predisposing factor "Elevation"

Table 2: Weight of influence for Topographical predisposing factor "Slope"

Table 3: Weight of influence for Topographical predisposing factor "Aspect"

Table 4: Weight of influence for Topographical predisposing factor "Planar curvature"

Table 5: Weight of influence for Topographical predisposing factor "Profile curvature"

Table 6: Weight of influence for Topographical predisposing factor "Surface roughness (radar)"

Table 7: Weight of influence for Hydrological predisposing factor "Distance to hydrology"

Table 8: Weight of influence for Hydrological predisposing factor "Topographical Wetness Index (TWI)"

Table 9: Weight of influence for Hydrological predisposing factor "Rainfall"

Table 10: Weight of influence for Soil predisposing factor "Surface soil moisture"

Table 11: Weight of influence for Soil predisposing factor "Soil Moisture Index (radar)"

Table 12: Weight of influence for Land cover predisposing factor "Land cover type"

Table 13: Weight of influence for Land cover predisposing factor "Forest biomass"

Table 14: Weight of influence for Geological predisposing factor "Geology"

Table 15: Weight of influence for Geological predisposing factor "Lineament density"

A - No of failure pixels in the particular class

B - No of whole pixels in the particular class

C - Whole failure pixels in the study area

D - Whole pixels in the study area

Table 1 : Weight of influence for Topographical predisposing factor "Elevation"

No of classes	break values	A	B	C	D	densclass	densmap	weight	*100	weight final	LOG	LOG final
1	446 - 600	6087	109273	36025	730895	0.05570	0.04929	1.13016	113.016	113	0.05314	0.053
2	600 - 710	4917	128866	36025	730895	0.03816	0.04929	0.77413	77.413	77	-0.11119	-0.111
3	710 - 790	3420	80067	36025	730895	0.04271	0.04929	0.86661	86.661	87	-0.06218	-0.062
4	790 - 900	4580	101449	36025	730895	0.04515	0.04929	0.91594	91.594	92	-0.03813	-0.038
5	900 - 1050	13724	133169	36025	730895	0.10306	0.04929	2.09088	209.088	209	0.32033	0.320
6	1050 - 1260	2805	118332	36025	730895	0.02370	0.04929	0.48093	48.093	48	-0.31792	-0.318
7	1260 - 1540	492	59739	36025	730895	0.00824	0.04929	0.16709	16.709	17	-0.77704	-0.777

No of classes	break value	A	B	C	D	densclass	densmap	weight	*100	weight final	LOG	LOG final
1	10	6901	126235	36025	730895	0.05467	0.04929	1.10913	110.913	111	0.04498	0.045
2	15	7698	219096	36025	730895	0.03514	0.04929	0.71284	71.284	71	-0.14701	-0.147
3	25	13304	159137	36025	730895	0.08360	0.04929	1.69614	169.614	170	0.22946	0.229
4	30	3353	111498	36025	730895	0.03007	0.04929	0.61012	61.012	61	-0.21458	-0.215

5	40	3056	73145	36025	730895	0.04178	0.04929	0.84766	84.766	85	-0.07178	-0.072
6	50	941	31880	36025	730895	0.02952	0.04929	0.59886	59.886	60	-0.22268	-0.223
7	80	772	9904	36025	730895	0.07795	0.04929	1.58146	158.146	158	0.19906	0.199

Table 2 : Weight of influence for Topographical predisposing factor "Slope"

No of classes	break value	A	B	C	D	densclass	densmap	weight	*100	weight final	LOG	LOG final
1	N	961	25065	36025	730895	0.03834	0.04929	0.77787	77.787	78	-0.10909	-0.109
2	NE	1925	18085	36025	730895	0.10644	0.04929	2.15955	215.955	216	0.33436	0.334
3	E	6599	58557	36025	730895	0.11269	0.04929	2.28639	228.639	229	0.35915	0.359
4	SE	9007	158397	36025	730895	0.05686	0.04929	1.15368	115.368	115	0.06208	0.062
5	S	7816	146386	36025	730895	0.05339	0.04929	1.08327	108.327	108	0.03474	0.035
6	SW	4924	123340	36025	730895	0.03992	0.04929	0.80996	80.996	81	-0.09153	-0.092
7	W	3141	121771	36025	730895	0.02579	0.04929	0.52333	52.333	52	-0.28122	-0.281
8	NW	1652	79294	36025	730895	0.02083	0.04929	0.42269	42.269	42	-0.37398	-0.374

Table 3 :Weight of influence for Topographical predisposing factor "Aspect"

No of classes	break value	A	B	C	D	densclass	densmap	weight	*100	weight final	LOG	LOG final
1	-116.87 - -16.34	276	7679	36025	730895	0.03594	0.04929	0.72921	72.921	73	-0.13714	-0.137
2	-16.34 - -7.74	1569	48647	36025	730895	0.03225	0.04929	0.65436	65.436	65	-0.18418	-0.184
3	-7.74 - -2.59	6388	133567	36025	730895	0.04783	0.04929	0.97032	97.032	97	-0.01308	-0.013
4	-2.59 - -0.8	5875	105724	36025	730895	0.05557	0.04929	1.12742	112.742	113	0.05209	0.052
5	-0.8 - 3.68	15828	287665	36025	730895	0.05502	0.04929	1.11632	111.632	112	0.04779	0.048
6	3.68 - 9.37	4897	109086	36025	730895	0.04489	0.04929	0.91078	91.078	91	-0.04059	-0.041
7	9.37 - 102.25	1192	38527	36025	730895	0.03094	0.04929	0.62771	62.771	63	-0.20224	-0.202

Table 4 : Weight of influence for Topographical predisposing factor "Planar curvature"

Table 5 :Weight of influence for Topographical predisposing factor "Profile curvature"

No of classes	break value	A	B	C	D	densclass	densmap	weight	*100	weight final	LOG	LOG final
1	-169.89 - -26.96	194	5838	36025	730895	0.03323	0.04929	0.67420	67.420	67	-0.17121	-0.171
2	-26.96 - -12.3	1626	47862	36025	730895	0.03397	0.04929	0.68926	68.926	69	-0.16162	-0.162
3	-12.3 - -3.28	8096	157249	36025	730895	0.05149	0.04929	1.04456	104.456	104	0.01893	0.019

4	-3.28 - 1.13	11857	220702	36025	730895	0.05372	0.04929	1.08999	108.999	109	0.03742	0.037
5	1.13 - 8.46	10459	201529	36025	730895	0.05190	0.04929	1.05294	105.294	105	0.02240	0.022
6	8.46 - 21.9	3458	85635	36025	730895	0.04038	0.04929	0.81926	81.926	82	-0.08658	-0.087
7	21.9 - 141.63	335	12080	36025	730895	0.02773	0.04929	0.56264	56.264	56	-0.24977	-0.250

Table 6 :Weight of influence for Topographical predisposing factor "Surface roughness (radar)"

No of classes	break value	A	B	C	D	densclass	densmap	weight	*100	weight final	LOG	LOG final
1	0.178186 - 0.330745	9679	237949	36025	730895	0.04068	0.04929	0.82527	82.527	82	-0.08340	-0.084
2	0.330745 - 0.390972	14294	219651	36025	730895	0.06508	0.04929	1.32030	132.030	132	0.12067	0.120
3	0.390972 - 0.414748	9093	120237	36025	730895	0.07563	0.04929	1.53433	153.433	153	0.18592	0.186
4	0.414748 - 0.474975	2433	67109	36025	730895	0.03625	0.04929	0.73555	73.555	74	-0.13339	-0.133
5	0.474975 - 0.627534	518	43885	36025	730895	0.01180	0.04929	0.23948	23.948	24	-0.62074	-0.620
6	0.627534 - 1.013976	8	29178	36025	730895	0.00027	0.04929	0.00556	0.556	1	-2.25471	-2.253
7	1.013976 - 1.992856	0	12886	36025	730895	0.00000	0.04929	0.00000	0.000	0	0.00000	0.000

Table 7 :Weight of influence for Hydrological predisposing factor "Distance to hydrology"

No of classes	break value	A	B	C	D	densclass	densmap	weight	*100	weight final	LOG	LOG final
1	20	6639	126235	36025	730895	0.05259	0.04929	1.06702	106.702	107	0.02817	0.028
2	65	12267	219096	36025	730895	0.05599	0.04929	1.13594	113.594	114	0.05535	0.055
3	115	8412	159137	36025	730895	0.05286	0.04929	1.07246	107.246	107	0.03038	0.030
4	175	4089	111498	36025	730895	0.03667	0.04929	0.74405	74.405	74	-0.12840	-0.128
5	250	3221	73145	36025	730895	0.04404	0.04929	0.89342	89.342	89	-0.04894	-0.049
6	350	1397	31880	36025	730895	0.04382	0.04929	0.88906	88.906	89	-0.05107	-0.051
7	565	0	9904	36025	730895	0.00000	0.04929	0.00000	0.000	0	0.00000	0.000

Table 8 : Weight of influence for Hydrological predisposing factor "Topographical Wetness Index (TWI)"

No of classes	break value	A	B	C	D	densclass	densmap	weight	*100	weight final	LOG	LOG final
1	0 - 3	15500	338442	36025	730895	0.04580	0.04929	0.92918	92.918	93	-0.03190	-0.032
2	3 - 5	6026	130315	36025	730895	0.04624	0.04929	0.93818	93.818	94	-0.02771	-0.028
3	5 - 10	7199	140498	36025	730895	0.05124	0.04929	1.03957	103.957	104	0.01685	0.017
4	10 - 80	6695	114448	36025	730895	0.05850	0.04929	1.18684	118.684	119	0.07439	0.074
5	80 - 5415	605	7192	36025	730895	0.08412	0.04929	1.70670	170.670	171	0.23216	0.232

Table 9 :Weight of influence for Hydrological predisposing factor "Rainfall"

No of classes	break value	A	B	C	D	densclass	densmap	weight	*100	weight final	LOG	LOG final
1	360 - 380	6326	91239	36025	730895	0.06933	0.04929	1.40669	140.669	141	0.14820	0.148
2	380 - 400	4166	123524	36025	730895	0.03373	0.04929	0.68426	68.426	68	-0.16478	-0.165
3	400 - 415	10685	95994	36025	730895	0.11131	0.04929	2.25830	225.830	226	0.35378	0.354
4	415 - 430	3450	101629	36025	730895	0.03395	0.04929	0.68874	68.874	69	-0.16195	-0.162
5	430 - 445	6173	111846	36025	730895	0.05519	0.04929	1.11976	111.976	112	0.04913	0.049
6	445 - 460	5225	103533	36025	730895	0.05047	0.04929	1.02390	102.390	102	0.01026	0.010
7	460 - 485	0	103130	36025	730895	0.00000	0.04929	0.00000	0.000	0	0.00000	0.000

Table 10 :Weight of influence for Soil predisposing factor "Surface soil moisture"

No of classes	break values	A	B	C	D	densclass	densmap	weight	*100	weight final	LOG	LOG final
1	-4.69 - -1.47	3311	60708	36025	730895	0.05454	0.04929	1.10653	110.653	111	0.04396	0.044
2	-1.47 - -0.96	10910	209281	36025	730895	0.05213	0.04929	1.05766	105.766	106	0.02434	0.024
3	-0.96 - -0.53	14265	256526	36025	730895	0.05561	0.04929	1.12821	112.821	113	0.05239	0.052
4	-0.53 - 0.06	7130	164138	36025	730895	0.04344	0.04929	0.88131	88.131	88	-0.05487	-0.055
5	0.06 - 2.91	409	40240	36025	730895	0.01016	0.04929	0.20621	20.621	21	-0.68568	-0.686

Table 11 : Weight of influence for Soil predisposing factor "Soil Moisture Index (radar)"

No of classes	break value	A	B	C	D	densclass	densmap	weight	*100	weight final	LOG	LOG final
1	-0.07 - 0.11	6055	17344	36025	730895	0.34911	0.04929	7.08298	708.298	713	0.85022	0.853
2	0.11 - 0.29	11825	201888	36025	730895	0.05857	0.04929	1.18834	118.834	119	0.07494	0.075
3	0.29 - 0.44	11141	285156	36025	730895	0.03907	0.04929	0.79267	79.267	79	-0.10091	-0.101
4	0.44 - 0.65	6365	153598	36025	730895	0.04144	0.04929	0.84074	84.074	84	-0.07534	-0.076
5	0.65 - 1.1	639	72909	36025	730895	0.00876	0.04929	0.17782	17.782	18	-0.75003	-0.756

Table 12 : Weight of influence for Land cover predisposing factor "Land cover type"

No of Classes	Land cover	A	B	C	D	densclass	densmap	weight	*100	weight final	LOG	LOG final
1	residential	327	6571	36025	730895	0.04976	0.04929	1.00964	100.964	101	0.00417	0.004
2	tea	21925	247420	36025	730895	0.08861	0.04929	1.79786	179.786	180	0.25476	0.255
3	scrub	12491	412088	36025	730895	0.03031	0.04929	0.61498	61.498	61	-0.21114	-0.211
4	forest	1273	64284	36025	730895	0.01980	0.04929	0.40177	40.177	40	-0.39602	-0.396
5	other	9	532	36025	730895	0.01692	0.04929	0.34323	34.323	34	-0.46442	-0.464

Table 13 : Weight of influence for Land cover predisposing factor "Forest biomass"

No of classes	break value	A	B	C	D	densclass	densmap	weight	*100	weight final	LOG	LOG final
1	-7.4312--5.764	13078	256419	36025	730895	0.36303	0.35083	1.03477	103.477	103	0.01484	0.015
2	-5.764-0.113	10514	209578	36025	730895	0.29185	0.28674	1.01783	101.783	102	0.00767	0.008
3	0.113-1.875	7811	174283	36025	730895	0.21682	0.23845	0.90929	90.929	91	-0.04130	-0.041
4	1.875-2.469	4025	69725	36025	730895	0.11173	0.09540	1.17119	117.119	117	0.06863	0.069
5	2.469-3.1914	597	20890	36025	730895	0.01657	0.02858	0.57981	57.981	58	-0.23671	-0.237

Table 14 : Weight of influence for Geological predisposing factor "Geology"

No of classes	break values	A	B	C	D	densclass	densmap	weight	*100	weight final	LOG	LOG final
1	Pmc	0	1146	36025	730895	0.00000	0.04929	0.00000	0.000	0	0.00000	0.000
2	Pmgga	0	2088	36025	730895	0.00000	0.04929	0.00000	0.000	0	0.00000	0.000
3	Pmgga_ga	878	79008	36025	730895	0.01111	0.04929	0.22546	22.546	23	-0.64693	-0.647
4	Pmgk	0	89	36025	730895	0.00000	0.04929	0.00000	0.000	0	0.00000	0.000

5	Pmgk_b	34074	523222	36025	730895	0.06512	0.04929	1.32126	132.126	132	0.12099	0.121
6	Pmgqf_ga	0	7	36025	730895	0.00000	0.04929	0.00000	0.000	0	0.00000	0.000
7	Pmq	1073	125335	36025	730895	0.00856	0.04929	0.17369	17.369	17	-0.76022	-0.760

Table 15 : Weight of influence for Geological predisposing factor "Lineament density"

No of classes	A	B	C	D	densclass	densmap	weight	*100	weight final	LOG	LOG final
0	1820	72180	36025	730895	0.02521	0.04929	0.51157	51.157	51	-0.29109	-0.291
1	2847	58857	36025	730895	0.04837	0.04929	0.98139	98.139	98	-0.00816	-0.008
2	5050	96920	36025	730895	0.05210	0.04929	1.05713	105.713	106	0.02413	0.024
3	6088	134472	36025	730895	0.04527	0.04929	0.91853	91.853	92	-0.03691	-0.037
4	6011	146154	36025	730895	0.04113	0.04929	0.83442	83.442	83	-0.07861	-0.079
5	3962	82686	36025	730895	0.04792	0.04929	0.97215	97.215	97	-0.01227	-0.012
6	9075	114113	36025	730895	0.07953	0.04929	1.61348	161.348	161	0.20776	0.208
7	1172	25513	36025	730895	0.04594	0.04929	0.93200	93.200	93	-0.03058	-0.031

APPENDIX B – Questionnaire Survey for MCDA based on AHP technique

Questionnaire for MCDA with AHP technique

Questionnaire Survey

PhD Research

University of Moratuwa, Sri Lanka

NO:

RESEARCH TITLE:

INTEGRATION OF RADAR AND OPTICAL REMOTE SENSING FOR LANDSLIDE PREDICTION. A CASE STUDY OF KOSLANDA, SRI LANKA

The importance of the criterion for landslide predictions is expected. The information derived from questionnaire survey will only be used for the above research. We thank you very much for your valuable cooperation.

1. Designation: .....
2. Answer the question **2** according to the given instructions.

Degree	Description of pair wise comparison judgment
1	Equally important
3	Moderately important

5	Strongly important
7	Very strongly important
9	Extremely important

2, 4, 6, 8 are intermediate values.

Main Criteria of the Research,

A – Elevation

B – Slope

C – Aspect

D – Planar Curvature

E – Profile Curvature

F – Topographical Wetness Index (TWI)

G – Land use

H – Lineament Density

I – Distance to Hydrology

J – Soil Moisture Index (SMI)

K – Geology

L – Rainfall

M – Surface Soil Moisture

N – Surface Roughness

O – Forest Biomass

Example: -

When you consider the criteria A is **strongly important** than B, then mark the suitability degree of the table as follows:

A	**9**	**7**	**5**	**3**	**1**	**3**	**5**	**7**	**9**	**B**

When you consider the criteria B is **strongly important** than A, then mark the suitability degree of the table as follows:

A	**9**	**7**	**5**	**3**	**1**	**3**	**5**	**7**	**9**	**B**

According to your preference, mark your desired degree of importance for the desired criterion.

A	**9**	**7**	**5**	**3**	**1**	**3**	**5**	**7**	**9**	B
A	**9**	**7**	**5**	**3**	**1**	**3**	**5**	**7**	**9**	C
A	**9**	**7**	**5**	**3**	**1**	**3**	**5**	**7**	**9**	D
A	**9**	**7**	**5**	**3**	**1**	**3**	**5**	**7**	**9**	E
A	**9**	**7**	**5**	**3**	**1**	**3**	**5**	**7**	**9**	F
A	**9**	**7**	**5**	**3**	**1**	**3**	**5**	**7**	**9**	G
A	**9**	**7**	**5**	**3**	**1**	**3**	**5**	**7**	**9**	H
A	**9**	**7**	**5**	**3**	**1**	**3**	**5**	**7**	**9**	I
A	**9**	**7**	**5**	**3**	**1**	**3**	**5**	**7**	**9**	J
A	**9**	**7**	**5**	**3**	**1**	**3**	**5**	**7**	**9**	K
A	**9**	**7**	**5**	**3**	**1**	**3**	**5**	**7**	**9**	L
A	**9**	**7**	**5**	**3**	**1**	**3**	**5**	**7**	**9**	M
A	**9**	**7**	**5**	**3**	**1**	**3**	**5**	**7**	**9**	N
A	**9**	**7**	**5**	**3**	**1**	**3**	**5**	**7**	**9**	O

.

B	**9**	**7**	**5**	**3**	**1**	**3**	**5**	**7**	**9**	C
B	**9**	**7**	**5**	**3**	**1**	**3**	**5**	**7**	**9**	D
B	**9**	**7**	**5**	**3**	**1**	**3**	**5**	**7**	**9**	E
B	**9**	**7**	**5**	**3**	**1**	**3**	**5**	**7**	**9**	F
B	**9**	**7**	**5**	**3**	**1**	**3**	**5**	**7**	**9**	G
B	**9**	**7**	**5**	**3**	**1**	**3**	**5**	**7**	**9**	H
B	**9**	**7**	**5**	**3**	**1**	**3**	**5**	**7**	**9**	I
B	**9**	**7**	**5**	**3**	**1**	**3**	**5**	**7**	**9**	J
B	**9**	**7**	**5**	**3**	**1**	**3**	**5**	**7**	**9**	K
B	**9**	**7**	**5**	**3**	**1**	**3**	**5**	**7**	**9**	L
B	**9**	**7**	**5**	**3**	**1**	**3**	**5**	**7**	**9**	M
B	**9**	**7**	**5**	**3**	**1**	**3**	**5**	**7**	**9**	N
B	**9**	**7**	**5**	**3**	**1**	**3**	**5**	**7**	**9**	O

C	**9**	**7**	**5**	**3**	**1**	**3**	**5**	**7**	**9**	D
C	**9**	**7**	**5**	**3**	**1**	**3**	**5**	**7**	**9**	E
C	**9**	**7**	**5**	**3**	**1**	**3**	**5**	**7**	**9**	F
C	**9**	**7**	**5**	**3**	**1**	**3**	**5**	**7**	**9**	G
C	**9**	**7**	**5**	**3**	**1**	**3**	**5**	**7**	**9**	H
C	**9**	**7**	**5**	**3**	**1**	**3**	**5**	**7**	**9**	I
C	**9**	**7**	**5**	**3**	**1**	**3**	**5**	**7**	**9**	J
C	**9**	**7**	**5**	**3**	**1**	**3**	**5**	**7**	**9**	K
C	**9**	**7**	**5**	**3**	**1**	**3**	**5**	**7**	**9**	L
C	**9**	**7**	**5**	**3**	**1**	**3**	**5**	**7**	**9**	M
C	**9**	**7**	**5**	**3**	**1**	**3**	**5**	**7**	**9**	N
C	**9**	**7**	**5**	**3**	**1**	**3**	**5**	**7**	**9**	O

D	**9**	**7**	**5**	**3**	**1**	**3**	**5**	**7**	**9**	E
D	**9**	**7**	**5**	**3**	**1**	**3**	**5**	**7**	**9**	F
D	**9**	**7**	**5**	**3**	**1**	**3**	**5**	**7**	**9**	G
D	**9**	**7**	**5**	**3**	**1**	**3**	**5**	**7**	**9**	H
D	**9**	**7**	**5**	**3**	**1**	**3**	**5**	**7**	**9**	I
D	**9**	**7**	**5**	**3**	**1**	**3**	**5**	**7**	**9**	J
D	**9**	**7**	**5**	**3**	**1**	**3**	**5**	**7**	**9**	K
D	**9**	**7**	**5**	**3**	**1**	**3**	**5**	**7**	**9**	L
D	**9**	**7**	**5**	**3**	**1**	**3**	**5**	**7**	**9**	M
D	**9**	**7**	**5**	**3**	**1**	**3**	**5**	**7**	**9**	N
D	**9**	**7**	**5**	**3**	**1**	**3**	**5**	**7**	**9**	O

E	**9**	**7**	**5**	**3**	**1**	**3**	**5**	**7**	**9**	F
E	**9**	**7**	**5**	**3**	**1**	**3**	**5**	**7**	**9**	G
E	**9**	**7**	**5**	**3**	**1**	**3**	**5**	**7**	**9**	H
E	**9**	**7**	**5**	**3**	**1**	**3**	**5**	**7**	**9**	I
E	**9**	**7**	**5**	**3**	**1**	**3**	**5**	**7**	**9**	J
E	**9**	**7**	**5**	**3**	**1**	**3**	**5**	**7**	**9**	K
E	**9**	**7**	**5**	**3**	**1**	**3**	**5**	**7**	**9**	L
E	**9**	**7**	**5**	**3**	**1**	**3**	**5**	**7**	**9**	M
E	**9**	**7**	**5**	**3**	**1**	**3**	**5**	**7**	**9**	N
E	**9**	**7**	**5**	**3**	**1**	**3**	**5**	**7**	**9**	O

F	**9**	**7**	**5**	**3**	**1**	**3**	**5**	**7**	**9**	G
F	**9**	**7**	**5**	**3**	**1**	**3**	**5**	**7**	**9**	H

F	**9**	**7**	**5**	**3**	**1**	**3**	**5**	**7**	**9**	I
F	**9**	**7**	**5**	**3**	**1**	**3**	**5**	**7**	**9**	J
F	**9**	**7**	**5**	**3**	**1**	**3**	**5**	**7**	**9**	K
F	**9**	**7**	**5**	**3**	**1**	**3**	**5**	**7**	**9**	L
F	**9**	**7**	**5**	**3**	**1**	**3**	**5**	**7**	**9**	M
F	**9**	**7**	**5**	**3**	**1**	**3**	**5**	**7**	**9**	N
F	**9**	**7**	**5**	**3**	**1**	**3**	**5**	**7**	**9**	O

G	**9**	**7**	**5**	**3**	**1**	**3**	**5**	**7**	**9**	H
G	**9**	**7**	**5**	**3**	**1**	**3**	**5**	**7**	**9**	I
G	**9**	**7**	**5**	**3**	**1**	**3**	**5**	**7**	**9**	J
G	**9**	**7**	**5**	**3**	**1**	**3**	**5**	**7**	**9**	K
G	**9**	**7**	**5**	**3**	**1**	**3**	**5**	**7**	**9**	L
G	**9**	**7**	**5**	**3**	**1**	**3**	**5**	**7**	**9**	M
G	**9**	**7**	**5**	**3**	**1**	**3**	**5**	**7**	**9**	N
G	**9**	**7**	**5**	**3**	**1**	**3**	**5**	**7**	**9**	O

H	**9**	**7**	**5**	**3**	**1**	**3**	**5**	**7**	**9**	I
H	**9**	**7**	**5**	**3**	**1**	**3**	**5**	**7**	**9**	J
H	**9**	**7**	**5**	**3**	**1**	**3**	**5**	**7**	**9**	K
H	**9**	**7**	**5**	**3**	**1**	**3**	**5**	**7**	**9**	L
H	**9**	**7**	**5**	**3**	**1**	**3**	**5**	**7**	**9**	M
H	**9**	**7**	**5**	**3**	**1**	**3**	**5**	**7**	**9**	N
H	**9**	**7**	**5**	**3**	**1**	**3**	**5**	**7**	**9**	O

I	**9**	**7**	**5**	**3**	**1**	**3**	**5**	**7**	**9**	J
I	**9**	**7**	**5**	**3**	**1**	**3**	**5**	**7**	**9**	K
I	**9**	**7**	**5**	**3**	**1**	**3**	**5**	**7**	**9**	L
I	**9**	**7**	**5**	**3**	**1**	**3**	**5**	**7**	**9**	M
I	**9**	**7**	**5**	**3**	**1**	**3**	**5**	**7**	**9**	N
I	**9**	**7**	**5**	**3**	**1**	**3**	**5**	**7**	**9**	O

J	**9**	**7**	**5**	**3**	**1**	**3**	**5**	**7**	**9**	K
J	**9**	**7**	**5**	**3**	**1**	**3**	**5**	**7**	**9**	L
J	**9**	**7**	**5**	**3**	**1**	**3**	**5**	**7**	**9**	M
J	**9**	**7**	**5**	**3**	**1**	**3**	**5**	**7**	**9**	N
J	**9**	**7**	**5**	**3**	**1**	**3**	**5**	**7**	**9**	O

K	**9**	**7**	**5**	**3**	**1**	**3**	**5**	**7**	**9**	L

K	**9**	**7**	**5**	**3**	**1**	**3**	**5**	**7**	**9**	M
K	**9**	**7**	**5**	**3**	**1**	**3**	**5**	**7**	**9**	N
K	**9**	**7**	**5**	**3**	**1**	**3**	**5**	**7**	**9**	O

L	**9**	**7**	**5**	**3**	**1**	**3**	**5**	**7**	**9**	M
L	**9**	**7**	**5**	**3**	**1**	**3**	**5**	**7**	**9**	N
L	**9**	**7**	**5**	**3**	**1**	**3**	**5**	**7**	**9**	O

M	**9**	**7**	**5**	**3**	**1**	**3**	**5**	**7**	**9**	N
M	**9**	**7**	**5**	**3**	**1**	**3**	**5**	**7**	**9**	O

N	**9**	**7**	**5**	**3**	**1**	**3**	**5**	**7**	**9**	O

APPENDIX C – AHP Calculation Procedure

AHP Calculations

There are two main matrices involved with AHP calculations. Pair-wise comparison matrix and normalized matrix. Relative weights for each factor, from questionnaire survey is generated in pair-wise comparison matrix and final relative weights are calculated in the normalized matrix for each predisposing factor with and without radar induced factors.

A – Elevation

B – Slope

C – Aspect

D – Planar curvature

E – Profile curvature

F – Topographical Wetness Index (TWI)

G – Land use

H – Lineament density

I – Distance to hydrology

J – Soil Moisture Index (NDVI-T domain)

K – Geology

L – Rainfall

M – Soil Moisture (Delta Index) - radar

N – Surface roughness - radar

O – Forest biomass - radar

Table 16 : Pair-wise comparison matrix generated from questionnaire survey for without radar induce factors

	A	B	C	D	E	F	G	H	I	J	K	L
A	1	1/5	3	3	3	1/5	1/5	1/3	1/3	1/5	1/5	1/5
B	5	1	7	7	7	3	1	5	5	3	1	3
C	1/3	1/7	1	3	3	1/7	1/7	1/3	1/5	1/7	1/7	1/7
D	1/3	1/7	1/3	1	3	1/5	1/7	1/5	1/5	1/7	1/7	1/7
E	1/3	1/7	1/3	1/3	1	1/5	1/7	1/5	1/5	1/7	1/7	1/7
F	5	1/3	7	5	5	1	1/3	3	3	1/3	1/5	1/5
G	5	1	7	7	7	3	1	3	5	3	1	1
H	3	1/5	3	5	5	1/3	1/3	1	3	1/3	1/5	1/5
I	3	1/5	5	5	5	1/3	1/5	1/3	1	1/3	1/7	1/7
J	5	1/3	7	7	7	3	1/3	3	3	1	1/3	1/3
K	5	1	7	7	7	5	1	5	7	3	1	3
L	5	1/3	7	7	7	5	1	5	7	3	1/3	1
SUM	38	5	54 2/3	57 1/3	60	21 2/5	5 5/6	26 2/5	35	14 5/8	4 5/6	9 1/2

Table 17 : Normalized Matrix for the final relative weights calculated from pair-wise comparison matrix (without radar induced factors)

	A	B	C	D	E	F	G	H	I	J	K	L	AVG
A	0.026	0.040	0.055	0.052	0.050	0.009	0.034	0.013	0.010	0.014	0.041	0.021	0.030
B	0.132	0.199	0.128	0.122	0.117	0.140	0.172	0.189	0.143	0.205	0.207	0.316	0.172
C	0.009	0.028	0.018	0.052	0.050	0.007	0.025	0.013	0.006	0.010	0.030	0.015	0.022
D	0.009	0.028	0.006	0.017	0.050	0.009	0.025	0.008	0.006	0.010	0.030	0.015	0.018
E	0.009	0.028	0.006	0.006	0.017	0.009	0.025	0.008	0.006	0.010	0.030	0.015	0.014
F	0.132	0.066	0.128	0.087	0.083	0.047	0.057	0.114	0.086	0.023	0.041	0.021	0.074
G	0.132	0.199	0.128	0.122	0.117	0.140	0.172	0.114	0.143	0.205	0.207	0.105	0.149
H	0.079	0.040	0.055	0.087	0.083	0.016	0.057	0.038	0.086	0.023	0.041	0.021	0.052
I	0.079	0.040	0.091	0.087	0.083	0.016	0.034	0.013	0.029	0.023	0.030	0.015	0.045
J	0.132	0.066	0.128	0.122	0.117	0.140	0.057	0.114	0.086	0.068	0.069	0.035	0.094
K	0.132	0.199	0.128	0.122	0.117	0.234	0.172	0.189	0.200	0.205	0.207	0.316	0.185
L	0.132	0.066	0.128	0.122	0.117	0.234	0.172	0.189	0.200	0.205	0.069	0.105	0.145
	1.000	1.000	1.000	1.000	1.000	1.000	1.000	1.000	1.000	1.000	1.000	1.000	1.000

Table 18 : Pair-wise comparison matrix generated from questionnaire survey (with radar induce factors)

	A	B	C	D	E	F	G	H	I	J	K	L	M	N	O
A	1	1/5	3	3	3	1/5	1/5	1/3	1/3	1/5	1/5	1/5	1/5	1/5	1/3
B	5	1	7	7	7	3	1	5	5	3	1	3	3	3	7
C	1/3	1/7	1	3	3	1/7	1/7	1/3	1/5	1/7	1/7	1/7	1/7	1/7	1/3
D	1/3	1/7	1/3	1	3	1/5	1/7	1/5	1/5	1/7	1/7	1/7	1/7	1/7	1/5
E	1/3	1/7	1/3	1/3	1	1/5	1/7	1/5	1/5	1/7	1/7	1/7	1/7	1/7	1/5
F	5	1/3	7	5	5	1	1/3	3	3	1/3	1/5	1/5	1/3	1/3	3
G	5	1	7	7	7	3	1	3	5	3	1	1	3	3	5
H	3	1/5	3	5	5	1/3	1/3	1	3	1/3	1/5	1/5	1/3	1/3	3
I	3	1/5	5	5	5	1/3	1/5	1/3	1	1/3	1/7	1/7	1/7	1/7	3
J	5	1/3	7	7	7	3	1/3	3	3	1	1/3	1/3	1/3	1/3	3
K	5	1	7	7	7	5	1	5	7	3	1	3	3	3	7
L	5	1/3	7	7	7	5	1	5	7	3	1/3	1	3	3	7
M	5	1/3	7	7	7	3	1/3	3	7	3	1/3	1/3	1	1	7
N	5	1/3	7	7	7	3	1/3	3	7	3	1/3	1/3	1	1	7
O	3	1/7	3	5	5	1/3	1/5	1/3	1/3	1/3	1/7	1/7	1/7	1/7	1
SUM	51	5 5/6	71 2/3	76 1/3	79	27 3/4	6 2/3	32 3/4	49 1/4	21	5 2/3	10 1/3	16	16	54

Table 19: Normalized matrix for the final relative weights calculated from pair-wise comparison matrix for with radar induce factors

	A	B	C	D	E	F	G	H	I	J	K	L	M	N	O	AVG
A	0.020	0.034	0.042	0.039	0.038	0.007	0.030	0.010	0.007	0.010	0.035	0.019	0.013	0.013	0.006	0.022
B	0.098	0.171	0.098	0.092	0.089	0.108	0.149	0.153	0.101	0.143	0.177	0.291	0.189	0.189	0.129	0.145
C	0.007	0.024	0.014	0.039	0.038	0.005	0.021	0.010	0.004	0.007	0.025	0.014	0.009	0.009	0.006	0.016
D	0.007	0.024	0.005	0.013	0.038	0.007	0.021	0.006	0.004	0.007	0.025	0.014	0.009	0.009	0.004	0.013
E	0.007	0.024	0.005	0.004	0.013	0.007	0.021	0.006	0.004	0.007	0.025	0.014	0.009	0.009	0.004	0.011
F	0.098	0.057	0.098	0.066	0.063	0.036	0.050	0.092	0.061	0.016	0.035	0.019	0.021	0.021	0.055	0.053
G	0.098	0.171	0.098	0.092	0.089	0.108	0.149	0.092	0.101	0.143	0.177	0.097	0.189	0.189	0.092	0.126
H	0.059	0.034	0.042	0.066	0.063	0.012	0.050	0.031	0.061	0.016	0.035	0.019	0.021	0.021	0.055	0.039
I	0.059	0.034	0.070	0.066	0.063	0.012	0.030	0.010	0.020	0.016	0.025	0.014	0.009	0.009	0.055	0.033
J	0.098	0.057	0.098	0.092	0.089	0.108	0.050	0.092	0.061	0.048	0.059	0.032	0.021	0.021	0.055	0.065
K	0.098	0.171	0.098	0.092	0.089	0.180	0.149	0.153	0.142	0.143	0.177	0.291	0.189	0.189	0.129	0.153
L	0.098	0.057	0.098	0.092	0.089	0.180	0.149	0.153	0.142	0.143	0.059	0.097	0.189	0.189	0.129	0.124
M	0.098	0.057	0.098	0.092	0.089	0.108	0.050	0.092	0.142	0.143	0.059	0.032	0.063	0.063	0.129	0.088
N	0.098	0.057	0.098	0.092	0.089	0.108	0.050	0.092	0.142	0.143	0.059	0.032	0.063	0.063	0.129	0.088
O	0.059	0.024	0.042	0.066	0.063	0.012	0.030	0.010	0.007	0.016	0.025	0.014	0.009	0.009	0.018	0.027
	1.000	1.000	1.000	1.000	1.000	1.000	1.000	1.000	1.000	1.000	1.000	1.000	1.000	1.000	1.000	1.000